Biophysical Studies of the G-protein coupled Neurotensin Receptor

Timothy Charles Hadingham

Thesis submitted to the Board of the Faculty of Biological Sciences

In partial fulfilment of the requirements for the

degree of Doctor of Philosophy

Pembroke College, Oxford

2006

Abstract

Neurotensin (NT) is an endogenous tridecapeptide neurotransmitter (pGlu-Leu-Tyr-Glu-Asn-Lys-Pro-Arg-Arg-Pro-Try-Ile-Leu-OH) (1673 Da), whose effects when administered centrally include analgesia, inhibition of food intake, modulation of dopaminergic systems, modulation of pituitary hormone secretion, regulation of digestive function, and it acts as a trophic factor on human colon, pancreatic, prostate, and lung cancer cell lines. Its receptor protein, the G-protein coupled neurotesin 1 (NTS1), therefore represents an interesting target for the treatment of pain, obesity, schizophrenia, and cancer. Here, NTS1 has been expressed in *E.coli* in the form of an N-terminally truncated fusion protein (NTS1-A) with maltose binding protein (N-terminally) and thyrodoxin (C-terminally) with typical yields of 2.7 nmols ± 2.3 nmols of active NTS1-A per 20 g of wet cell base and a novel protocol for the reconstitution of the receptor into a model membrane was elucidated. Solid phase peptide synthesis was used to produce NT and a variety of derivative peptides of NT to facilitate the studies of the receptor carried out in this thesis. Surface plasmon resonance (SPR) was utilised to study the kinetics of the interaction of NTS1-A with its ligand NT, using the receptor molecule as the analyte in order to enhance the response on binding; the data yielded an overall apparent K_D in the nanomolar range of 37.3 ± 11.3 nmols. SPR was also applied in a new way to investigate techniques for the direct kinetic study of reconstituted receptor. Electron spin resonance (ESR) was used to study the dynamics of NT bound to NTS1-A, where it was demonstrated that there is an induced restriction of motion in the N-terminal region of NT upon binding to NTS1-A, with the correlation time increasing approximately by an order of magnitude at least (1.9 ns to 11.4 ns) in the presence of excess receptor binding sites. This study has suggested that an area of the peptide previously believed to have little biological relevance is, in fact, implicated in binding. Solid state nuclear magnetic resonance (NMR) was used to investigate the assignment of resonances arising from labelled NT bound to NTS1-A. Using the $R14^5_4$ single quantum-double quantum correlation (1Q-2Q) experiment it has been possible to filter resonances arising from labelled ligand from the natural abundance background. This is the first time that this type of experiment has been used to study a ligand bound to a membrane protein. Finally, in order to investigate a possible solution to the difficulties in obtaining crystals of membrane proteins, NTS1-A was used as a test subject with repeating arrays of DNA Holliday junctions, with covalently attached NT. The success of this method was shown in the production of 2D crystals of NTS1-A, and were validated by electron microscopy.

Contents

Acknowledgements

This work was supported by the Biotechnology and Biological Sciences Research Council CASE award with GlaxoSmithkline and the Bionanotechnology IRC.

There are many people I would like to thank for their help and support over the course of this thesis. I would like to express my gratitude to Professor Anthony Watts who has repeatedly given me the opportunities, resources and support which enabled me to complete the work for this thesis, without his confidence in me none of this would have been possible. Thank you to my supervisor from GSK Claus Spitzfaden for facilitating the access to instrumentation for large scale fermentation and SPR and his discussion about detergents, also to Mark Hessey at GSK for his aid with handling the massive fermentation he described to someone used to working with shaker flasks as pilot scale. A huge thank you to Jude Watts for his help with the ESR work an idea I muted to him in the Swan, for drinks and valued discussion, for his tireless sarcastic red pen and putting a rocket up me when I was finding it all far too much to handle and wallowing in self pity. A big thank you to George Wadham, for ganging up on me with Jude, for his swift review of chapters, for ruby games in the Radcliff Arms and for not giving up on me when I had. Thank you Peter Harding for your work with me on your part two project and later joining the lab as a DPhil student, for long hours in the cold room, working with me on all of the SPR experimentation. Thank you Rene Verel for having the patience to explain NMR to a biochemist, for allowing me to have Christmas day off while he went in and filled the heat exchanger, sharing a taste in literature and for understanding that when he blew a sample up at the time we were working together it took another six months to reproduce it. Many thanks to Christoph Meier and Andrew Tuderfield in the Physics department for foolishly wanting to attempt to use a membrane protein with their DNA arrays and letting me come along for the ride. I would also like to thank the members of the Watts group both past and present especially and in no particular order Peter Fisher, Liz Mitchell, Tracy Lam, Chris Kim, Vincent Lemetre, Lubica Aslimovska, Helen Attrill, Wolfgang Fischer, Xin Xho, Scott Goodall, Gerhard Grobner, Phil Williamson, Stephan Grage, Paul Spooner, Boyan Bonev, and James Mason.

Thank you to my parents, Ted and Pauline, for their constant love and unshaking support and for providing a haven in Belgium away from the pressures of work. Finally, thank you Petra for understanding, for your strange taste in men, for everything, but most of all for your love.

Abbreviations and Symbols

A – Adenine

APD – Antipsychotic drugs

APHH – Adiabatic passage through the Hartman-Hann condition

Bio-NT – N-terminally biotinylated NT

Bp – Base pairs

BPL – Brain polar lipid extraction

C – Cytosine

cAMP – Adenosine 3',5'-cyclic monophosphate

cAR – cAMP receptors

CCR5 – Chemokine receptor

cGMP – Guanodine 3',5'-cyclic monophosphate

CHAPS - 3-[(3-cholamidopropyl)dimethylammonio]-1-propanesulfonate

CHS - cholesteryl hemisuccinate Tris salt

CMC – Critical micellar concentration

CNS – Central nervous system

COSY – Correlation spectroscopy

CP – Cross polarization

Cpm – Scintillation counts per minute

CSA – Chemical shift anisotropy

CTC – Cubic ternary complex

CW – Continuous wave decoupling

CXCR4 – Chemokine receptor

Cys-NT – Neurotensin with the addition of a cysteine residue N-terminally

DA – Dopaminergic

DCM – dichloromethane

DDM - dodecyl-β-D-maltoside

DIPEA – diisopropylethylamine

DMF – dimethylforamide

DNA – Deoxyribonucleic acid

dO_2 – Dissolved oxygen

DTT – Dithiotheritol

E1 – Extracellular loop one

E2 – Extracellular loop two

E3 – Extracellular loop three

EDC - 1-Ethyl-3-(3-dimethylaminopropyl) carbodiimide hydrochloride

EDT – 1-2-ethanedithiol

EDTA – Ethylenediaminetetraacetic acid

EFG – Electric field gradient

EM – Electron microscopy

ESI – Electro-spray ionization

ESR – Electron spin resonance

Fc – Flow cell

FID – Free induction decay

FPLC – Flow pressure liquid chromatography

Fv – variable fragment

G – Guanine

GABA – Gamma-aminobutyric acid

GABA-B - Gamma-aminobutyric acid B

GDP – Guanosine 5'-diphosphate

GPCR – G-protein coupled receptor

GTP - Guanosine 5'-triphosphate

HBTU - 2-(H-Benzotriazole-1-yl)-1,1,3,3-tetramethyluronium hexafluorophosphate

hNTS1 – Human neurotensin receptor 1

hNTS2 – Human neurotensin receptor 2

HOBt - N-Hydroxybenzotriazole

HPLC - High pressure liquid chromatography

HPS-EP – Hepes buffer saline with EDTA and surfactant P

HRP – Horseradish peroxidase

I1 – Intracellular loop one

I2 – Intracellular loop two

I3 – Intracellular loop three

IPTG – Isopropyl β-D-1-thiogalactopyranoside

LB – Luria Bertani bacteria growth media

LF – Laboratory frame

MALDI-TOF – Matrix assisted laser disorption – time of flight

MAS – Magic angle spinning

MBP – Maltose binding protein

mGluRs – Glutamate receptor

mNTS2 – Mouse neurotensin receptor 2

NCCN-$NT_{(8\text{-}13)}$ – N-terminal six amino acids of NT with (1, 2, 3, 4, 5 ^{13}C, ^{15}N)Pro and (^{15}N)Try

NHS - N-Hydroxysuccinimide

Ni-NTA – Nickle affinity resin

NMR – Nuclear magnetic resonance

NN – Neuromedin N

NOE – Nuclear Overhauseer effect

NT - Neurotensin

$NT_{(8-13)}$ – Angonist analogue of Neurotensin consisting of the C-terminal size amino acids

NTS1 – Neurotensin receptor 1

NTS1-A – T43 truncated fusion construct of neurotensin receptor one

Nts2 – Neurotensin receptor 2

Nts3/gp95/sortilin – Neurotensin receptor 3

NTspin0 – Cys-NT with a spin label attached to the N-terminal cysteine residue

NTspin6 – Neurotensin with the sixth amino acid substituted for cysteine and modified with a spin label

OD – Optical density

PACAP - Pituitary adenylate cyclase-activating polypeptide

PAGE – Polyacrylamide gel electrophorises

PAS – Principle axis frame

PBS – Phosphate buffered saline

PCR – Polymer chain reaction

PDEA - 2-(2-Pyridinyldithio)ethaneamine hydrochloride

RAP – Receptor-associated protein

Rf – radio frequency

rNTS1 – Rat neurotensin receptor 1

rNTS2 – Rat neurotensin receptor 2

ROSEY – Rotating frame Overhauser effect spectroscopy

RU – Response units

SDS – Sodium lauryl sulphate

SPPS – Solid phase peptide synthesis

SPR – Surface plasmon resonance

T – Thyamine

TES – Triethylsilane

TFA – Trifluoroacetic acid

TM – Trans-membrane

TMD – Trans-membrane domain

TPPM – Two pulse phase modulated decoupling

UV – Ultra violet

VIP - Vasoactive intestinal peptide

Vvm – Volume per volume per minute

1Q – Single quantum

2Q – Double quantum

Chapter 1 Introduction

1.1 Biological Membranes

Biological membranes consist of amphipathic lipids forming a stable sheet-like bilayers, with the polar lipid head groups externaly to a core of hydrophobic acyl chains and with proteins both bisecting the sheets and attached on their surfaces Figure 1.1.

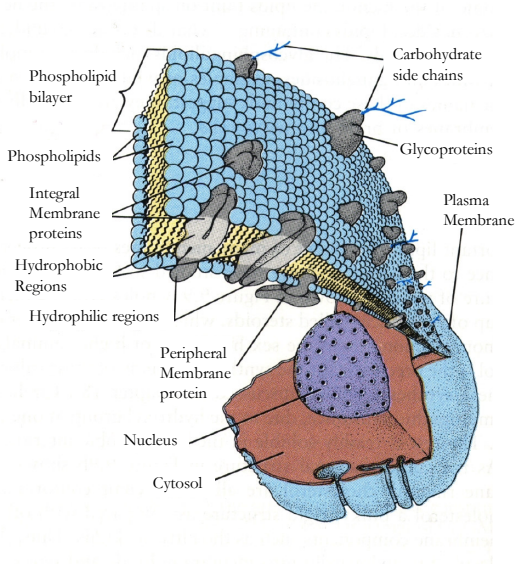

Figure 1.1 - Structure of a typical cell membrane. In this schematic view of a membrane, drawn according to the fluid mosaic model of Singer and Nicholson, a strip of the plasma membrane of a eukaryotic cell has been peeled off to reveal the lipid bilayer: polar head groups exposed to the aqueous interior and exterior, non-polar carbon chain tails self associated and interdigitated in the membrane core; and the proteins embedded and peripheral in it which are free to diffuse laterally in the plane of the membrane [1].

These membranes play a vital role in both the structure and function of living cells. They serve not only to compartmentalise the cell, but also to regulate the passage of information, in the form of chemicals and electrical potential gradients, into and out of these compartments.

1.1.1 The Pivotal Role of Membrane Proteins

Membrane-spanning proteins acting as channels, pumps, receptors and enzymes largely mediate the passage of molecules and information across cell membranes. These proteins perform many tasks: they control electrochemical gradients across the membranes; receive signals from the environment or from other cells; and harness proton gradients to generate the energy consumed in metabolism. Indeed, of the estimated 56,960-81,273 genes in the human genome[2, 3], some 20-40% is thought to encode for membrane proteins.

Unlike soluble proteins, membrane proteins are not well suited to study by the principal high-resolution structural methods, X-ray diffraction and solution NMR. Practical problems routinely hamper the use of these methods and to date there are 92 unique membrane proteins in the PDB database (includes proteins of same type from different species; e.g. photosynthetic reaction centres from R. viridis and R. sphaeroides are considered unique, structures of mutagenized versions of proteins already in the database are excluded as unique, proteins that differ only by substrate bound or by physiological state are also excluded.), with 169 coordinate files of high-resolution membrane protein structures that have been solved. Diffraction studies of membrane proteins are limited by the difficulty in obtaining well-ordered crystals [4]. Solution NMR approaches rely on rapid isotropic molecular motion to produce high-resolution spectra. As a result, these methods are not generally applicable to membrane systems where proteins exhibit slow and anisotropic motions due to their size (M_r^{eff} greater than 30k) and association with detergent or lipids, increasing this effective M_r^{eff} to >> 10^3 k.

1.2 G-Protein-Coupled Receptors

The evolution of multicellular organisms has been highly dependent on the capacity developed by their cells to communicate with each other and with their environment. Membrane-bound receptors, dedicated to recognizing intercellular messenger molecules (such as hormones, neurotransmitters, growth and developmental factors), and several sensory messages (such as light, odors and gustative molecules), belong to four or five protein families; the most common one is the G protein-coupled receptor (GPCR) family. In vertebrates, this family contains 1000–2000 members (1% > of the genome) including 1000 coding for odorant and pheromone receptors [5]. Similarly, the Caenorhabditis elegans genome encodes ~1100 GPCRs (5% of the genome, which is now entirely known) [6], in this organism, this is the family of genes which comprises the most members. GPCRs are certainly among the oldest devices devoted to signal transduction being present in plants [7], yeast [8] and slime mould (Dictyostelium discoıdeum) [9], as well as in protozoa and the earliest diploblastic metazoa [10, 11]. However, the range of sequence data is currently too small to be able to make reasonable inference as to the evolutionary emergence of most of the GPCRs present in vertebrates.

The first GPCRs to be purified were rhodopsin, the photon receptor from retinal rod outer segments, and the β-adrenergic receptor. They were the fruits of completely independent research efforts, directed on the one hand towards understanding the mechanism of light activation of cGMP phosphodiesterase and or the other toward the mechanism of activation of adenyl cyclase by epinephrine. Differences in the agonists (catecholamines and photons) and effectors (adenyl cyclase and cGMP phosphodiesterase) provided an early hint of the remarkable diversity of situations in which G-protein-coupled receptors are employed to select,

amplify, and transmit signal from the external environment to elicit cellular responses and functions.

Sequence comparison of GPCRs has revealed the existence of different receptor families sharing no sequence similarity, suggesting a remarkable example of convergence in molecular evolution. However, all these receptors have in common a central core domain constituted of seven transmembrane helices (TM) (TM-I through -VII) connected by three intracellular (I1, I2 and I3) and three extracellular (E1, E2 and E3) loops [12]. Two cysteine residues (one in e1 and one in e2) which are conserved in most GPCRs, form a disulfide link which is probably important for the packing and for the stabilization of a restricted number of conformations of these seven TMs. Aside from sequence variations, GPCRs differ in the length and function of their N-terminal extracellular domain, their C-terminal intracellular domain and their intracellular loops. Each of these domains provides specific properties to these various receptor proteins, as discussed below.

Figure 1.2 (A) shows three main families (1, 2 and 3), which can be easily recognized when comparing their amino-acid sequences. Family 1 contains most GPCRs including receptors for odorants, group 1a GPCRs for small ligands including rhodopsin and β-adrenergic receptors the binding sites are localized within the seven TMs; group 1b receptors for peptides whose binding sites can include the N-terminals, the extracellular loops and the superior parts of TMs; and group 1c GPCRs for glycoprotein hormones characterized by a large extracellular domain and a binding site which is mostly extracellular but at least with contact with extracellular loops E1 and E3.

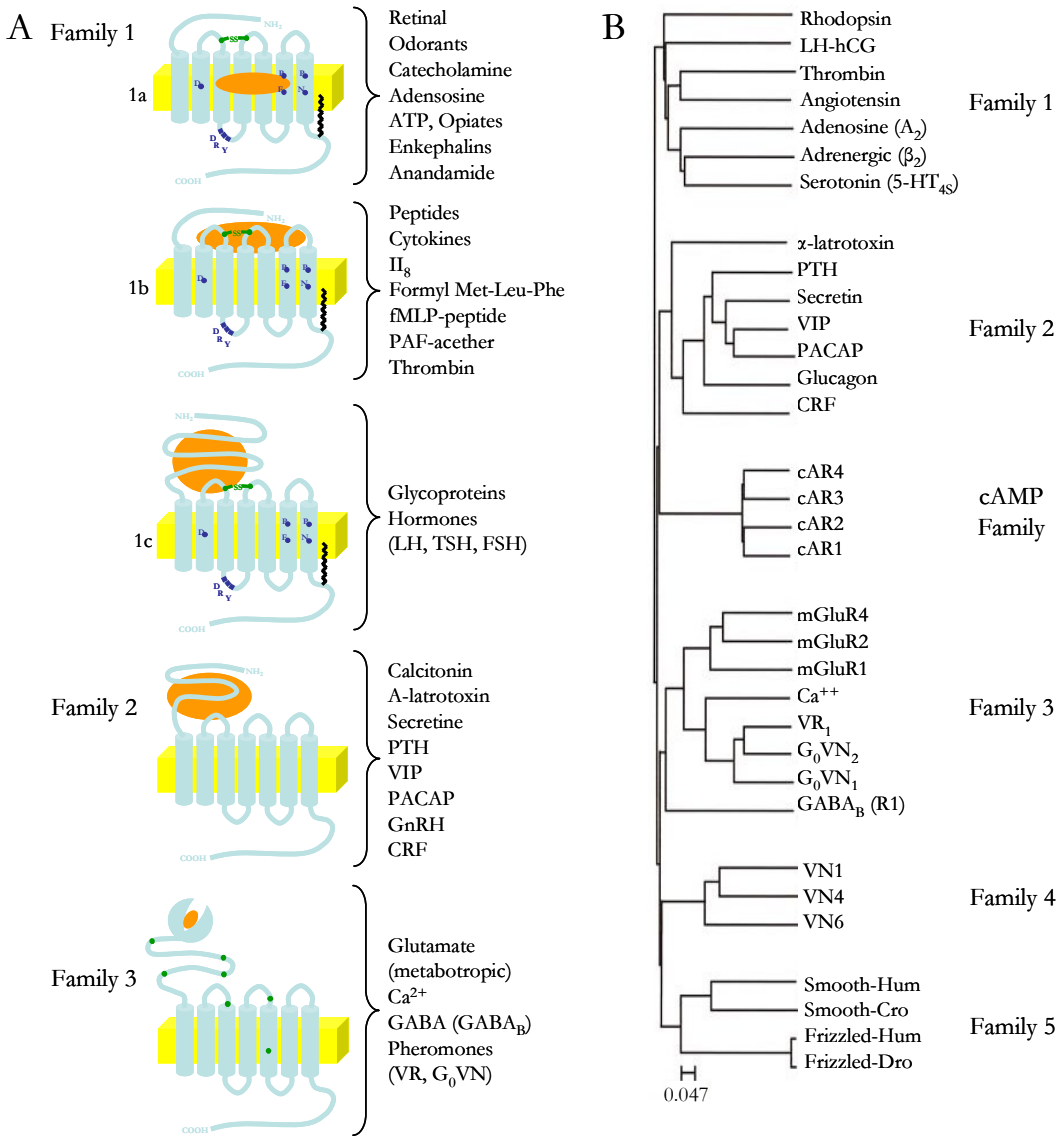

Figure 1.2 – A diagram to demonstrate the classification and diversity of GPCRs. (**A**) the three main families of GPCRs with their topography and conserved amino acids highlighted. (**B**) A dendrogram for the evolutionary diversion of GPCRs and their respective family groups; the dendrogram has been established with Clustal W.

Family 2 GPCRs have a similar morphology to group 1c GPCRs, but they do not share any sequence homology; their ligands include high molecular weight hormones such as glucagon, secretine, VIP-PACAP and the Black widow spider toxin, α-latrotoxin [13, 14]. Family 3 contains mGluRs and the Ca^{2+} sensing receptors [15]. In 1998, however, GABA-B receptors

[16] and a group of putative pheromone receptors coupled to the G protein G_o (termed VRs and G_o-VN) became new members of this family [17]. Figure 1.2 (B) shows three additional family members; family 4 comprises pheromone receptors (VNs) associated with Gi [18]; family 5 includes the 'frizzled' and the 'smoothened' (Smo) receptors involved in embryonic development and in particular in cell polarity and segmentation. Finally, the cAMP receptors (cAR) have only been found in *D.discoideum* but its possible expression in vertebrate has not yet been discovered. The receptors signal is transduced via heterotrimeric G proteins, constisting of three subunits (Gα, Gβ, and Gγ) with several different isoforms of each; activation is mediated by exchange of GDP for GTP leading to the dissociation of alpha from beta-gamma subunits which then leads to the activation of various effecter enzymes and/or channels.

The GPCR in this study, Neurotensin receptor 1 (NTS1), is part of the 1b family and is discussed in detail below.

1.2.1 Neurotensin receptors (NTS)

Tissue specific regions of neurotensin (NT) binding were originally identified by radioligand binding studies [19]. NT mediates its effects through cell surface receptors, which have both high and low affinity sites for the peptide. Three receptors have been cloned, all of which share the same recognition for the C-terminal six amino acids of NT ($NT_{(8-13)}$): NTS1 [20], nts2 [21, 22], and nts3/gp95/sortilin [23]. NTS1 and nts2 share 43% amino acid identity and 64% homology whereas the nts3 belongs to an entirely different family of proteins.

NTS1, the high affinity receptor originally cloned from rat, is a G-protein coupled receptor (GPCR) with seven putative transmembrane domains (7TMD) [20], and cGMP, inositol 1,4,5-triphosphate and Ca^{2+} identified as secondary messengers. The human NTS1 (hNTS1) shares 84% homology with the rat NTS1 (rNTS1) [24] and they are 418 and 424 amino acids long respectively. The receptor is sensitive to Na^+ ions and GTP, which both decreases the affinity

of NTS1 for NT. The effects mediated by NTS1 are blocked by the non-peptide antagonist SR48692 which targets NTS1 selectively [25], or by the promiscuous antagonist SR 142948A [26].

NTS2, the low affinity receptor, is also a GPCR with a putative 7TMD structure though it has a longer third cytoplasmic loop and a shorter extracellular N-terminal region than found in NTS1. As with the NTS1, human NTS2 (hNTS2) is six amino acids shorter than rat (rNTS2) and mouse (mNTS2) being 410 and 416 amino acids long respectively. NTS2 is less sensitive to Na^+ ions than NTR1 and insensitive to GTP concentration. The antihistamine-1 drug levocabstine selectively blocks the binding of NT to NTS2. The signalling pathway of NTS2 is still poorly understood, the only cross-species consistent result is the agonist action of SR 48692. Surprisingly, NT itself may act as an agonist [27] or as an antagonist of the inositol phosphate stimulation induced by SR 48692 [28].

NTS3 is unlike the other two NTSs and on its discovery as a NT receptor was found to share 100% identity with the gp95sortilin, a sorting protein originally identified by its ability to interact with a receptor-associated protein (RAP) [29]. NTS3 is 800 amino acids (100 kDa) in length and has a single putative TMD.

1.2.2 Neurotensin

NT (1673 Da) is an endogenous tridecapeptide neurotransmitter (pGlu-Leu-Tyr-Glu-Asn-Lys-Pro-Arg-Arg-Pro-Try-Ile-Leu-OH) originally isolated and sequenced from bovine hypothalamus [30] then later in the intestines [31], distributed heterogeneously in the central nervous system (CNS) as well as the gastrointestinal tract and is responsible for the activation of the neurotensin receptor (NTR) family.

NT exerts potent CNS effects including stimulation of and modulation of dopamine neurotransmission [32], anterior-pulmonary hormone secretion, antinociception [33, 34], and hypothermia [35, 36]. NT interacts with dopaminergic (DA), cholinergic, serotonergic, as well as noradrenergic, neuronal systems. All of these systems, together with other neurotransmitter systems, including glutamate and gamma-aminobutyric acid (GABA), have been implicated in mediating the effects of antipsychotic drugs (APDs) in the treatment of schizophrenia, Parkinson's disease and other disorders [37, 38]. Peripherally, neurotensin acts as a paracrine and endocrine peptide of both the digestive and cardiovascular systems; it induces hypotension, decreases gastric acid secretion, and activates lipid digestion [39, 40]. Additionally, there is evidence to support a role for neurotensin in the growth of normal and cancerous cells [41, 42]. Commercially/Pharmaceutically, the peptide is involved in the hypothalamic-pituitary-adrenocortical axis; it plays a tonic stimulatory role linked to depressive disorders, gut cell proliferation, and pro-inflammatory responses.

The discovery that only the C-terminal six amino acids of the parent compound, namely $NT_{(8-13)}$ (Arg-Arg-Pro-Try-Ile-Leu), are all that are needed for biological activity is quite surprising, since it appears that $NT_{(8-13)}$ is not one of the fragments generated *in vivo* by NT degradation. This is a C-terminal motif NT shares in common with the family of bioactive peptide ligands including xenopsin, bradykinin, and neuromedin N [39].

In free solution, proton NOEs and J-couplings have revealed that NT has no preferred conformation [43]. These studies were extended to investigate the conformation of NT in the presence of membrane mimetic sodium dodecyl d_{25}-sulfate and indicated that charge-charge interactions with the surface of the detergent micelles ordered the charged residues within NT. No preferred conformation was adopted by NT however. To date, no crystallographic data has been published for NT as a free ligand or bound to its receptor.

1.2.3 Nonpeptide NT Antagonists

The first highly selective non-peptide NTS antagonist to be discovered, SR 48692 (Figure 1.3)[44], is orally active, crosses the blood brain barrier and has a long-lasting action; it shows higher affinity for NTS1 than for NTS2.

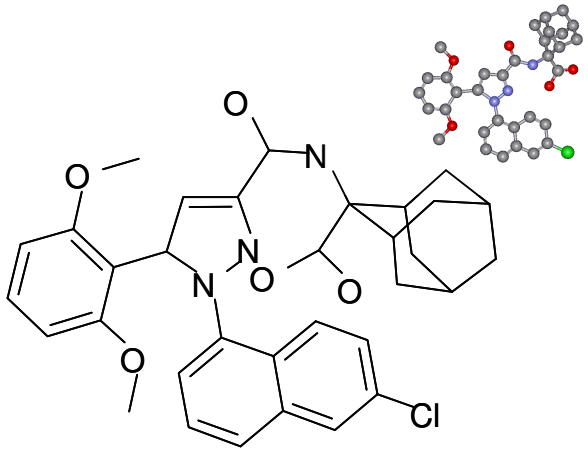

Figure 1.3 – The chemical structure of SR 48692; with oxygen atoms in red, nitrogen in blue, and chlorine in green.

This antagonist has been shown to counteract the effects of NT *in vitro* and *in vivo*. However, SR 48692 is unable to inhibit NT-induced hypothermia and analgesia in rats and mice [25]. This compound also fails to reverse dopamine release in the nucleus accumbens evoked by NT injection in the ventral tegmental area [45], as well as the hypolocomotion induced by intracerebroventricular administration of the peptide [46]. These findings suggest that these effects of NT could be mediated through a NTS subtype which is insensitive to SR 48692 [47]. SR 48692 has a number of properties that limit its usefulness, in particular, it has very low aqueous solubility and 100 times lower affinity for the rat brain when compared to the guinea pig brain [44].

Sanofi Recherche have developed a second non-peptide antagonist of NTSs, SR 14948A (Figure 1.4), which is chemically related to SR 48692 but has better solubility and increased affinity in the rat brain [26].

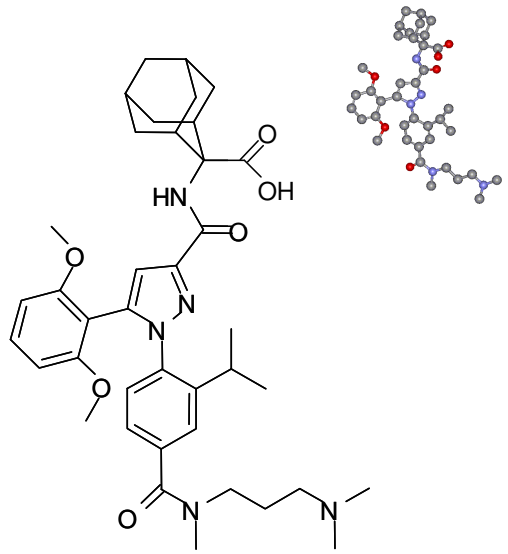

Figure 1.4 – Chemical structure of SR 142948A with oxygen atoms in red, and nitrogen in blue.

SR 142948A recognises with similar affinity (in the nanomolar range) both NTS1 and NTS2[26]. In contrast to SR 48692, SR 14298A prevents the hypothermia and analgesia induced by central injection of NT, revealing a wider spectrum of action which is probably achieved through inhibition of different NTS subtypes [26].

1.2.4 NT structure-activity relationships

$NT_{(8-13)}$ analogues have been used to help define the interaction of NT with its receptors. Pseudopeptides were compared for there ability to cause hypothermia (*in vivo*), antiociception (*in vivo*), and dopamine release (*in vitro*). Arg^{8} can be replaced with D-Lys, or L- and D-

Ornithine (Orn) with the resulting peptides exhibiting greater potency at the NTR1 than NT (with D-Lys<L-Orn<D-Orn) (Figure 1.5).

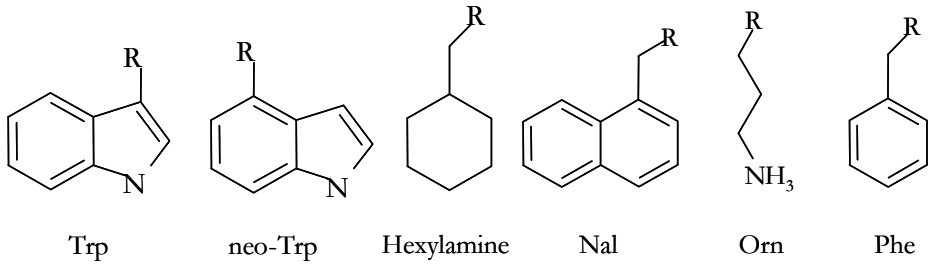

Figure 1.5 – Chemical structures of the amino acid substituted into NT(8-13). The R group in the diagram represent the alpha carbons of the amino acid.

A critical aspect of these experiments is the metabolic stability of the analogue since if the peptide is degraded; it must be administered centrally for an effect to be seen (Table 1.1).

Peptide	K_d/nM		P_I Turnover EC_{50}/nM
	hNTR1	rNTR1	
$NT_{(8-13)}$	0.14 ± 0.01	0.16 ± 0.01	1.5 ± 0.1
[L-Orn^8]$NT_{(8-13)}$	0.41 ± 0.03	1.2 ± 0.2	3.1 ± 0.2
[D-Orn^8]$NT_{(8-13)}$	0.26 ± 0.02	1.2 ± 0.2	2.9 ± 0.2
[L-Orn^9]$NT_{(8-13)}$	0.73 ± 0.04	0.51 ± 0.06	3.2 ± 0.6
[D-Orn^9]$NT_{(8-13)}$	1 ± 0.1	0.8 ± 0.1	1.5 ± 0.3
[Hexylamine^{11}]$NT_{(8-13)}$	700 ± 100	280 ± 20	3100 ± 20
[L-Phe^{11}]$NT_{(8-13)}$	3.4 ± 0.2	0.74 ± 0.03	22.3 ± 0.9
[L-Nal^{11}]$NT_{(8-13)}$	89 ± 9	3.9 ± 0.2	320 ± 60
[neo-Trp^{11}]$NT_{(8-13)}$	0.09 ± 0.01	0.1 ± 0.01	

Table 1.1 – Binding and functional parameter of NT analogues[48].

The substituted peptide exhibits almost equal effectiveness at cGMP stimulation as $NT_{(8-13)}$, though with less potentency [49]. If Arg^9 is replaced with D-Orn, the resulting peptide causes a potent hypothermic reaction but no analgesia when delivered to rats and mice. L-Orn substitution at the same position causes hypothermia in both rats and mice, as with D-Orn,

and is accompanied by analgesic properties in mice. The two peptides, [D-Orn^{9}]($NT_{(8-13)}$) and [L-Orn^{9}]($NT_{(8-13)}$), when compared have a 190- and 700-fold increase in binding potency (picomolar affinity) at the human and rat receptors, respectively [48]. This stereoselectivity is also seen in phosphatylinositol turnover.

Substitutions for Tyr at position 11, whereby the delocalised π-electron system is replaced by a hexyl moiety, cause a drastic decrease in affinity, 5000-fold with respect to $NT_{(8-13)}$, implying π-π or cation-π interactions with the receptor. [L-Phe^{11}]($NT_{(8-13)}$) shows a significant decrease in potency value upon the loss of the OH group, implicating it in possible hydrogen bond formation. [L-napthylalanine(Nal)^{11}]($NT_{(8-13)}$) shows a species-selective binding with a 23-fold greater affinity for rNTS1 than hNTS1 [48]. Changes in the residue at position 11 affects the K_d values more dramatically for hNTS1 and rNTS1 [50]. The orientation of the steric bulk of Tyr^{11} is crucial for binding to NTS1 and it has been demonstrated that the binding site of $NT_{(8-13)}$ in hNTS1 is slightly smaller than in rNTS1. hNTS1 exhibits a preference for molecules that are larger than Tyr and smaller than napthylalane at position 11. For the substitution [L-4-indole-tryptophan[neo-Trp^{11}]($NT_{(8-13)}$) for both hNTS1 and rNTS1 results in an increase in affinity over that of $NT_{(8-13)}$ results [51]. The orientation of the aromatic indole side chain of neo-Trp would reorientate the steric bulk and thus be better accommodated by the relatively smaller hNTR; neo-Trp also maintains any π-π or cation-π interactions that may be important for binding in the receptor.

1.2.5 Mutagenesis and modelling of NTS1

The third extracellular loop (E3) was identified as a potential contributing region for NT binding. The E3 region has the highest percentage of aromatic residues in the receptor containing 10 aromatic residues in both hNTS and rNTS, which accounts for 48% of the residues compared to only 11% aromatic amino acids over the whole protein. Alignment

studies of rNTS and other GPCRs have also determined that this region, when compared across the whole family, contains the greatest structural variation [20]. Homology modelling of E3 reveals that the backbone of the loop forms a predominantly aromatic pocket in 3D space. In hNTS1 this is composed of Phe^{326}, Ile^{329}, Trp^{334}, Phe^{337}, Tyr^{339}, Phe^{341}, Tyr^{342}, and Tyr^{344}; and in rNTS1 Phe^{331}, Ile^{334}, Trp^{339}, Phe^{342}, Phe^{344}, Phe^{346}, Tyr^{347} and Tyr^{349}. The difference in the sequence of E3 from hNTS1 to rNTS1 is thought to be responsible for the hNTS1 binding cavity binding being smaller than that of rNTS1 [50](Figure 1.6).

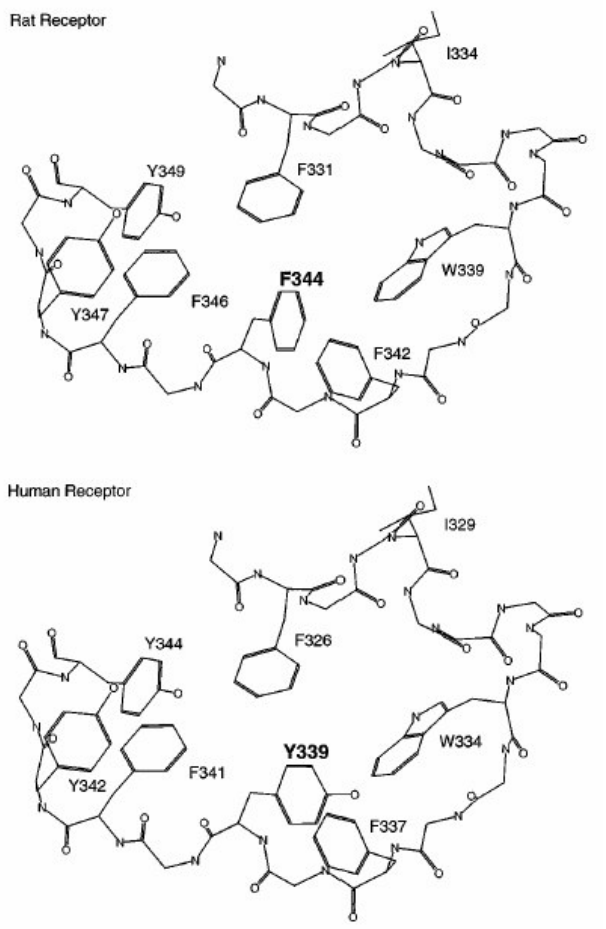

Figure 1.6 – Three-dimensional structure of the E3 in human and rat NTR1 as a putative $NT_{(8-13)}$ binding site [50].

Manual docking of $NT_{(8-13)}$, into the model by Pang *et al* of the E3 region, shows that the ligand adopts a compact conformation with the Arg^{9}-Pro^{10}-Trp^{11}-Ile^{12} adopting a proline type I turn,

while the guanidium groups of Arg^{8} and Arg^{9} interact with the hydroxyl group of Tyr^{11} (Figure 1.7).

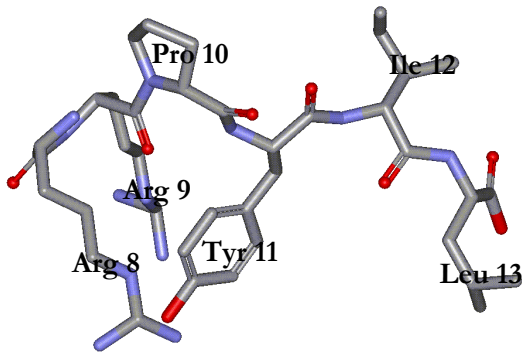

Figure 1.7 - Proposed three dimensional structure of the bound conformation of $NT_{(8-13)}$ from manual docking to the homology model of the E3 loop region [50].

$NT_{(8-13)}$ contains, at neutral pH, three positive and one negative charge which may engage in ionic interactions with the receptor. To identify the charged amino acids important for ligand binding, point mutations at every charged amino acid in the extracellular loops and TMs have been introduced into the rat NTS1 [52]. A 2-3 fold decrease in affinity for $NT_{(8-13)}$ is observed when Arg^{213} and Asp^{216}, in the second extracellular loop (E2) of NTS1; and also when Asp^{336}, Glu^{337} and Asp^{345} in E3 are substituted. Substitution of Asp^{139}, Arg^{143}, Arg^{327} or Arg^{328} (in the first extracellular loop (E1) and the sixth transmembrane region (TMVI) respectively) virtually abolishes all $NT_{(8-13)}$ binding. These positively charge amino acids located close to the external surface of the bilayer are critical for the preservation of the interaction with NT. SR 48692 and NT have been used in a comparative mutagenesis modelling study (Table 1.2)[53]. All of the residues determined to be critical for SR 48692 binding, except for Asp^{139} and Met^{208}, are found in putative TMs 6 and 7, or lying at the external surface of the bilayer between these two

helices on E3. The majority of mutations affecting the binding properties of SR 48692 have little effect on the binding of NT; the converse is also true substitutions; resulting in the loss of NT binding do not affect the affinity of SR 48692 for rNTS1. These data lead to the conclusion that SR 48692 and NT bind to distinct epitopes on the rNTS1.

TM/E	Mutation	K_d, K_i[a]	
		NT	SR 48692
		nM	
	Wild type	0.12 ± 0.02 0.18 ± 0.01[a]	2.60 ± 0.20 5.88 ± 0.11[a]
E1	D139A D139G	ND ND	ND
TM4	M208A	1.26 ± 0.26 1.91 ± 0.59[a]	ND 56.0 ± 17.0[a]
TM6	Y324A F331A R327M R327E	0.20 ± 0.07 0.28 ± 0.03[a] 1.29 ± 0.15 3.02 ± 0.51[a] ND ND	ND 106 ± 7[a] ND 124 ± 19[a] ND ND
TM7	Y347A Y351A Y359A	ND 0.90 ± 0.27 1.18 ± 0.12[a] 0.40 ± 0.07 0.40 ± 0.09[a]	3.99 ± 0.73 ND 1625 ± 470[a] ND 29.2 ± 2.2[a]

Table 1.2 – Kd and Ki values for NT and SR 48692 binding to wild type and mutated rNTR[53]. Kd values were determined from Scatchard analysis of saturation binding experiments employing either 125I-NT or [3H]SR 48692 as labelled ligand. aKi values were derived from competition binding experiments with unlabelled NT and SR 48692 as the competitors and 125I-NT as the labelled ligand. ND, not detectable [53].

The Y351A mutation exhibits a 300-fold decrease in affinity for SR 48692 and a 10-fold decrease for NT binding; Y347A seems to have the opposite effect with no detectable NT binding and only a 2-fold decrease in antagonist binding. These two Tyr residues in E3; are close to the external terminus of TM7 and are therefore in spatial proximity, and appear to be responsible for discriminating the two binding activities. TM6 and 7, together with E3, contain most of the residues responsible for the binding of both NT and SR 48692, suggesting that the two binding sites are close to each other and could overlap. If this is the case, the

overlap could explain the observation that SR 48692 behaves as a competitive antagonist of NT binding and NT mediated effects [44].

Decreases in affinity caused by the Y352A and Y347A mutations are compatible with the removal of hydrogen bonding and π-π interactions between a Tyr residue and the pyrazole; and dimethylphenol of the antagonist and the Tyr^{11} residue of NT. The R327M mutant is devoid of any detectable binding activity for both SR 48692 and NT. It is possible that Arg^{327} forms an ionic interaction with the acidic function of the antagonist and the C-terminus of NT [54]. A similar loss in the magnitude of affinity is observed after a reciprocal modification of interacting partners (Y347A and Y11A; A327M and Leu^{13}-COOH to Leu^{13}-NH_2) which is consistent with the interactions described above.

It has been proposed in complementary mutagenesis studies, mutating both receptor and agonist, that the side chains of Ile^{12} and Leu^{13} interact with Met^{208} and Phe^{331} respectively [54]. The decreases in potency cause by the M208A and F331A substitutions exhibit a 30-fold decrease in binding, which is 500 times smaller than that observed in the corresponding I12A and L13A mutations in the $NT_{(8-13)}$ sequence. This observation suggests that there may be interactions with residues yet to be identified, or that the side chains of Ile^{12} and Leu^{13} are important in the positioning of the C-terminus of NT in the binding site. A cation-π interaction between the guanidinium group of Arg^{9} and Phe^{331} has been postulated due to the 70-fold decrease in potency observed for [L-Citrulline $(Cit)^{9}$]$NT_{(8-13)}$ [54]. The substitutions D139G and D139A result in complete loss of agonist and antagonist binding; it had been proposed that this was due to the loss of an ionic interaction with Arg^{8}, though if this was the case then the [Cit^{8}] $NT_{(8-13)}$ would be expected to have a greater loss in potency than the 2-fold loss observed. To reconcile these inconsistencies, it has therefore been proposed that loss of

residue Asp[139] results in a conformational change in the receptor which precludes both agonist and antagonist binding.

Figure 1.8 highlights the residues involved in binding NT and SR 48692 discussed above; it also shows the TM2 Asp that is highly conserved in most GPCRs [55] and is responsible for the modulation of NTS by Na^+ ions. Asp[113] in NTS1 is also responsible for efficient coupling of the receptor to phospholipase C.

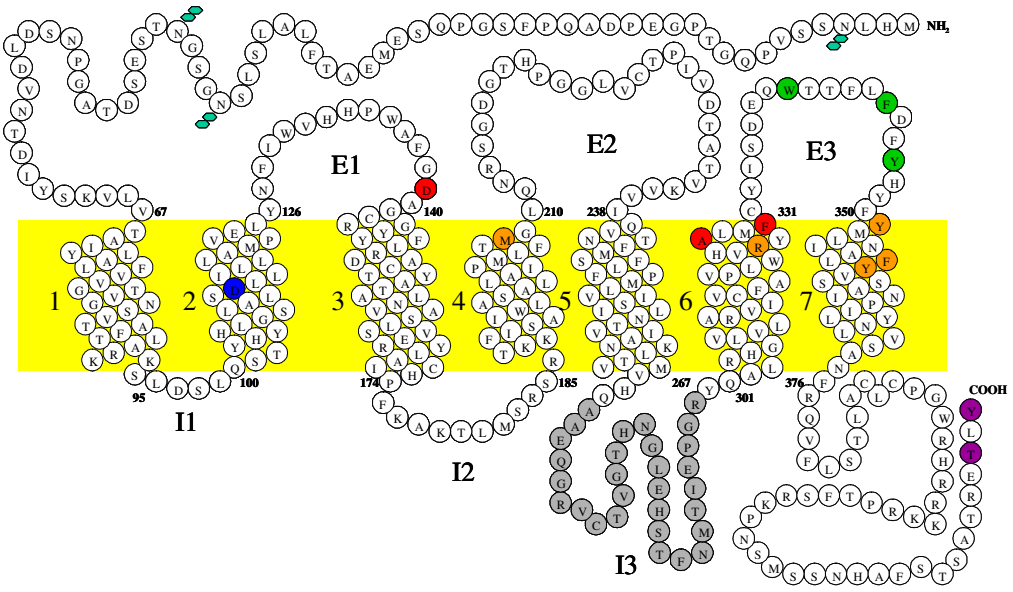

Figure 1.8 – Summary of the residues critical for agonist and antagonist binding in rat neurotensin receptor, NTS1 [54]. The N-terminal (1), C-terminal (424) and the first residues of each extracellular segments of the NTS1 receptor are numbered. The Na^+ binding site (Asp[113]) of NTR1 is shown in blue. Residues involved in the binding of NT (green), SR48692 (orange) or both (red) are indicated. Residues crucial for NTS1 internalisation are in violet. The region of the third intracellular loop (I3) that is essential for coupling to phospholipase C is in grey. Glycosylation sites are highlighted.

1.3 Aims of the Thesis

Chapter 2 details the materials and methods used in the rest of the thesis, which are then referred to throughout the following chapters of this thesis.

Chapter 3 describes the production, quantification and reconstitution of active NTS1-A in sufficient quantities to use in subsequent biophysical studies in later chapters of this thesis.

Chapter 4 describes a study in which surface plasmon resonance (SPR) was used to demonstrate and quantify the specific interaction of NTS1-A with its ligand NT, in both detergent solubilized and membrane reconstituted receptor.

Chapter 5 describes a study in which spin-labelled full-length NT analogues and NTS1-A were observed by conventional electron spin resonance (ESR) methods in order to compare the relative mobilisation of the N-terminal seven amino acids of NT to gain an insight into the binding of this important neuropeptide to its GPCR.

Chapter 6 describes a study utilising various solid state NMR approaches and labelling schemes to obtain assignment of labelled NT ligand bound to NTS1-A

Chapter 7 describes how arrays of DNA Holiday junctions could possibly be used to generate regular arrays of membrane protein for possible future crystallographic study.

Chapter 8 outlines the overall conclusions of this body of work.

Chapter 2 Materials and Methods

2.1 Aims of this Chapter

This chapter details the materials and methods used in the rest of the thesis, which will be referred to throughout the rest of the thesis.

2.2 Materials

2.2.1 Bacterial growth media

2.2.1.1 SOC medium

Per litre: 20 g bacto-tryptone, 5 g yeast extract, 0.5 g NaCl were added to 950 ml of milli Q water and shaken well until all the solutes had dissolved. Then 10 ml of a 250 mM solution of KCl was added, the pH was adjusted to 7.0 and the volume made up to 1 litre with milli Q water before sterilization by autoclaving for 20 minutes at 15 lb per sq. in. on liquid cycle. Just prior to use, 5 ml of sterile 2 M $MgCl_2$ and 20 ml of 1 M glucose was added.

2.2.1.2 Luria-Bertani (LB) bacterial growth medium

Per litre: 10 g bacto-tryptone, 5 g yeast extract and 10 g NaCl were added to 950 ml of milli Q water and shaken well until all the solutes had dissolved. The pH was then adjusted to 7.0 and

the volume made up to 1 litre with milli Q water before sterilization by autoclaving for 20 minutes at 15 lb per sq. in. on liquid cycle.

2.2.1.3 LB agar

As LB medium with 15 g, per litre, of bacto-agar added before adjusting the pH and sterilization.

2.2.1.4 2x TY

Per litre: 16 g bacto-tryptone, 10 g yeast extract and 5 g NaCl were added to 950 ml of milli Q water and shaken well until all the solutes had dissolved. The pH was then adjusted to 7.0 and the volume made up to 1 litre with milli Q water before sterilization by autoclaving for 20 minutes at 15 lb per sq. in. on liquid cycle.

2.2.2 Antibiotic stock solution

Ampicillin stocks were made, 1 $g.ml^{-1}$ in Milli Q water, filter sterilised and stored in aliquots at -20 °C.

2.2.3 Reagents and buffers for the purification of NTS1-A

The detergents dodecyl-β-D-maltoside (DDM) and 3-[(3-cholamidopropyl)dimethylammonio]-1-propanesulfonate (CHAPS); and cholesteryl hemisuccinate Tris salt (CHS), stock solutions (6 % CHAPS / 1 % CHS and 10 % DDM) were made freshly prior to each purification. Complete, EDTA-free protease inhibitors (Roche) were present in all buffers used. The following buffers were used:

2x solubilization buffer: 100 mM Tris/HCL pH 7.4, 60 % glycerol, 400 mM NaCl.

NiA buffer: 50 mM Tris/HCL pH 7.4, 30 % glycerol, 200 mM NaCl, 0.6 % CHAPS / 0.1 % CHS, 0.1 % DDM.

NiB buffer: as NiA with 50 mM imidazole.

NiC buffer: as NiA with 350 mM imidazole.

NT0 buffer: 50 mM Tris/HCl pH 7.4, 30 % glycerol, 1 mM EDTA, 0.6 % CHAPS, 0.1 % CHS, 0.1 % DDM.

NT50 buffer: as NT0 with 50 mM NaCl.

NT1K buffer: as NT0 with 1 M NaCl.

2.2.4 Buffers for SDS-PAGE gels and Western blotting

2.2.4.1 X cell II invitrogen pre-poured gels

The buffers for denaturing glycine gels:

4x sample loading buffer: 25 % 1M tris-HCl, pH 6.8; 20 % glycerol; 40 % a 10 % (w:v) SDS solution; 5 % a 0.1 % solution of bromophenol blue; 10 % Milli Q water and 10x running buffer: 29 g Tris Base, 144 g glycine, 10 g SDS in a litre of Milli Q water.

4x sample loading buffer: 30 % 6 M Tris-HCl; 24 % glycerol; 8 % (w:v) SDS; 15 % a 0.1 % solution of Coomassie Blue G; 5 % a 0.1% solution of phenol red; 18 % Milli Q water and 10x running buffer: 121 g Tris base, 179 g tricine, 10 g SDS in a litre of Milli Q water.

2.3 Methods

2.3.1 Molecular Biology

2.3.1.1 Production of Competent Cells

Competent cells were prepared using the $CaCl_2$ method, a variation of that of Cohen *et al.* (1972) [56]. Briefly, a 2 ml overnight culture of the desired cell strain in LB media was used to

inoculate 50 ml of LB media in a 250 ml flask. This culture was grown, at 37 °C 200 rpm shaking, until the cells had reached an absorbance $OD_{600} \approx 0.4$ but no greater than 0.5. The culture was cooled on ice for 10 mins and then centrifuged, to harvest the cells (3000g 15 mins at 4 °C). The cell pellet was then resuspended into 20 ml of ice cold sterile 0.1 M $CaCl_2$ and incubated on ice for 20 mins before harvesting again in the above manner. The pellet from this harvest was resuspended in 4 ml of ice cold sterile 0.1 M $CaCl_2$ and incubated on ice for a further 15 mins. 1 ml of ice cold sterile < 99 % glycerol solution was added to the solution before it was separated into 50 µl aliquots, and snap frozen using liquid nitrogen before storage at -80 °C until required.

2.3.1.2 Preparation of plasmid DNA

Plasmid DNA was prepared using Qiagen mini and maxi prep kits according to the manufactures protocols.

2.3.1.3 Transformation

A 50 µl aliquot of the desired competent cells was thawed on ice, 1 µg of plasmid DNA stock was added and allowed to incubate on ice for 10 mins. After this incubation the cell solution was heat shocked (45 °C for 90 s) then placed on ice for a further 5 mins. 450 µl of pre-warmed (to 37 °C) SOC media was added to the cell solution, which was then shaken at 37 °C 200 rpm, for 1 hour. The cell solution was then plated out onto agar plates containing appropriate antibiotic at 37 °C overnight.

2.3.2 Expression and Purification methods for NTS1-A

2.3.2.1 Bacterial inner membrane preparation

Spheroplasts were prepared by the method of Witholt *et al* [57]. The pellet of harvested cells was resuspended (20 ml 2x solubilization buffer (2.2.3)) and benzonase (Sigma) (2.5 $\mu g.ml^{-1}$).

Lysozyme was added to a concentration of 0.1 $mg.ml^{-1}$ and after 45 seconds the cells were lysed by osmotic shock with ice cold deionised water, making up the total volume to 40 ml, containing protease inhibitors (Roche) for 2 hours. The membranes were isolated by ultracentrifugation (40,000 g, 1 hour, 4 °C). The resulting pellet was flash frozen in liquid nitrogen and stored at -80 °C.

2.3.2.2 Production of NT affinity column

HiTrap streptavidin HP (Amersham) was soaked then washed with 3 volumes of buffer (50 mM Tris, 150 mM NaCl pH 7.4). 1 mM of Bio-NT, produced using the methods in 2.4 (results shown in 3.2), per ml of streptavidin resin was then added to the resin and it was incubated with gentle stirring at room temperature for 1 hr. After incubation the resin was packed into a column and packed under pressure (as per the suppliers guidelines) using the buffer above and the column was then stored in 20% ethanol in Milli Q.

2.3.3 SDS-PAGE Gels

2.3.3.1 X cell II invitrogen pre-poured gels.

Pre-poured tris-glycine and tricine gels (Invitrogen) were used. Crude and purified protein samples were made by adding 15 µl of sample to 5 µl of sample loading buffer and heated for 2 minutes at 85 °C. The gel cassettes were loaded into the X cell II gel tank and immersed in 1x gel running buffer. Samples were loaded and run at a constant voltage of 120 V.

2.3.3.2 Staining gels

2.3.3.2.1 Coomassie brilliant blue

Coomassie brilliant blue R250 (0.25g) (Sigma) was dissolved in 90 ml of methanol:water (1:1 v/v) and 10 ml of glacial acetic acid and the solution was filtered through a 0.2 µm membrane.

The gel was immersed in 5 ml of this solution and placed on a rocker for a minimum of 4 hours at room temperature. The gel was destained in methanol:water (1:1 v:v) and 10 ml of glacial acetic acid for up to 24 hours.

2.3.3.2.2 Silver stain

Proteins were fixed by incubating the gels in at least 5 ml of a solution of ethanol:glacial acetic acid:water (30:10:60 v:v:v) for 4-12 hours at room temperature. The fixing solution was then discarded and the gels were washed twice in 5 ml of 30 % ethanol for 30 minutes. The gel was then washed four times in Milli Q. Following the last water wash, the gel was placed into 5 ml of 0.1 % solution of $AgNO_3$ and incubated at room temperature with gentle shaking for 30 minutes. The $AgNO_3$ solution was discarded and the gel washed under a stream of Milli Q for approximately 20 seconds on each side, after which 5 ml of a freshly prepared aqueous solution of 2.5 % $NaCO_3$, 0.02 % formaldehyde was added and the gel was incubated at room temperature with gentle agitation. When the desired level of colour was achieved the reaction was quenched by washing the gel in 1 % acetic acid for a few minutes, after which the gel was washed (4 x 10 mins Milli Q) before flatbed scanning to obtain a digital image.

2.3.4 Western Blotting

Tris-glycine gels were run as in 2.3.3.1, and equilibrated in transfer buffer (25 mM Tris, 192 mM glycine, 20 % methanol, pH 8.3) for 15 minutes prior to blotting with Bio-Rad semi-dry blotting apparatus. An extra thick filter paper pad, which had been presoaked in transfer buffer, was placed onto the anode of the transfer apparatus. A nitrocellulose membrane (Amersham Biosciences), presoaked in transfer buffer, was placed onto the top of the pad and the soaked gel was placed on top of the membrane. A second presoaked pad of extra thick filter paper was then placed on top of the gel. The cathode was then placed on top of the transfer sandwich and pushed down until the catches engaged. The current was then set to 5.5

$mA.cm^{-3}$ of gel being transferred until the molecular weight markers are visible on the membrane.

The nitrocellulose membrane, prepared above, was placed in 10 ml of the appropriate blocking solution (0.5 % Hammersten casein in PBS pH 7.0, 0.4 % Tween 20) in a square Petri dish and incubated for 30 minutes on a rotary shaker set at 1 $revolution.sec^{-1}$. The blocking solution was then decanted off and the membrane was washed twice (20 ml of milli Q water, 5 mins). The membrane was then incubated with 10 ml of primary antibody solution (blocking solution (WesternBreeze, Invitrogen) with a 1:3000 dilution of antibody added) for 1 hour, then decanted and washed (4x for 5 minutes with 20 ml of a solution of PBS pH 7.0, 0.4 % Tween 20). The membrane was then incubated in 10 ml of secondary antibody solution (WesternBreese kit, Invitrogen) for 30 minutes, before being washed 4x for 5 minutes with 20 ml of a solution of PBS pH 7.0, 0.4 % Tween 20. The membrane was then washed three times with 20 ml of water for 2 minutes. The membrane was then placed on a sheet of overhead-projector transparency plastic (without allowing the membrane to dry out) and 2.5 ml of the chemiluminescent substrate (Invitrogen) with enhancer was applied evenly to the membrane surface. The reaction was allowed to develop (5 min) before the excess chemiluminescent substrate solution (Invitrogen) was blotted from the membrane surface with the filter paper. The membrane was covered with another clean piece of transparency plastic prior to exposure to X-ray film (Kodak X-OMAT AR film) to the membrane sandwich for between 1 second and several minutes.

2.3.5 Protein Assay

2.3.5.1 Introduction

The high concentrations of detergent used to maintain soluble, active NTS1-A causes problems with protein determination, such that even commercially available detergent

compatible protein assays are adversely affected. To overcome this problem and achieve effective protein determination a reducing agent compatible assay (Reductant Compatible Detergent Compatible (RC DC) assay from Biorad) was used. This protocol starts with a protein precipitation step and buffer exchange before addition of a modified Lowry assay. Using this method and standards made up in the same detergent buffers and treated in the same manner it is possible to get reproducible quantification of the protein content of samples.

2.3.5.2 Methods

Samples were all tested in triplicate, all solution were obtained using the Biorad RC DC assay kit. A range of 25 μl aliquots of BSA standards and unknowns were diluted in 125 μl of RC reagent I, vortexed and incubated at room temperature for 1 minute. After incubation, RC reagent II (125 μl) was added, the sample was vortexed and centrifuged (15000 g for 5 min). The supernatant was discarded and the tubes left to drain thoroughly.

Reagent A' was produced by adding reagent S (5 μl) to reagent A (250 μl). After the microfuge tubes were completely drained, reagent A' (127 μl) was added to each and the tubes were then incubated (5 min) at room temperature or until all the precipitate was completely dissolved. When all the precipitate had gone into solution reagent B (1 ml) was added to the tubes before vortexing again. This solution was then incubated for a further 15 minutes at room temperature. After this final incubation, the absorbance of the solutions in each tube was measured at 750 nm within a one hour window during which the colour that has developed is stable.

2.3.6 Binding assay of NT binding to NTS1-A

Stock solutions of H^3-NT (New England Nuclear), $3.7x10^6$ Bq/nmol, radio active peptide in NT50 buffer (2.2.3) was doped such that it was 20% of the total NT in solution giving a specific activity of $7.4x10^5$ Bq/nmol.

All binding assays were done in triplicate and at 4 °C unless otherwise stated. The test NTS1 sample was diluted one in ten in NT50 Buffer to produce a total volume of 100 µl, which was then split into two eppendorfs 50:50. To each these 10 µl of the doped H^3-NT solution was added, and to one of these 2 µl of 0.2nM unlabelled NT solution was added, and then the solution was incubated on ice for 1 hour. During this time two Ni-NTA affinity spin columns were equilibrated in 600 µl of NT50 buffer, the buffer was added onto the top of the columns and they are then centrifuged at 700 g for 2 minutes. After incubation the samples were added to the spin columns and centrifuged at 700 g for 2 minutes collecting the flow through in an eppendorf, and then the columns were washed with 700 µl NT50. 200 µl of the flow through was then added to 3ml of scintillant, the bottles were then placed into a scintillation counter; the average scintillations per minute (cpm) were measured over five minutes.

2.4 Reconstitution of NTS1-A into model membranes

2.4.1 Preparation of brain polar lipids (BPL) liposomes

A lipid film was formed by dissolving 4mg/ml brain polar lipids (BPLs) in chloroform/methanol (50:50% v:v). The solvent was evaporated off under a stream of nitrogen and placed under vacuum overnight. The resultant film was then resuspended in aqueous buffer (50 mM Tris, 50 mM NaCl, pH 7.4) by vortexing, sonication (3 mins in a sonication bath) and freeze thawing (20 times using liquid nitrogen, thawing under a cold tap), to a final concentration of 4 mg/ml.

The solution was then freeze thawed ten times to remove any small lipid structure induced by sonication before extrusion 20x through a 400nm polycarbonate filter to form unilamellar liposomes of homogenous size of 400nm diameter.

2.4.2 BPLs liposome detergent titrations

Liposomes were then titrated with detergents, DDM and CHAPS the major detergent components of the lysis buffer, in 0.5 mM steps. Aliquots with a range of increasing detergent concentration (0-10 mM) were then left over night at 4°C before their absorbance at 540nm was measured to observe their turbidic state.

2.4.3 Reconstitution of NTS1-A into destabilised lipid vesicles meditated by Bio Beads

Unilamellar lipid vesicles were generated as in 2.4.1, and incubated (overnight at 4 °C) with 4 mM DDM to destabilize them. Detergent solubilized receptor and doped lipid vesicles were then combined to the desired lipid:protein ratio and allowed to incubate at 4 °C for two hours with mild shaking. During this incubation period, 320 mg of Bio-beads per ml of protein-lipid mixture above, were treated with an equal volume of 0.4 mg BPL as used in the reconstitution, at 4°C with mild shaking, to saturate the lipid binding sites on the Bio-beads, and then washed once with buffer (50 mM Tris, 50 mM NaCl, pH 7.4). Pre-saturated Bio-beads (80 $mg.ml^{-1}$) were then added to the incubated protein-lipid solution and this mixture was shaken (4 °C for 4 hrs). After incubation the Bio-beads were allowed to settle down and the liposome solution was removed, added to 80 $mg.ml^{-1}$ of fresh pre-saturated Bio-Beads and incubated (2 hrs, 4 °C) with mild shaking. This exchanging of Bio-Beads was repeated twice, with the last addition incubated overnight at 4 °C with mild shaking. The Bio-beads were allowed to settle and the proteoliposomes solution was filtered off and harvested by centrifugation at 60000 g. The resulting pellet from the centrifugation was then resuspended into buffer (50 mM Tris, 50 mM NaCl, pH 7.4) and a fraction of this was then loaded onto a SDS-PAGE gel for Western blot analysis using an anti-His-tag antibody to determine whether the NTS1-A constructs were associated with the pelleted material (Figure 3.18).

2.5 Peptide synthesis

2.5.1 Introduction

The amide bond, formed by the condensation of an α-amine group of one amino acid with the α-carboxyl group of another, is the crucial linkage in any polypeptide chain. Chemical construction of peptides on an insoluble solid support, Solid Phase Peptide Synthesis (SPPS), has obvious benefits: separation of intermediate peptides from the soluble reagents and solvents used during synthesis is a simple case of filtration and washing the beads; many of the operations in chain extension on the solid support are amenable to automation; excess reagent can be employed to help drive the reactions to completion and the physical losses can be minimized as the peptide remains attached to the support throughout the synthesis. SPPS does, however, have its attendant limitations; by-products arising from incomplete reactions, side chain reactions, or impure reagents will accumulate on the resin during chain assembly and may contaminate the final product.

In general in solid phase peptide synthesis (SPPS) the C-terminal amino acid residue of the target peptide is attached to an insoluble support via its carboxyl group. Any functional groups in amino acid side chains must be masked with *permanent* protecting groups that are not affected by the reactions conditions implied during peptide assembly. The *temporary* protecting group masking the α-amino group during the initial resin loading is removed. An excess of the second amino acid is introduced, with the carboxy group of this amino acid being activated for amide bond formation through generation of an activated ester or by reaction with a coupling reagent. After coupling, excess reagents are removed by washing and the protecting group removed from the N-terminus of the dipeptide, prior to the addition of the third amino acid residue. This process is repeated until the desired peptide sequence is assembled. In a final step, the peptide is released from the support and the side-chain protection removed.

The general scheme which outlines the strategy of 9-fluorenylmethyloxycarbonyl (Fmoc) amino acid SPPS is shown in Figure 2.1.

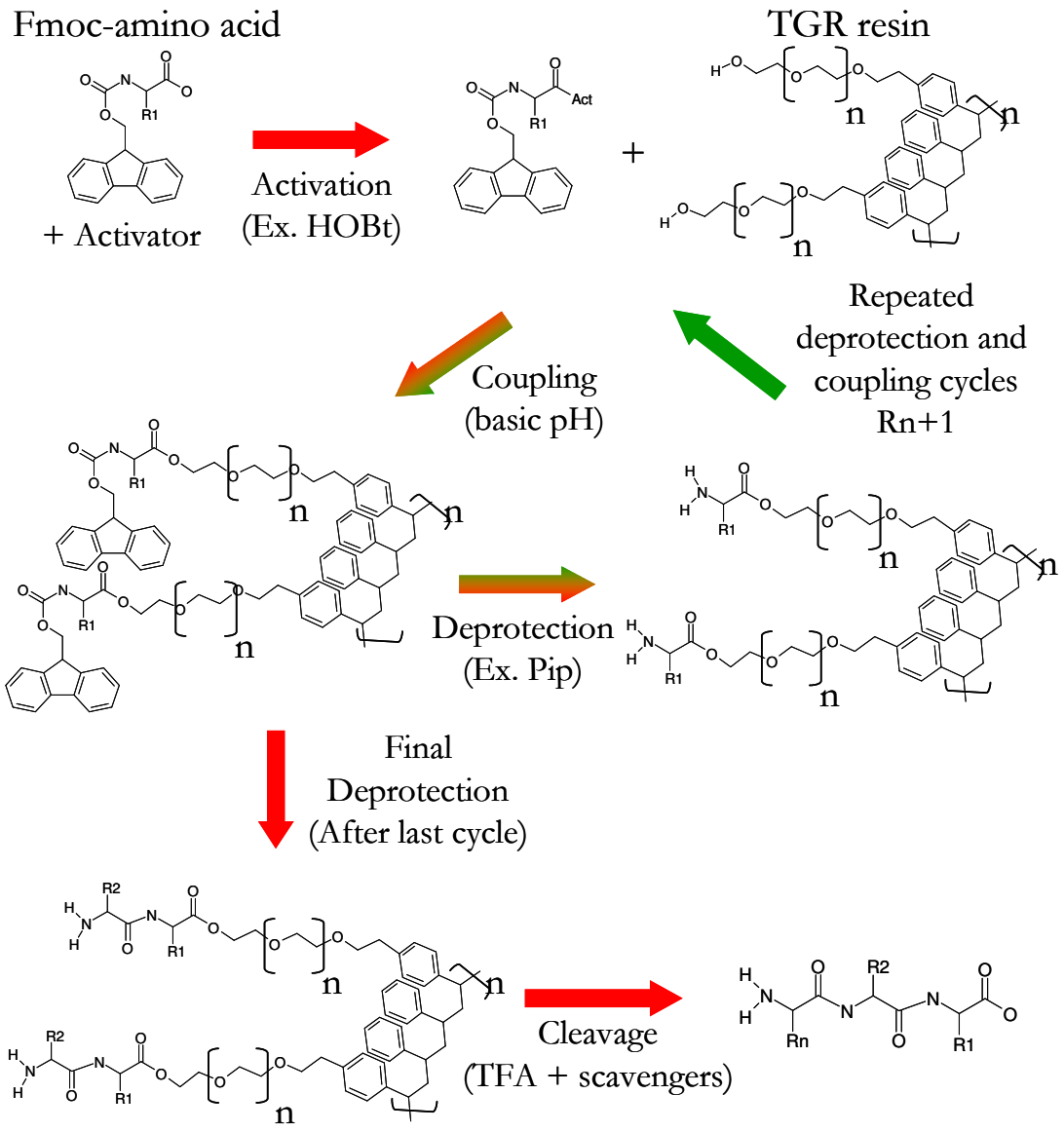

Figure 2.1 – General scheme for Fmoc synthesis of polypeptides, with red arrows representing single reactions and green arrows cycling of reaction stages. Initially, the first Fmoc amino acid is attached to an insoluble support resin via an acid labile linker. Deprotection of the Fmoc, is accomplished by treatment of the resin with a base, usually piperidine. The second Fmoc amino acid is coupled utilizing a pre-activated species or *in situ* activation. These steps are cycled until the desired peptide has been synthesized, the resin bound peptide is deprotected and detached from the solid support via TFA cleavage in the presence of chemical scavengers to neutralise the reactive leaving groups generated from the removal of side chain protection.

2.5.2 Methodology

2.5.2.1 Fmoc protection of amino acids

An L-amino-acid (Sigma) (5 mmol) and solid Na_2CO_3 (5 mmol) were added to 15 ml of ice-cold water in a round-bottomed flask with stirring. A solution of Fmoc (CM biosciences) reagent (5 mmol) in acetone (15 ml) was then added to the flask and the pH adjusted with 0.1 M NaOH to be 9-10. The solution was left to stir overnight at 0 °C. After this time, the mixture was then allowed to warm up to RT and was acidified to pH 2 with concentrated HCl. The acetone was removed under vacuum and the product extracted in chloroform. The product was washed in 0.1 M HCl and then in H_2O. The organic phase, from the chloroform extraction and washes, was then dried under vacuum and the final Fmoc product crystallised in a minimum amount of hot ethylacetate (~60 °C). Warm petroleum ether (40-60 °C), an equal quantity to the amount of ethylacetate, was then added and the product was allowed to precipitate at 4 °C. The pure Fmoc amino acid was then collected by filtration through a fine glass sinter. The product was purified by recrystalisation and purity verified by ESI positive mass spectrometry.

2.5.2.2 Solid-phase synthesis of peptides

Syntheses were carried out both by hand in fume-hood and also on a Pioneer peptide synthesizer (PerSeptive Biosystems). The reagents used for both methods were the same, the decision to use one method or the other comes from the complexity of the peptide required and the presence or absence of labels.

Novasyn TGR resin (Novabiochem) was used for the synthesis of NT, NT derivatives and NT_{8-13} (loading of 0.29 $mmol.g^{-1}$ resin (the stoiciometric amount of peptide that can be synthesized per gram of resin)). Resin was swelled in excess dichloromethane (DCM) for 30

minutes, washed with 10 ml dimethylformamide (DMF) and swelled for a further 30 minutes in excess DMF.

All coupling reagents and Fmoc-protected amino acids were supplied by CN Biosciences. Coupling was carried out using a three times excess of the coupling reagents N-Hydroxybenzotriazole (HOBt) and 2-(H-Benzotriazole-1-yl)-1,1,3,3-tetramethyluronium hexafluorophosphate (HBTU) and a four times excess of Fmoc-protected amino acids. Coupling reagents and amino acid were dissolved in a minimal amount of DMF and 200 µl diisopropylethylamine (DIPEA) added to start the reaction. This was left for 2 minutes before the addition to the resin. The coupling reaction mixture was agitated for 45 minutes, drained, washed with DMF and tested with ninhydrin for the presence of primary amine groups. If a positive result was obtained, further coupling was carried out as shown in Figure 2.1.

Fmoc deprotection was carried out using 5 ml 20% piperidine in DMF and agitating for 30 minutes. A positive ninhydrin test result indicated deprotection had been successfully carried out.

The resin was washed with DCM and methanol in order to collapse the beads, followed by a diethyl ether wash. The resin was then dried for 24 hours in a dessicator under vacuum. Cleavage was achieved using 5ml of the solution trifluoroacetic acid (TFA) (95 %), triethylsilane (TES) (2.5 %) and water (2.5 %) by agitating for 2-3 hours at room temperature. The resultant liquid was drained off under vacuum and the resin washed 3 times with TFA. Excess TFA was then evaporated off under a stream of nitrogen until around 1 ml remained. 5-10 ml of ice cold diethyl ether was added followed by centrifugation at 3000 g 4 ^{o}C for 15 minutes. The ether extraction process was then repeated on the peptide pellet and the resulting pellet suspended in minimal water and lyophilised until dry.

The lyophilised peptide cleavage product was taken up into Milli Q water to produce a concentration of 5-10 $mg.ml^{-1}$, for purification using reverse phase HPLC with acidified Milli Q water and acetonitrile regime using a C18 column.

2.5.2.3 Ninhydrin test for primary and secondary amines

A small number of resin beads were removed from the reaction mixture and gently dried on a hot plate, before being sprayed liberally with ninhydrin solution (0.5 % ninhydrin in butan-1-ol) and heated again on a hotplate; solution and beads turn purple in the presence of primary or secondary amide groups.

2.5.2.4 Solid-phase synthesis of biotinylated peptide

After synthesis, as per the method set out above (2.5.2.1), leaving the Fmoc on the last amino acid, the resin was then transferred from the synthesizer and deprotected in the fume hood before coupling the biotinylation reagent (Biotin OSu, Novabiochem) with 5x excess HOBt and HBTU, this reaction was then monitored using ninhydrin until completion, as it is more sluggish than a standard amino acid coupling step.

2.5.2.5 Reverse-phase purification of NT and its derivative peptides

All the peptides synthesized here were purified using Kromasil 100-5C18 reverse phase high pressure liquid chromatography (HPLC) columns (HiCHROM) with (filtered and degassed) milli Q water with 0.1 % TFA and (filtered and degassed) acetonitrile with 0.1 % TFA gradient.

2.6 Surface Plasmon Resonance (SPR)

2.6.1 Immobilisation of ligand to sensor surfaces

2.6.1.1 Biotin coupling to sensor chip SA (BiaCore)

The flow cells were conditioned with three consecutive one minute injections of 1 M NaCl in 50 mM NaOH before Biotinylated ligand was injected in HBS-EP until the desired number of response units (RU) had been immobilised.

2.6.1.2 Thiol coupling to sensor chips C1 and CM4

A 1:1 (v:v) solution of 0.4 M 1-Ethyl-3-(3-dimethylaminopropyl) carbodiimide hydrochloride (EDC) and 0.1 M N-Hydroxysuccinimide (NHS) was injected into the flow cell at 10 $\mu l.min^{-1}$ for a contact time of 2 mins. A, freshly prepared, solution of 80 mM 2-(2-Pyridinyldithio)ethaneamine hydrochloride (PDEA) in a 50 mM $Na_2B_4O_7$ buffer pH 8.5 was then injected in the same manner for a contact time of 4 mins. Thiol ligand was then injected for a contact time of 7 mins and/or the desired number of RU had been immobilised after which the remaining reactive sites were blocked by a 4 min injection of a 50 mM cysteine solution.

2.7 Electron Spin Resonance

2.7.1 Spin labelling cystinylated peptides

The reaction between methanethiosulphonate spin label derivatives and protein/peptide sulphur hydride groups is spontaneous. Five times excess of spin label regent was added to Cys-NT in a solution of 20 % ethanol in Milli Q water pH 7.0 and incubated at room temperature for 2 hours. The labelled peptide was then separated from the excess free spin label by use of a 5 mm by 150 mm G10 resin (Amersham) size exclusion column on an AKTA flow pressure liquid chromatography (FPLC).

2.7.2 Preparation of samples for ESR

Spin labelled peptide was incubated with each sample at 4 ˚C for one hour with mild agitation. 20 µl was then placed into a 3 cm long blind ended 0.84 mm quartz capillary tube which was then sealed with a plug of parafilm. Samples were then placed into a 4 mm width NMR tube to hold them within the ESR machine's cavity.

2.7.3 ESR measurements

ESR measurements were made with a Bruker ESP-300 spectrometer operating at 9 GHz (X-band) equipped with a nitrogen gas-flow temperature regulation system. Sample capillaries, prepared as stated above in 2.7.2, were accommodated within standard 4-mm quartz ESR tubes in the standard TE_{102} microwave cavity. All spectra were acquired using 10 mW incident microwave power and ca. 1 G field modulation amplitude at 100 kHz. Temperatures were measured with a thermocouple placed just below the cavity within the quartz tube to within ± 0.5 °C. Spectra were processed and analysed using Origin, with a baseline subtraction and normalisation of intensity.

2.8 NMR

2.8.1 One pulse with decoupling

A one pulse NMR experiment was performed in the liquid phase, therefore magic angle spinning (MAS) was not required since anisotropic interactions were averaged due to rapid thermal motion. The pulse sequence is shown in Figure 2.2.

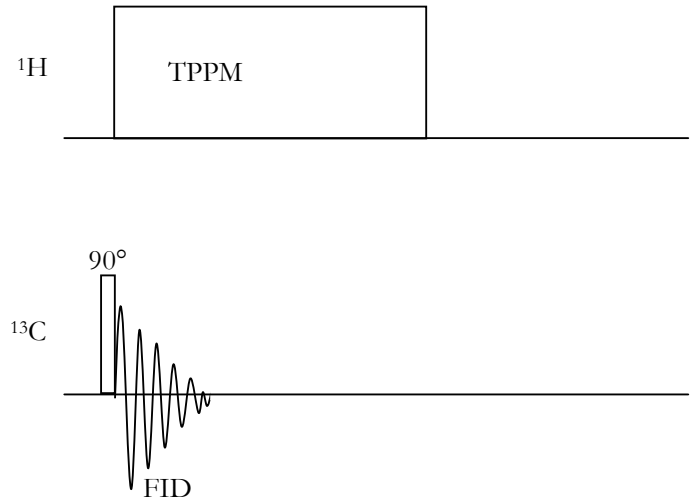

Figure 2.2 - Pulse sequence for ^{13}C one pulse experiment with TPPM proton decoupling during acquisition.

2.8.2 Cross Polarisation Magic Angle Spinning (CP MAS)

The pulse sequence for a CP MAS experiment is shown in Figure 2.3 [58].

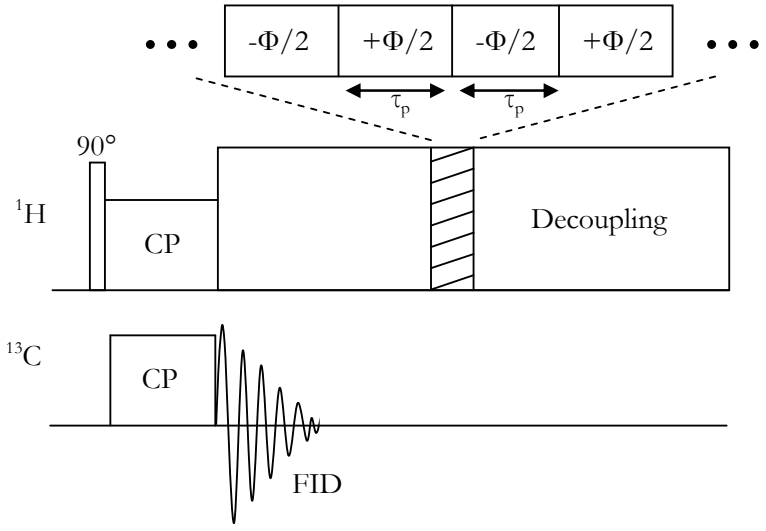

Figure 2.3 - Pulse sequence for CP MAS experiment with the addition of phase modulated TPPM decoupling period is expanded in order to illustrate the rapid alternation of the phase of the rf excitation between two values $-\Phi/2$ and $+\Phi/2$ with overall period $2\tau_p$, which is carried out throughout the acquisition of the FID.

The large heteronuclear dipolar couplings inherent in solid state NMR can lead to insufficient averaging by MAS, and result in residual proton dipolar couplings that will broaden the resonances in the spectrum. Strong couplings of protons in solid-state samples necessitate proton decoupling in most experiments. Proton decoupling field strengths of 10-100 kHz are therefore commonly used to eliminate large dipolar couplings. A simple two pulse phase modulation (TPPM) scheme greatly reduces the residual line widths arising from insufficient proton decoupling power in double resonance MAS experiments.

2.8.3 R14$^5_4$ two dimensional ^{13}C Carbon-Carbon Correlation Experiment

A 2D MAS ^{13}C-^{13}C correlation experiment, pulse sequence shown in Figure 2.4, allows the assignment of individual resonances in the labelled peptide and couplings between neighbours allows structure and positions of labels to be confirmed. The pulse sequence for a single quantum-single quantum correlation experiment is shown in Figure 2.4.

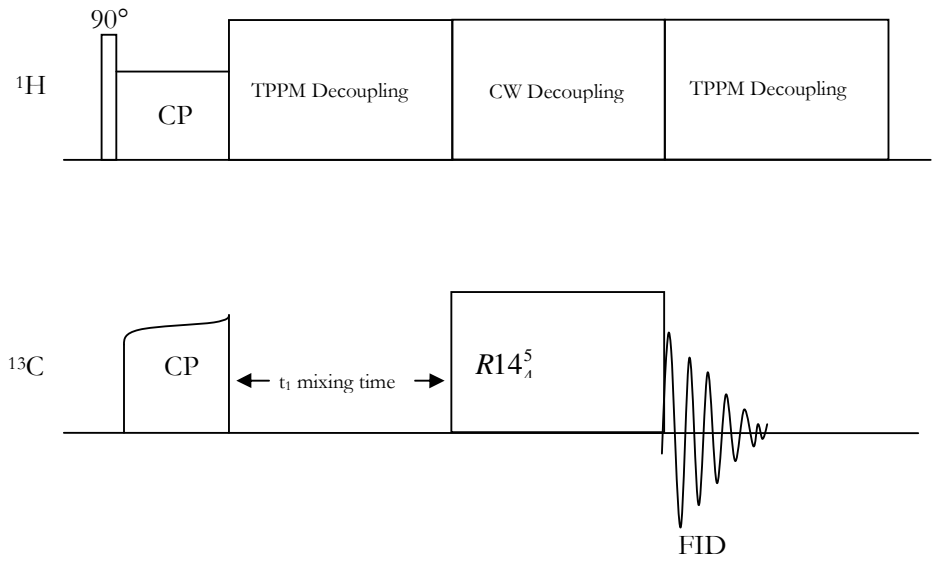

Figure 2.4 - 2D ^{13}C-^{13}C Correlation $R14^5_4$ Pulse Sequence. A $\pi/2$ pulse is applied to the ^{1}H Channel, followed by cross polarisation to the ^{13}C channel by utilising the APHH technique [59]. This is followed by a t_1 mixing period, during which no rf is applied on the ^{13}C channel, while TPPM decoupling [60] is applied on the ^{1}H channel. An $R14^5_4$ symmetry-based recoupling pulse sequence [61, 62] is then applied on the ^{13}C channel, along with CW decoupling on the ^{1}H channel.

The recoupling pulse sequence is required due to the nature of the MAS experiment itself [63]. As mentioned before, MAS is used to improve sensitivity and resolution by employing mechanical rotation to eliminate dipole-dipole couplings and other second-rank anisotropic interactions. In order to measure the attenuated dipolar couplings, they must be reintroduced into MAS experiments with rotor-driven or rf-driven recoupling techniques [64].

The $R14_4^5$ pulse sequence is a method of rf-driven recoupling. It consists of 14 separate π pulses (experimentally actually a $-\pi/2$, $3/2\pi$ composite pulse), with alternating phase, occurring in exactly 4 rotor periods ($4\tau_r$). The FID (t_2) can then be measured in the presence of TPPM decoupling. A slight alteration to the above experiment results in a double quantum-single quantum correlation, the pulse sequence of which is shown in Figure 2.4.

Passing signals through double-quantum coherences allows the suppression of signals from isolated spins-1/2, pulse sequence shown in Figure 2.5.

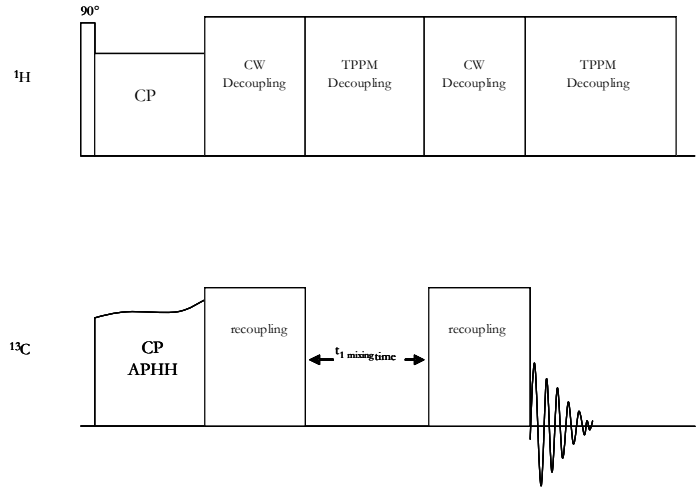

Figure 2.5 - Pulse sequence for an $R14^5_4$ double quantum-single quantum ^{13}C correlation. It is similar to the single-quantum-single quantum pulse sequence except it contains two $R14^5_4$ sequences, each half as long as in the single quantum-single quantum experiment. The first $R14^5_4$ sequence introduces double quantum coherence, whilst the second refocuses back to single quantum for measurement as an FID.

This is particularly useful when spectra of NT_{8-13} bound to the receptor are observed since the double quantum filters out background signals from naturally-occurring isolated ^{13}C nuclei in the receptor itself.

2.9 DNA arrays

2.9.1 Preparation of DNA arrays

Mixtures of NT-bound and unmodified oligonucleotides were prepared in Tris/HCl buffer (pH 8), 13 mM $MgCl_2$ at a concentration of 3.1 μM per oligonucleotides. Using a PCR thermocycler, this mixture was heated to 70 °C, the temperature was then lowered to 10 °C over the course of 5 days; at 30 °C, concentrated DDM was added to a final concentration of 0.1% (w/v); at 20 °C, when protein bound arrays were produced, NTS1-A was added to a final concentration of ~0.2 μM.

2.9.2 Spectrophotometric analysis of array annealing

Mixtures of oligonucleotides (3.3 μM per nucleotide of each in 10 mM Tris-HCl, 10 mM $MgCl_2$ (pH=8), to a total volume 650 μl) were cooled from 90 °C to 10 °C and then heated back up to 90 °C. In both cases the rate of temperature change was ± 0.1 °.min^{-1}. The absorbance was measured at 260nm against of buffer blank.

2.9.3 Electron microscopy and image processing

Specimens were absorbed onto 400-mesh carbon-coated, glow-discharge copper grids. A drop of the sample was placed onto the carbon-coated grid on a flat surface with the support film facing upwards and allowed to absorb for 30 mins. After absorption the sample is removed with a pipette and the grid is washed with Milli Q water before it is stained at 4 °C with 2% uranyl acetate pH 4.4 for 10 secs [65]. Electron micrographs were recorded on Kodak SO163 film under low dose conditions using a Philips CM120 electron microscope at 100-kV

acceleration. The nominal defocus range was between 400 and 700 nm, the nominal magnification was 45000×.

Electron micrographs were scanned with a UMAX Powerlook 3000 scanner at a sampling raster of 8.33 μm corresponding to a pixel size of 1.9Å. Image processing was carried out using the MRC program package [66] as well as the CCP4 package [67].

Chapter 3 Expression, Purification and Reconstitution of the G-Protein Coupled Receptor (GPCR) NTS1

3.1 Introduction

3.1.1 Expression of GPCRs

The over-expression of membrane proteins has proved extremely difficult, with relatively few expression systems able to produce sufficient quantities of materials for biophysical studies [68]. The low natural abundance of most GPCRs, an exception being rhodopsin in the retina, precludes the use of such methods of investigation. To date the most successfully overexpressed GPCR has been rhodopsin, with systems established in a baculovirus/Sf 9 cell expression system and stably in HEK293S cells [69], for solid state NMR [70] and electron spin resonance [71] experimentation. Though yielding sufficient quantities of protein for studies including crystallisation no crystal structure has been obtained from any recombinant eukaryotic membrane protein.

E. coli is an attractive organism for an expression system as it is easy to scale-up and cheap to grow and has the potential for labelling, but there are drawbacks associated with the prokaryotic nature of the organism for expressing eukaryotic proteins. For example, the low

percentage of GC nucleotides in the genome when compared to mammalian genes or the existence of rare codons often result, at least for soluble proteins, in low expression levels or truncated forms [72, 73]. Heterologuous expression in bacteria also suffers from the inability of prokaryotes to perform any post translational modifications (e.g. glycosylation, fatty acid acylation, phosphorylation) some of which are known to be critical for protein function. Also the lack of GPCRs in bacteria affects the properties of the expressed GPCRs, though successful interaction with a Gα subunit (in fusions or added to the membrane-bound receptor) has been demonstrated in *E. coli* [74].

In spite of many efforts invested in the design of fusion proteins and/or selection and engineering of bacterial strains, GPCR expression levels at the inner membrane are still poor (most often less than 200 receptors/cell), and receptor production is often found to be toxic to the cell. However, in the best cases, up to 3500 copies per cell of functional muscarinic m_1 receptor (0.66 $mg.l^{-1}$ culture) have been produced in *E. coli*, allowing for the purification of milligrams of receptor [75]. Folding of some heterologuous membrane proteins may be hindered by the lack of appropriate chaperones leading to accumulation of misfolded proteins in the cytoplasm and formation of inclusion-bodies.

3.1.2 Expression of NTS1

The expression system and subsequent purification strategy for NTS1 has been elucidated by Grisshammer and has been developed to overcome a lot of the inherent difficulties in expressing membrane proteins in general, and in particular in a heterologuous system such as *E. coli*. The vector is derived originally from the vector pBR322 with the protein expression being under the control of a wild type *lac* promoter and with plasmid loss prevented using the *hok*/*sok* plasmid maintenance system. The choice of this promoter and plasmid for expression of NTS1 leads to something short of the classical ideas of overexpression, due to the low copy

number of the plasmid [76] and the relatively weak nature of the wild type *lac* promoter [77]. Stronger promoters are available, such as the cut down version of *lac* itself *tac* however, these promoters appear to offer little advantage for the expression of membrane proteins as the rate determining step is not that of transcription and translation, during the production of the polypeptide chain, but rather the insertion and folding of that chain into the membrane [77]. Systems in which the membrane targeting and insertion machinery are co-expressed with the protein of interest have met with only limited success [77], and in the absence of these processing systems the build-up of unprocessed polypeptides has been shown to be toxic to the cell and can lead to reduced growth rates and the exportation of the plasmid [77]. Stringency is another concern when expressing these proteins, especially as in the case where cell base is generated in standard growth conditions before a reduction in temperature on induction. Strong promoters such as T7 are leaky and allow a basal level of expression detectable before induction which can produce a toxic build up of translation products and concurrent loss of expression levels after induction [77].

The rat NTS-1 receptor has been expressed in *E.coli* as a fusion protein (termed NTS1-A) (Figure 3.1) from the pRG/III-hs-MBPP-T43NTR-TrxA-H10 plasmid. The plasmid expresses a hybrid protein composed of a truncated rNTS1, to remove the N-terminal sites of glycosylation, with a maltose binding protein attached to the N-terminus, together with its periplasmic targeting sequence. Thyrodoxin and a deca-His tag, which aid stability and purification, are attached to the C-terminus. Functional expression of NTS1-A is highest (800 receptors.cell^{-1}) when thyrodoxin is placed between the receptor and the affinity tag, indicating the stabilizing effect of the thyrodoxin moiety [68].

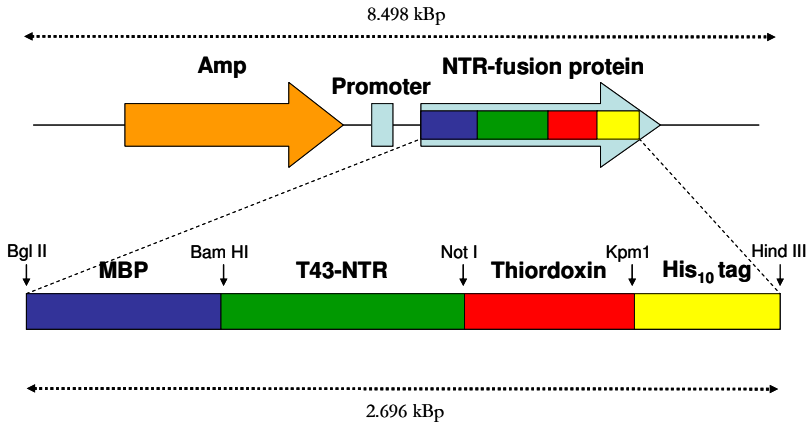

Figure 3.1 - Schematic diagram representing the fusions used to express functional NTS1

3.1.3 Aims of this chapter

Here the production, quantification and reconstitution of active NTS1-A in quantities sufficient for use in the biophysical studies in later chapters of this thesis, will be described.

3.2 Synthesis of Biotinylated NT (Bio-NT)

Biotinylated NT Bio-NT (pBiotin-Glu-Leu-Tyr-Glu-Asn-Lys-Pro-Arg-Arg-Pro-Try-Ile-Leu-OH), the full length NTS1 ligand with a biotin moiety on the N-terminus well away from the 8-13 region which is the site required for ligand binding and activity, was produced. This peptide was created to facilitate the use of streptavidin resins in the purification of the receptor and also in avidin derivised SPR chips (Chapter 4). The synthesis of this peptide was carried out in a peptide synthesizer for the NT section instructing the synthesizer to leave the last Fmoc on the peptide, as per the method set out in 2.5.2.4. This synthesis was carried out at the 0.2 mM scale giving it a theoretical maximum yield of 0.383 g. The lyophilised cleavage product was then purified using HPLC using the method in 2.5.2.5, Figure 3.2.

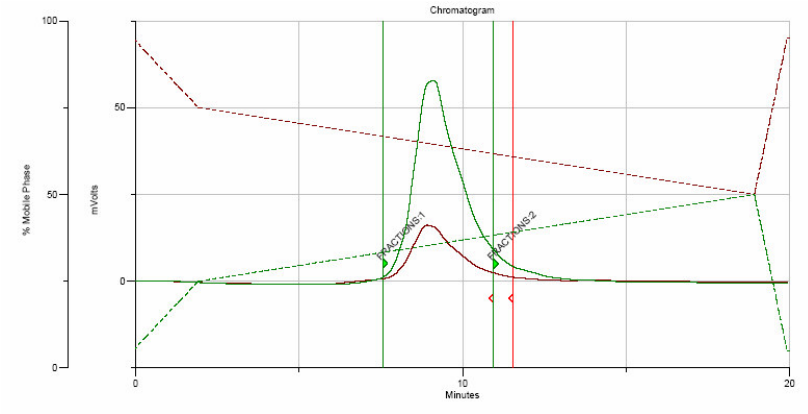

Figure 3.2 – Reverse phase HPLC trace of the lyophilised products from the solid phase synthesis of Bio-NT. With the absorption at 254 nm as a solid green line and the absorption at 280 nm as a solid red line and the percentages of H_2O and acetonitrile in dashed red and green lines respectively.

The HPLC trace shows that the cleavage product from the synthesis is very pure as would be expected from a solid phase synthesis of a simple peptide. The large peak in this trace has been separated into two fractions by the collector; this is due to overloading the column which causes broadening of the base (footing) of the peak. Analysis of the fraction by mass spectrometry of this peak shows that it is indeed Bio-NT; Figure 3.3 shows an electro-spray mass spectrum of the dominant peak from the HPLC trace above.

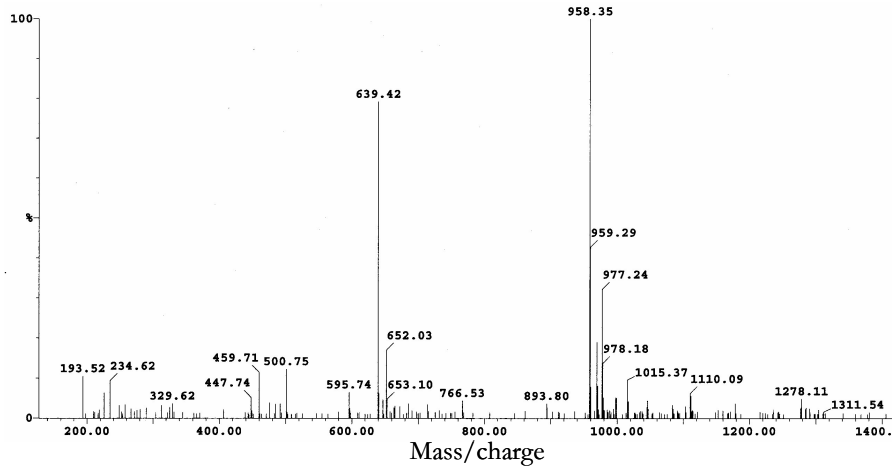

Figure 3.3 – Electro spray ionisation mass spectrum of the dominant peak in the HPLC purification of solid phase synthesised Bio-NT.

The mass spectrum shows two main peaks at 958.35 corresponding to the doubly charged ion and 639.42 corresponding to the triply charged peptide species, confirming that this HPLC fraction is pure Bio-NT with a molecular mass of 1917 Da. A typical yield from these syntheses was 0.362 g, a final yield of 95 % of the theoretical maximum.

3.3 Expression of NTS1-A in *E. coli* DH5α in shaker flasks

3.3.1 Transformation

1 µl of 1 $\mu g.\mu l^{-1}$ pNTS1-A DNA vector was added to DH5α cells in the transformation method set out in 2.3.1.3.

3.3.2 Growth

Double-strength TY broth was prepared as described in 2.2.1.4. 10 ml 2x TY overnight cultures were prepared containing ampicillin (100 $\mu g.ml^{-1}$) and 0.2 % (w:v) glucose and inoculated with bacterial colonies from freshly transformed plates of pNTS1-A in DH5α. Ampicillin (100 $\mu g.ml^{-1}$) and glucose (0.2 % w:v) were added to the conical flasks containing sterilized TY and inoculated with 1ml of overnight culture. The culture was incubated at 37 °C until the cells reached an OD_{600} of around 0.6 (using a 2x TY blank). Expression was induced by adding isopropyl β-D-1-thiogalactopyranoside (IPTG) to a final concentration of 0.5 mM and reducing the temperature to 20 °C for 40 hours. The cells were harvested by centrifugation at 3000 g for 15 mins, frozen in liquid nitrogen and stored at -80 °C.

3.3.3 Purification of NTS1-A Fusion Protein from flask scale growths

All steps were carried out at 4 °C or on ice, and all buffers used can be found in 2.2.3. Membranes containing NTS1-A, prepared using the method in 2.3.2.1, were solubilised in buffer NiA at a concentration of 5 mg of crude membrane per ml of buffer. The mixture was homogenised with a hand held glass homogeniser, sonicated to disrupt the cells (10 sec

sonication 20 sec resting on ice for 2 mins), gently stirred for 30 minutes, and then centrifuged at 100,000 g for 1 hour at 4 °C to clarify the solution. The supernatant was loaded onto a 5 ml Nickel affinity column (Ni-NTA Superflow (Qiagen) resin) in buffer NiA 2 $ml.min^{-1}$ using an AKTA prime FPLC (Amersham). The column was washed with four column volumes of buffer NiB followed by elution of receptor using buffer NiC. The eluate was then diluted with NT0 to reduce the imidazole concentration from 350 mM to <70 mM and the NaCl concentration from 150 mM to <50 mM, this Ni-NTA eluate was then concentrated using YM30 membranes (Amicon) in a stirred cell, to reduce the volume from 15 ml to 5 ml before loading the sample onto an NT column (produced using the method set out in 2.3.2.2).

5 ml of Ni-NTA eluate, obtained above, was then loaded onto a 1 ml NT column (biotinylated NT, produced following the protocol in 2.4, bound to tetrameric avidin resin) at a flow rate of 1 ml/min. The column is then washed with four column volumes of NT50 buffer followed by elution of the receptor off the NT column with NT1K buffer. The NT-column eluate is then immediately diluted with NT0 to reduce the concentration of NaCl to 50mM and again concentrated as above with the Ni-NTA eluate. Fractions were collected at every stage of preparation and purification for gel analysis.

3.3.4 Results from expression of NTS1-A in *E.coli* DH5α in shaker flasks

The coomassie stained gels (for methods see 2.3.3) of the NTS1-A purification are shown below (Figure 3.4); samples were concentrated using YM30 centricons (Eppendorf) before loading so that the purification profile could be observed on this scale of cell growth.

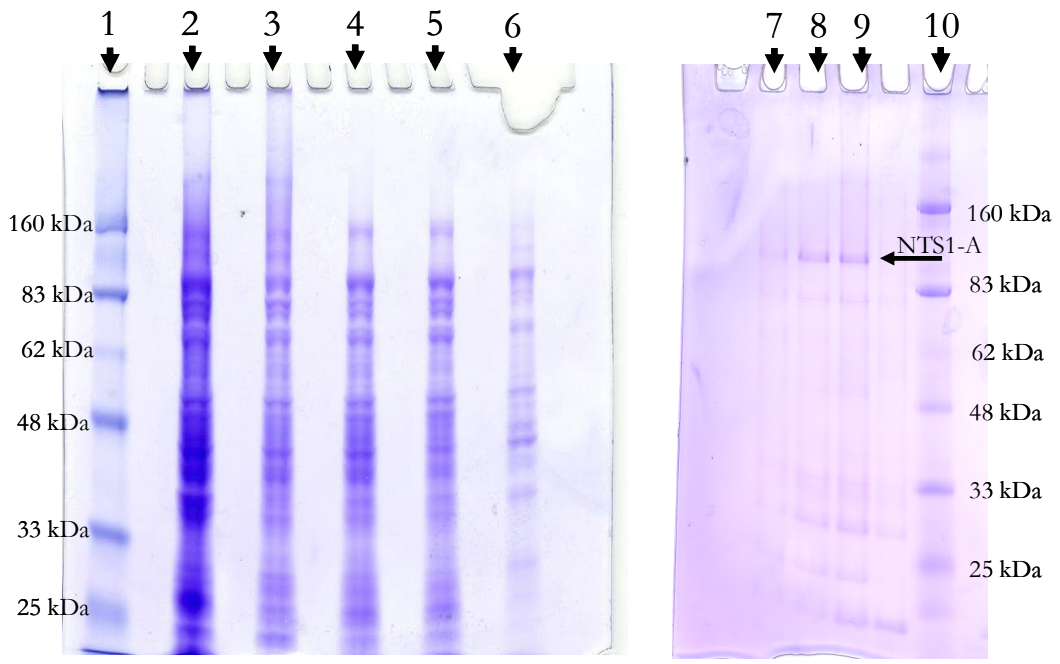

Figure 3.4 - Tricine (10-20%) SDS-PAGE gels showing the purification procedure of NTS1-A, the gels are stained for protein using Coomassie Brilliant Blue dye. The lane numbers correspond to: 1 molecular weight markers; 2 whole cells from the expression protocol; 3 cell lysate; 4 Ni-NTA column load; 5 Ni-NTA column flow-through; 6 Ni-NTA column wash; 7 NT-column load; 8 NT-column flow-through; 9 NT-column elute and 10 molecular weight markers.

Lane 2 of the gel above (Figure 3.4) shows the protein profile of whole cells expressing NTS1-A before solubilization with detergent; as would be expected there is a large amount of protein present and it runs together in a smear. The solubilised clarified cell lysate fraction (lane 3) can be seen to still contain large amounts of protein with a similar but clearer band pattern to the whole cells in lane 2. After filtering through a 0.2 μm membrane, Ni-NTA column load lane 4, has much of the highest molecular weight species (>160 kDa) removed whilst retaining those below this weight. Much of the protein content of the Ni-NTA column load apparently runs straight through the nickel affinity column without binding, as shown by the large amount of protein in the Ni-NTA flow through (lane 5) and it is a similar profile to the Ni-NTA column load (lane 4). The 50 mM imidazole wash (lane 6) removes a large amount of weakly bound non-specific proteins from the column. A protein band can be seen in the 200 mM imidazole

elution fraction (lane 7), which is also the column load for the NT-column, with a molecular weight (between the 83-175 kDa molecular weight markers) which corresponds well with the predicted molecular weight of 103 kDa for the NTS1-A fusion protein. The NT-column separates active from inactive protein by the use of its own ligand in affinity purification, and this can be seen clearly in lanes 9 and 10: lane 9 shows the protein that failed to bind to the NT-column and lane 10 shows the eluted active NTS1-A from the NT-column. However, the low intensity of the bands, even after concentration, indicates a relatively low-level of expression, in line with results obtained by Grisshammer [78], where a yield of only 800 receptor molecules per bacterial cell was obtained.

Figure 3.5 shows a Western blot, with bands on the film corresponding to protein that has bound anti-His-Horseradish peroxidase (HRP) antibody.

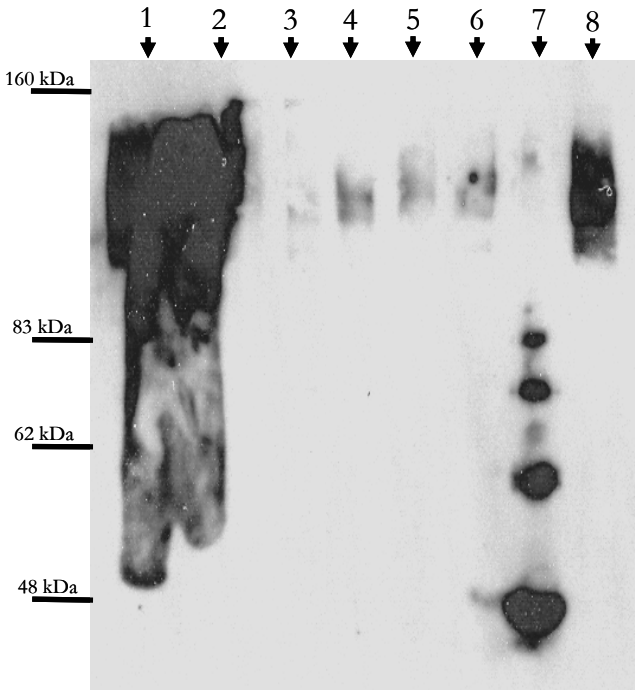

Figure 3.5 - Western Blot of purification fractions run on a Tris-Glycine (10%) SDS-PAGE gel. Bands were transferred onto nitrocellulose membrane and hybridised to anti-His-Horseradish peroxidase (HRP) antibody. The lane numbers correspond to: 2 insoluble fraction of cell base; 1 cell lysate; 3 Ni-NTA column elute; 4NT-column load; 5 NT-column flow-through, 6 NT-column elute, 7 is a standard His tagged protein (dip Z) which oligomerises and 8 concentrated NT-column elution.

There is clearly a considerable amount of non-specific binding of the anti-His antibody to native *E. coli* proteins in the early stages of the purification (lanes 1 and 2), however, a band in the imidazole elution fraction (lane 3) with the same approximate molecular weight as the NTS1-A fusion protein can be seen. This becomes clearer after the concentration of the Ni-NTA elution fraction to make NT-column load (lane 4) and again it can be seen that the second column step is needed to separate out inactive NTS1-A polypeptide (lane 5) from active receptor (lane 6). A standard His tagged protein (lane 7) was also used in this Western blot to test the specificity of the primary anti-His-tag antibody. A binding assay using radioactive NT was used to calculate the amount of active NTS1-A in the 200 mM imidazole elution fractions.

3.3.4.1 Discussion

The expression of NTS1-A, at the flask scale, yielded relatively small amounts of active NTS1-A, indicating that as expected, the expression system is quite inefficient. The use of a His_{10} tag allows the efficient enrichment of receptors by immobilized metal affinity chromatography. The subsequent NT affinity column selects for functional protein. However, improvement of the system in the short term is unlikely, given that extensive trials have already taken place with only limited success [78]. Although the number of active receptors per cell may not be increased, the time taken to produce a sample can be cut drastically by using large scale fermenters which not only allow for much larger volumes to be processed at any one time but also give much more automated control and fine tuning of the growth conditions, for example by controlling the dissolved oxygen content and pH of the media.

3.4 Large-scale fermenter production of NTS1-A in *E. coli* DH5α

Freshly transformed DH5α with pNTS1-A were prepared as in 3.3.1 above. 500 litres of 2x TY medium (2.2.1.4) and ampicillin (2.2.2) was inoculated with 500 ml of DH5α transformed with pNTS1-A overnight culture $O.D_{600} \approx 0.4$. Cells were then grown at 37 °C to an $O.D_{600}$ of 0.5 with constant stirring (200 rpm) and air sparging level of 1 vvm (volume per volume per minute). On reaching the required $OD_{600} = 0.5$, the temperature was decreased to 22 °C and the culture was induced with 0.5 mM ITPG. The cells were harvested after 40 hours of induction using continuous flow centrifugation at a flow rate of 100 litres per hour and snap frozen in liquid nitrogen and stored at -85 °C.

3.4.1.1 Purification of NTS Fusion Protein for fermenter scale growths

All steps were carried out at 4 °C or on ice and all buffer solutions used below can be found in 2.2.3. 250 g wet weight of cell pellet was homogenized in 500 ml of 2x solubilisation buffer using a Waring blender for 3-5 minutes (Figure 3.6).

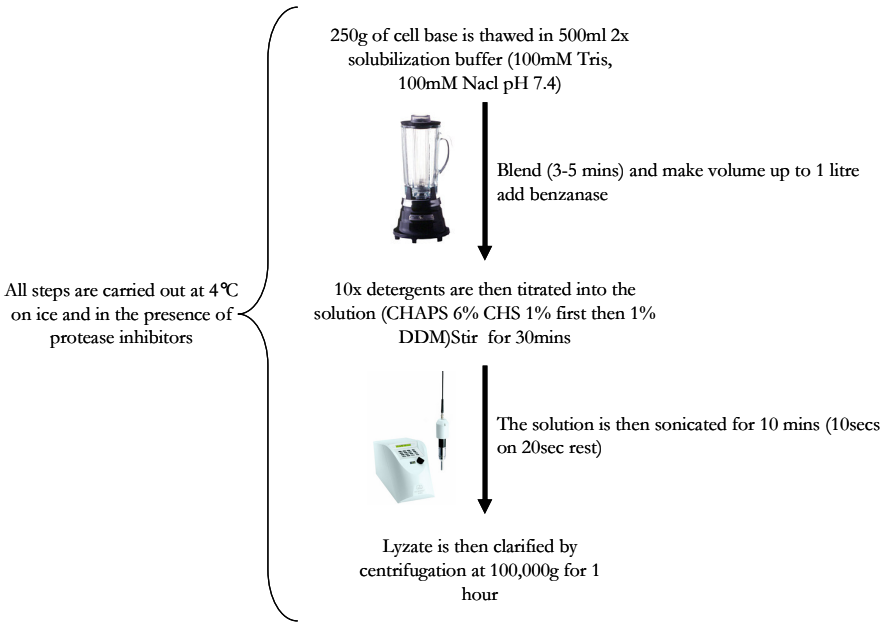

Figure 3.6 – Schematic of the process of solubilisation of cell base in the large scale NTS1 prep.

300 µl of Benzanase (10 $mg.ml^{-1}$) was then added to the homogenized mixture before drop-wise titration of 100 ml of each detergent stock solution, first CHAPS/CHS then DDM, with gentle stirring of the homogenate. The mixture was then sonicated for 10 minutes (10 seconds on 20 seconds rest) on ice. The volume was then adjusted to 1 litre with ice cold Milli-Q water containing protease inhibitors, and the mixture was stirred for a further 30 minutes (Figure 3.6). The homogenate was then clarified by centrifugation (100,000 g for 1 hour at 4 ^{o}C), and the supernatant was then passed through a 0.2 µm filter (Millipore) for subsequent purification by immobilized metal affinity chromatography.

The supernatant was loaded onto a 100 ml Nickel affinity column (Ni-NTA Superflow (Qiagen) resin) in buffer NiA 5 $ml.min^{-1}$ using an AKTA purifier (Amersham), recirculating the supernatant over the affinity column over-night. The column was washed with four column volumes of buffer NiB followed by elution of receptor using buffer NiC.

The eluate was then diluted with NT0 to reduce the imidazole concentration to <70 mM and the NaCl concentration to <50 mM, and then concentrated using YM30 membranes (Amicon) in a stirred cell, to reduce the volume to ~ 60 ml before loading the sample onto an NT column Figure 3.7. This sample was then loaded onto a 20 ml NT column (biotinylated NT bound to tetrameric avidin resin) 2 $ml.min^{-1}$ using an AKTA purifier, by recirculating the Ni-NTA elute over the affinity column. The column was then washed with four column volumes of NT50 buffer followed by elution of the receptor off the NT column with NT1K buffer.

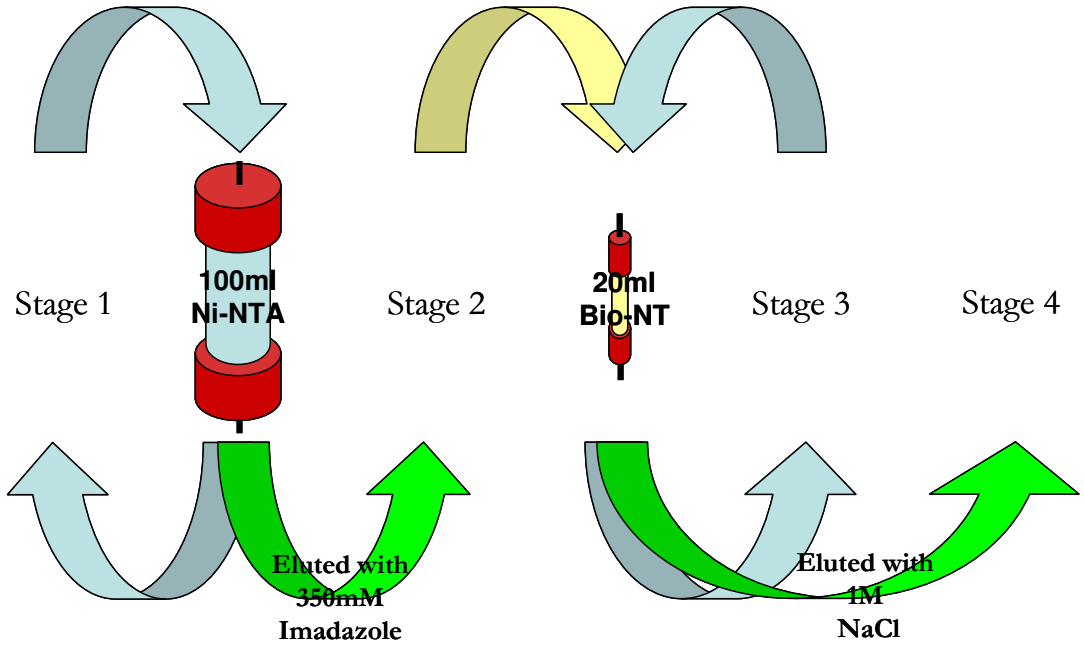

Figure 3.7 – Schematic representation of the two stage purification of NTS1-A, with: stage 1 Clarified Cell lysate is loaded onto the Ni-NTA column by cycling overnight; stage 2 Elute from Ni-NTA column is diluted to lower the concentration of Na to < 50 mM and Imidazole to < 70 mM, then concentrated to lower the volume; stage 3 Concentrated diluted Ni-NTA column eluate is loaded onto the NT column by cycling overnight and stage 4 Elute from Bio-NT column is diluted to lower the concentration of Na to 50 mM, then concentrated to lower the volume

The NT-column eluate is then immediately diluted with NT0 to reduce the concentration of NaCl from 1 M to 50 mM and again concentrated as above with YM30 membranes before snap freezing with liquid nitrogen and storing at -80 °C. 100 µl was collected at every stage of preparation and purification, snap frozen with liquid nitrogen and stored at -80 °C for us in assays of protein content and specific activity and for gel analysis.

3.4.2 500l Fermentation of pNTS1-A in DH5α

The fermentation trace from a 500 L scale growth is shown in Figure 3.8 below. The CO_2 difference in red, the difference between the CO_2 entering the vessel and that in the exhaust, is a direct indication of the cell density during the 37 °C growth phase. After five hours of

growth the temperature was reduced to 20 °C, as the cell density had reached the required level for induction.

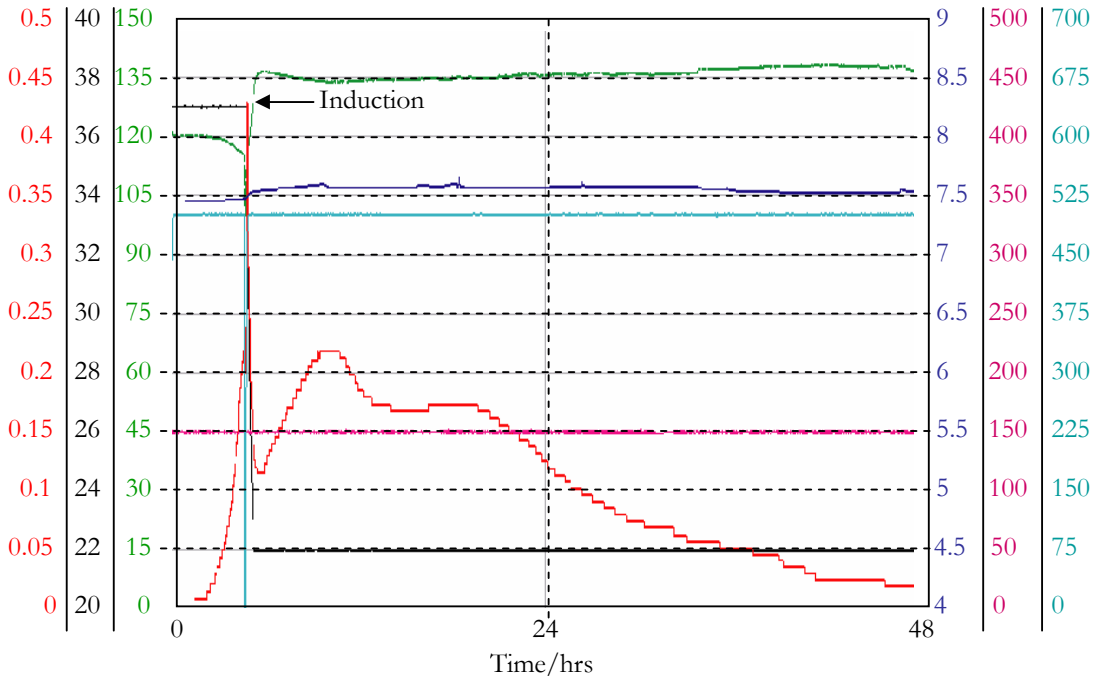

Figure 3.8 – A status trace for 500L Fermentation, of pNTS1A in DH5α, with: CO_2 difference in red, the difference between the CO_2 coming into the vessel and that being expelled; temperature, °C, in black; dO_2 in green, the amount of oxygen dissolved in the media this is a percentage value; pH in blue; stirring speed, in rpm, in pink and air flow, in volume per volume per minute, in cyan.

On induction a slower rate of growth is observed, by CO_2 difference, though this is expected as both the temperature and the addition of IPTG will have an effect on the rate of bacterial respiration. At the end of 40 hours of induction, the cells were harvested by flow through centrifugation, yielding a cell pellet of 1.5 kg, which was then flash frozen and stored at -85 °C. Throughout this time the pH of the medium was constantly being adjusted to maintain it at pH 7.4.

250 g of frozen cell base from the fermentation was used for each large scale purification of NTS1-A. The AKTA FPLC trace from the first stage of the affinity purification, a 100 ml nickel affinity column, of which the wash and subsequent elution is shown in Figure 3.9.

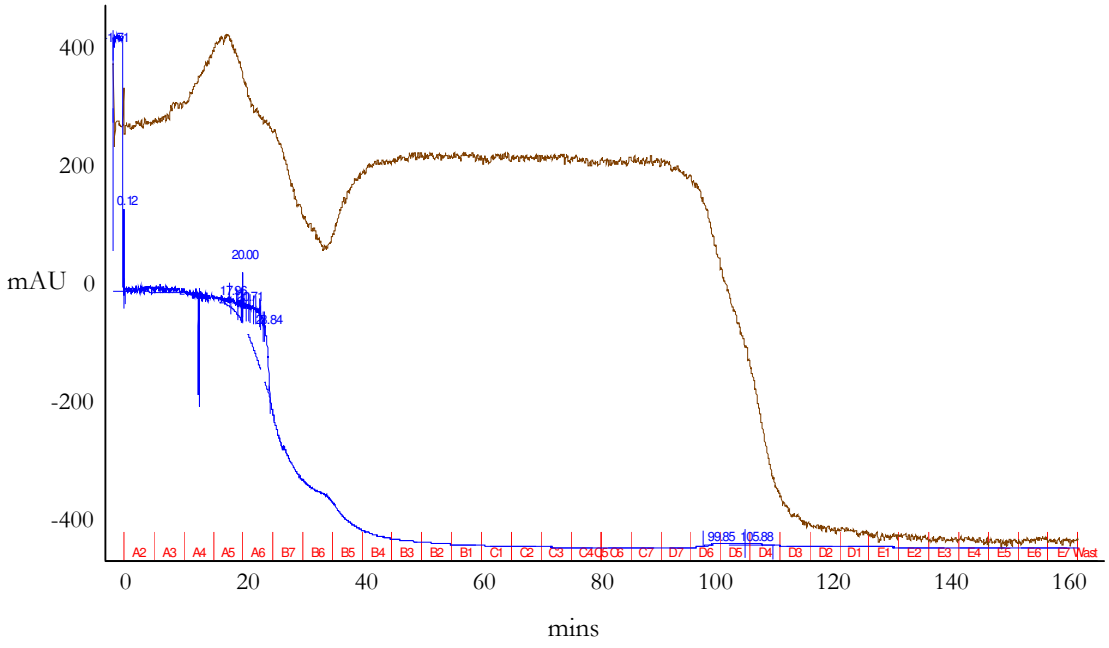

Figure 3.9 - AKTA FPLC purifier trace of the 100ml Ni-NTA column purification, the Abs_{280} in blue and the conductance in brown, and the fractions collected off the column marked in red along the x-axis.

The clarified detergent cell lysate was passed over the Ni-NTA column 3 times then the wash and the elution of the NTS1-A was observed and graphed here above. The column is washed with 4 column volumes of NiB buffer in the first 80mins of the graph and eluted using 4 column volumes of NiC buffer. Around 100 mins, in fractions D6-D3, a broad flat peak occurs in the UV trace; this represents the NTS1-A eluting off the Ni-NTA.

After dilution to reduce the concentration of imidazole and NaCl, and subsequent concentration, the NTS1-A eluate off the Ni-NTA column was loaded onto a NT-affinity column. Again the sample to be loaded is passed over the column 3 times and the AKTA FPLC trace in Figure 3.10 is of the column wash and elution.

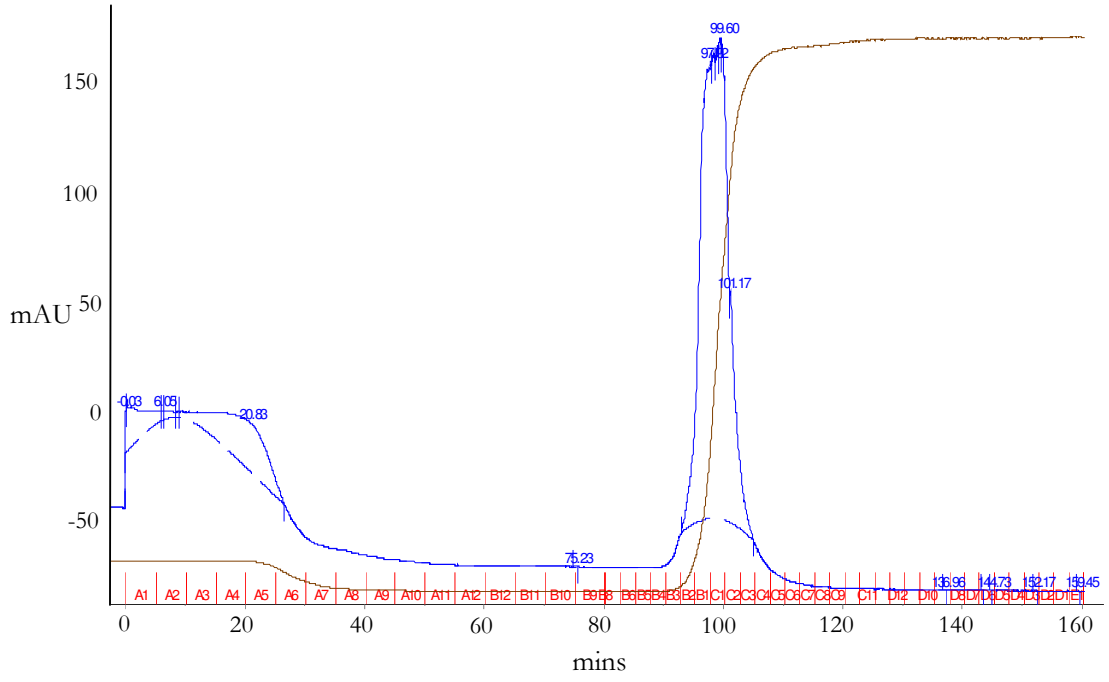

Figure 3.10 – AKTA FPLC purifier trace of the 20ml NT-streptavidin column purification, the Abs_{280} in blue and the conductance in brown, and the fractions collected off the column marked in red along the x-axis.

The column was washed with 4 column volumes over the first 80mins; as can be seen on the graph above the absorbance and conductance reaches a minimum in this time reflecting the clean nature of the column. The salt concentration was raised to 1 M, to disrupt the interaction of the receptor with the immobilised NT, and there is a clear elution peak of the active receptor off an affinity column made of its ligand.

A silver stained gel was run of the purification profile to determine the quantity of receptor present through the purification process, shown in Figure 3.11.

Figure 3.11 – Silver stained, Tris-glycine (4%-12%) SDS PAGE, gel of the purification profile of a large scale preparation of NTS1-A. The lane numbers correspond to: 1 cell lysate; 2 100ml Ni-NTA column wash; 3 NT-column load; 4 NT-column wash; 5 NT-column Load, 6 molecular weight markers, 7 NT-column flow-through and 8 NT-column elution.

It was difficult to track the NTS1-A band through the purification profile due to the large volumes and dilute nature of the protein during the majority of the purification, though there is a clear band in the NT-column load, flow-through and eluate at the correct molecular weight confirming that the peak from the AKTA was indeed NTS1-A. The fact that there is a band in the NT-column flow-through shows that as expected the Ni-NTA column purified both active and inactive receptor, thus this second affinity column provides a means of distinguishing and separating active protein from inactive mis/unfolded polypeptide.

A western blot, using an anti His-tag antibody, of the purification was also carried out in an attempt to visualise the receptor through more stages of the purification process.

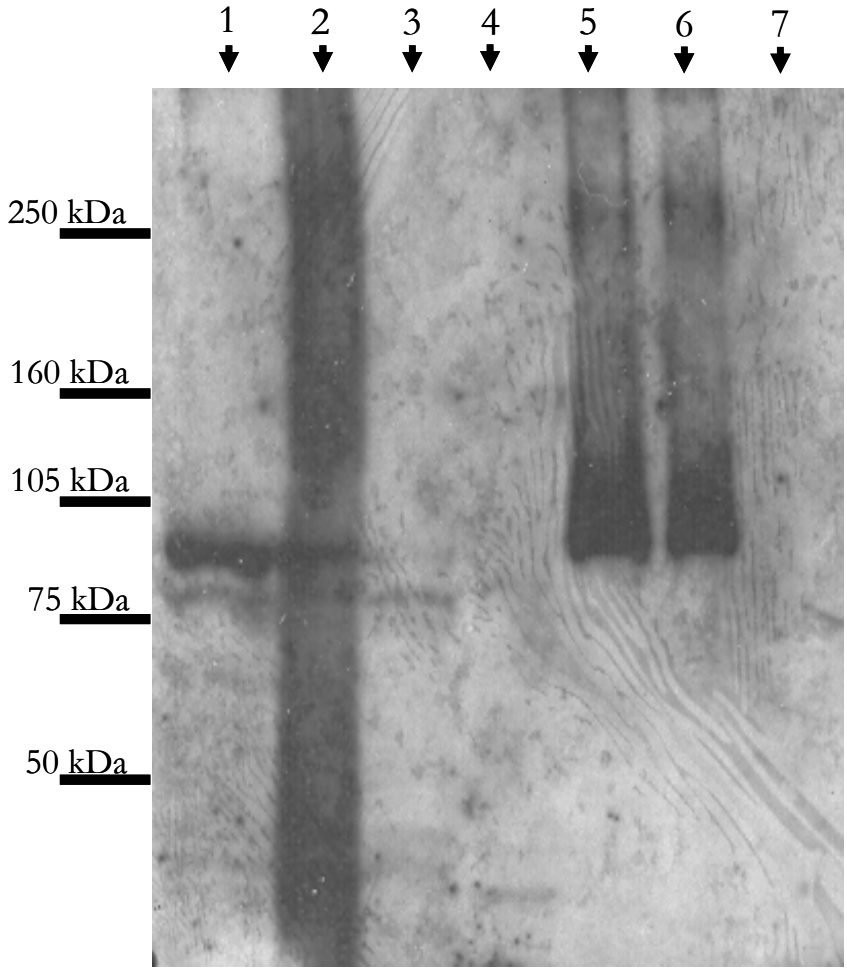

Figure 3.12 – Western blot from a Tris-glycine (4%-12%) SDS PAGE gel of the purification profile of a large scale preparation of NTS1-A. Bands were transferred onto nitrocellulose membrane and hybridised to anti-His-Horseradish peroxidase (HRP) antibody. The lanes correspond to: 1 cell lysate; 2 insoluble fraction from cell lysis; 3 100ml Ni-NTA column flow through; 4 100ml Ni-NTA wash; 5 NT-column elute; 6 NT-column flow-through; and 7 NT-column wash.

The western blot shows the NTS1-A in the cell lysate though no other new bands appear even after longer exposure of the film, this is due to the scale of the preparation and the volume of

the individual stages of the purification diluting out NTS1-A to such an extent that even using western blotting it is not visible.

3.4.2.1 Protein assay

Using the protocol set out in 2.3.5, the protein content across all the stages of a 200 g of cell base, purification was assessed with the results shown in Figure 3.13.

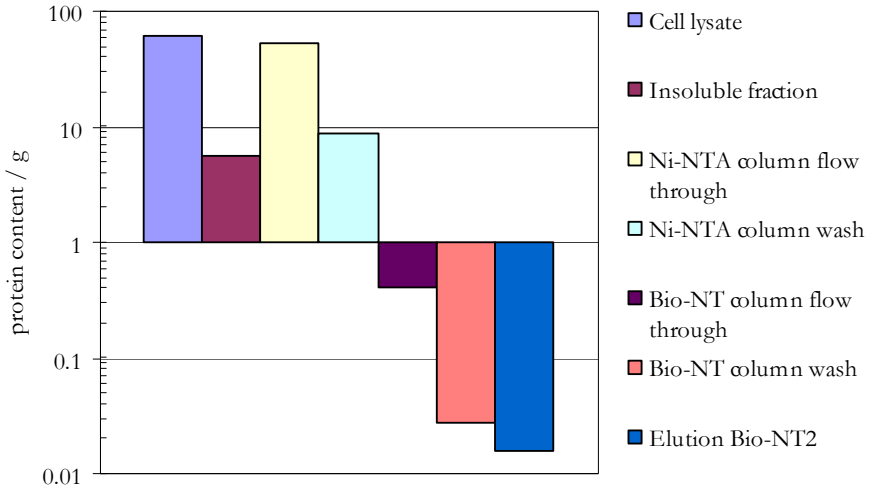

Figure 3.13 – A graph to show the amount of protein present at each stage of the purification of 200 g of *E. coli* cell base expressing NTS1-A

From the 200 g of wet cell base there was a total of 68 g of protein, taking the sum of the soluble and insoluble fractions to be total protein. From the 62 g of solubilised protein that was loaded onto the Ni-NTA column 0.9 g remains on the column after washing. After concentration 0.43 g of protein is loaded onto the NT-column of which 15.6 mg was retained to be eluted as active NTS1-A, a typical yield from this stage for the preps carried out at this scale. After dilution to remove the high concentration of salt and concentration this tends to fall to 6 mg of active receptor on average, these losses are likely to occur due to the high salt concentration used for the NT-column elution and also the stability of the receptor over the

time it takes for concentration at 4 °C (the protein has a half-life of approximately 50 hours at this temperature) with unfolded protein crashing out onto the concentration membrane. This assay shows that the quantity of un/misfolded NTS1-A polypeptide is large even after the steps that were taken in the expression method to slow the production of translation products to allow for correct folding of the receptor.

3.4.3 Discussion

As expected large scale fermentation yielded a relatively large amount of cell base in the space of just one growth time, it has also shown that the conditions in the shaker flasks in terms of pH and dissolved oxygen are likely to be be detrimental to the growth of healthy bacterial cells. There was a clear acidification of the media occurring right from the start of inoculation which was compensated for in the fermenter but would be left unchecked in the flasks, and therefore possibly contributed to lower yields per gram of cell base than in the more regulated system of the fermenter. This aside fermentation on this scale enabled the stock piling of NTS1-A and alleviated the need for constant batch growing in shaker flask before a large scale purification could be made for use of the NTS1-A in the biophysical applications detailed in this thesis.

The large-scale purification of NTS1-A fusion protein is simple and robust. It reliably provides high-quality receptor material for SPR, ESR and NMR on the scale of ~ 6 mg per large scale purification. Receptors are solubilized from whole cells as starting material, rather than crude membranes as in the shaker flask prep, which are time-consuming to prepare especially with the volumes involved in cell lysis of such a large amount of cell base.

3.4.4 Assays of NT binding to NTS1-A

3.4.4.1 Introduction

A radioligand is a radioactively labelled agonist/antagonist of a receptor, transporter, enzyme, or any protein of interest. Measuring the rate and extent of binding provides information on the number of binding sites, and their affinity and pharmacological (biological) characteristics. There are three commonly used experimental protocols: Saturation binding experiments; in these experiments the extent of binding is measured in the presence of different concentrations of the radioligand; from an analysis of the relationship between binding and ligand concentration, we can determine the number of binding sites, B_{max}, and ligand affinity, K_D: Kinetic experiments; saturation and competition experiments are allowed to incubate until binding has reached equilibrium; kinetic experiments measure the time course of binding and dissociation to determine the rate constants for radioligand binding and dissociation, together, these values also permit a calculation of the K_D: and competitive binding experiments, measuring the binding of a single concentration of radioligand at various concentrations of an unlabeled competitor, analysing this data gives information on the affinity of the receptor for the competitor.

The equations that describe the law of mass action include the variable F ([Ligand]), the free radioligand concemtration. In many experimental situations, you can assume that only a very small fraction of the ligand ever binds to receptors. In these situations, you can assume that the free concentration of ligand is approximately equal to the concentration added. This assumption vastly simplifies the analysis of binding experiments, and the standard analysis methods depend on this assumption. In other situations, a large fraction of the ligand binds to the receptors. This means that the concentration of ligand free in solution does not equal the concentration you added, and the discrepancy is not the same in all tubes or at all times, the free ligand concentration is depleted by binding. Many investigators apply the approximation

that, if less than 10% of the ligand binds, to receptors, ligand depletion may be discounted; if more than 10% of the ligand binds, there are three approaches available: (i) Change the experimental conditions, the simplest approach being to decrease the amount of receptor in the incubation, the problem being that this will decrease the number of radioactive counts, the way around this is to increase the reaction volume, the problem with this approach is that it requires more radioligand, which is usually very expensive; (ii) Measure the free concentration of ligand in every tube; this is fairly straightforward, and one can also estimate the free concentration by subtracting the total bound from the total added; (iii) Use analysis techniques that adjust for the difference between the concentration of added ligand and the concentration of free ligand.

To determine the activity of NTS1 samples produced we measure the free concentration of radioligand separating it from bound ligand using Ni-NTA affinity spin columns (Qiagen) which trap the receptor in the resin matrix using the His_{10} tag or in the case of membrane reconstituted samples centrifugation is used. Non-specific binding is determined by running a parallel experiment where excess unlabelled ligand is added along with the radio labelled ligand to determine the extent of non-specific binding.

3.4.5 Methods

Methods for this are set out in 2.3.6 above.

3.4.6 Results

3.4.6.1 Synthesis of NT

The full length NTS1 ligand NT (pGlu-Leu-Tyr-Glu-Asn-Lys-Pro-Arg-Arg-Pro-Try-Ile-Leu-OH) was synthesized for use in competition with other labelled ligands in experiments to determine non-specific binding. The synthesis was carried out at a 0.2 mmol scale with a

theoretical yield of 0.338 g of peptide. The HPLC trace of the lyophilised Fmoc synthesis cleavage produce can be seen in Figure 3.14. A large peak (fraction 3 Figure 3.14) with absorbance at 254 nm (wavelength corresponds to peptide bonds) and 280 nm (wavelength corresponds to aromatic amino acids) eluted at 32 % acetonitrile after 23 minutes during the purification process, corresponds to NT.

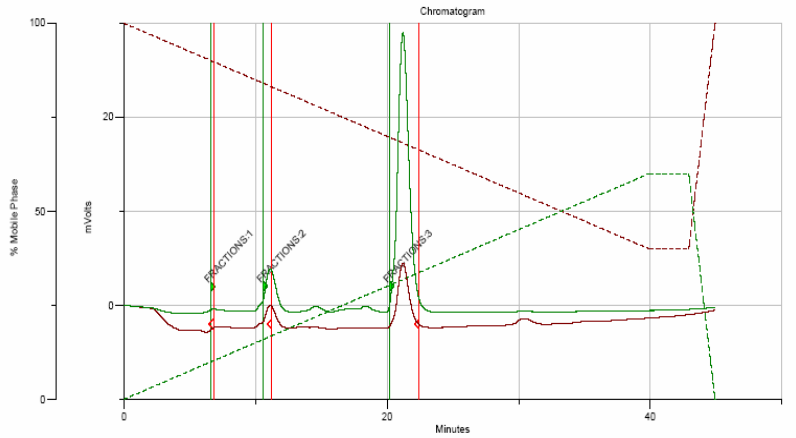

Figure 3.14 – Reverse phase HPLC trace of the lyophilised products from the solid phase synthesis of NT. With the absorption at 254 nm as a solid green line and the absorption at 280 nm as a solid red line and the percentages of H_2O and acetonitrile in dashed red and green lines respectively.

This was verified using matrix assisted laser disorption time of flight (MALDI-TOF) mass spectrum of the peak Figure 3.15.

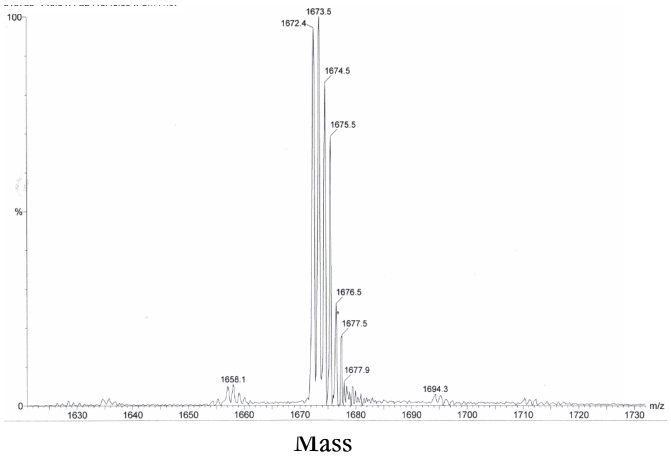

Figure 3.15 – MADLI-TOF mass spec of the dominant peak in the HPLC purification of solid phase synthesised NT.

The mass spectograph shows the correct peptide weight of 1673 Da with isotope stepping as the dominant feature and component of fraction 3 from the HPLC (Figure 3.14). The yield from one of these syntheses was 0.297 g which is a yield of 88% of the theoretical maximum for this synthesis.

3.4.6.2 Radio ligand Assay

The scintillation counting from the activity assays carried out on two separate large scale NTS1-A preparations are shown below in Table 3.1.

Sample	Counts per minute						Mean
	1	2	3	4	5	6	
Prep 1a Non Specific	116357.6	87965.88					102161.8
Prep1a	163494.8	116294.8					139894.8
Prep1b Non Specific	149112	81152.97					115132.5
Prep 1b	105556.7	151362.3					128459.5
Prep 1c Non Specific	28301.61	28556.03	24990.04	26315.86	26691.07	30541.3	27565.99
Prep 1c	28086.61	34421.36	32673.97	34226	41774.07	39616.07	35133.01
Prep 2a Non Specific	150370.4	87103.91					118737.2
Prep 2a	147122	119702.8					133412.4
Prep 2b Non Specific	242642.2	21109.5					131875.8
Prep 2b	122301.9	166619.6					144460.8

Table 3.1 – Results from scintillation counting of the NTS1-A radio ligand activity assay on the concentrated NT-column eluate of 2 separate large scale purifications of NTS1-A. The different purifications are labelled 1 and 2, the lettering refers to differing volumes of the eluate tested.

The average of each of the repeats was then taken; the specific counts subtracted from the non-specific to produce give a cpm value for the amount of radio ligand bound to the receptor

in each sample. These values were then used to calculate the activity of the eluates from the purification process the results are shown in Table 3.2

Sample	cpm observed on NTS1-A	cps observed on NTS1-A	cps in total collected	cps per 50µl	cps in sample	dps in sample	nmol in elution sample
Prep 1a	37733.03	628.8838	4716.629	5659.955	7923936	17432660	23.55765
Prep 1b	13326.99	222.1165	1665.874	1999.049	1399334	3078535	4.160182
Prep 1c	7567.028	126.1171	1639.523	1967.427	4590664	10099460	13.64792
Prep 2a	14675.23	244.5871	1834.403	2201.284	22012838	48428243	65.44357
Prep 2b	12584.91	209.7485	1573.114	1887.737	9438683	20765102	28.06095

Table 3.2 – Calculated activity, from radio ligand assay, of two separate purification preparations of the NTS1-A from fermenter grown cell base.

From this radio ligand assay the activity the average activity of NTS1-A purified from 200 g of cell base is 27 nmol ± 23 nmol of binding sites for NT which equates to roughly half of the total protein content of the average purification being active. The error is reflected in the specific activity, of each purification, and is indicative of the process which regularly halves in yield between different purification runs due to varying times needed for concentration and the half life of the receptor in detergent solution at 4 °C. Even with that level of variance between the different processes this method generates a constant supply of functionally active NTS1-A for biophysical studies.

3.5 Reconstitution of NTS1-A back into a model membrane

3.5.1 Introduction

Studies of native membrane proteins in their native environment can be difficult due to their natural abundance levels being low and the complexity of the native membranes where the influence of other constituents can not be differentiated from the test protein. It is therefore advantageous to reintroduce a detergent micellar protein back into a known lipid membrane as a tool for elucidating both functional and structural characteristics in a near native environment. Though many membrane proteins have been reincorporated into membranes, the molecular mechanisms for reconstitution are largely unknown and, largely, the efficacy of the process is only qualitatively assessed. Data on the structural complexes formed by the interaction of membrane proteins with lipids and detergents and the mechanisms of protein insertion into lipid bilayers are limited.

Detergent mediated reconstitution has been the most successful and frequently used technique for the production of proteoliposomes [79], simply because most membrane proteins are purified in the presence of detergent. This technique generally involves cosolubilisation of phospholipids and protein in an appropriate detergent forming an isotropic solution of lipid-protein-detergent micelles and lipid-detergent micelles. Then the detergent is gradually removed, through either dialysis or SM2 Bio-Beads, resulting in the self assembly of bilayers structures containing protein. Optimization of the reconstitution process can be made by looking at the stepwise solubilisation of preformed liposomes and the incorporation of protein at various stages [79, 80] and the temperature and speed at which the detergent is removed.

3.5.2 Aim of this study

This section aims to demonstrate the incorporation of NTS1-A into a model membrane system from its detergent purified form generated above (3.4).

3.5.3 Methodology

3.5.3.1 BPL liposome detergent titrations

Preparation methods for stock solutions of BPLs are found in 2.4.1 and the titration experiments are described in 2.4.2.

3.5.3.2 Reconstitution of NTS1-A into destabilised lipid vesicles mediated by Bio Beads

Stock solutions of lipids were prepared as above and the method for bio bead mediated reconstitution of NTS1-A is shown in 2.4.3.

3.5.4 Results

3.5.4.1 BPL liposome detergent titrations

First, the solubilisation of BPLs with DDM was analysed, by examining the detergent induced changes in the turbidity of lipid suspensions. The results, shown in Figure 3.16, show an initial decrease in turbidity followed by a slight rise before it then decreases to a minimal value. Studies of the interaction of model lipid membranes with detergent [81-83] have shown that these turbidity curves can be interpreted in terms of a "three-stage" model.

Stage I, 0 to 4 mM DDM (Figure 3.16), involves a partitioning of detergent monomers between the aqueous environment and the lipid bilayers.

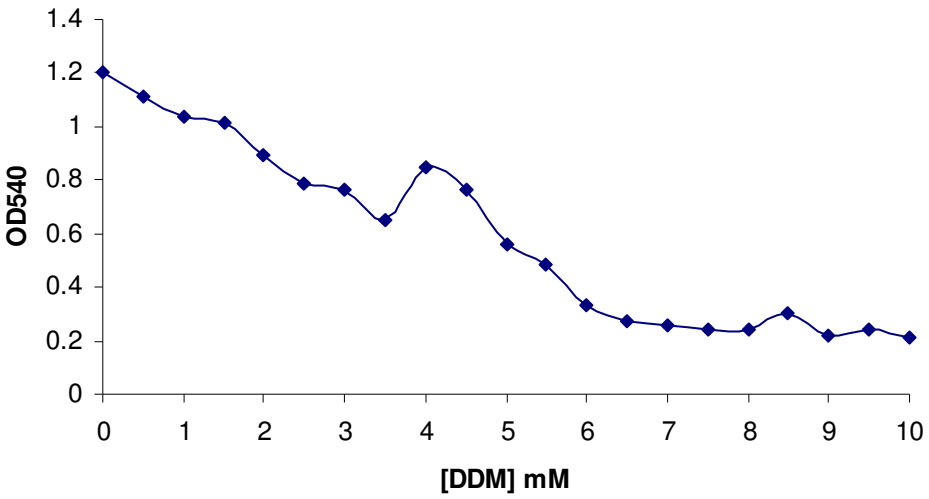

Figure 3.16 – Turbidity dependence for BPLs titrated with DDM.

During this stage we see a slight increase in the turbidity as the detergent saturates the lipid vesicles in solution, the maximum of this increase is termed R_{sat}, where whole vesicular structures are still present saturated with detergent. In stage II, between 4 and 7 mM (Figure 3.16), increased detergent concentrations promote gradual liposome solubilisation with mixed micelles forming of much lower molecular weight with a subsequent decrease in turbidity. Stage III is the total solubilisation of lipid by the detergent (Figure 3.16 above between 7 and 10 mM) and condition also termed R_{sol} such that the detergent concentration precludes any lipid structures from forming. The concentration of DDM in the solubilized protein is 2 mM DDM falling clearly within stage I.

The second detergent present in the NTS1 solubilisation buffer is CHAPS; titrations of BPLs with this detergent gave a very different turbidity profile (Figure 3.17). CHAPS seems not to have a stage I of the above model, going straight to the formation of mixed micelles and the gradual solubilisation of the lipid vesicles (stage II) and onto total solubilisation (stage III).

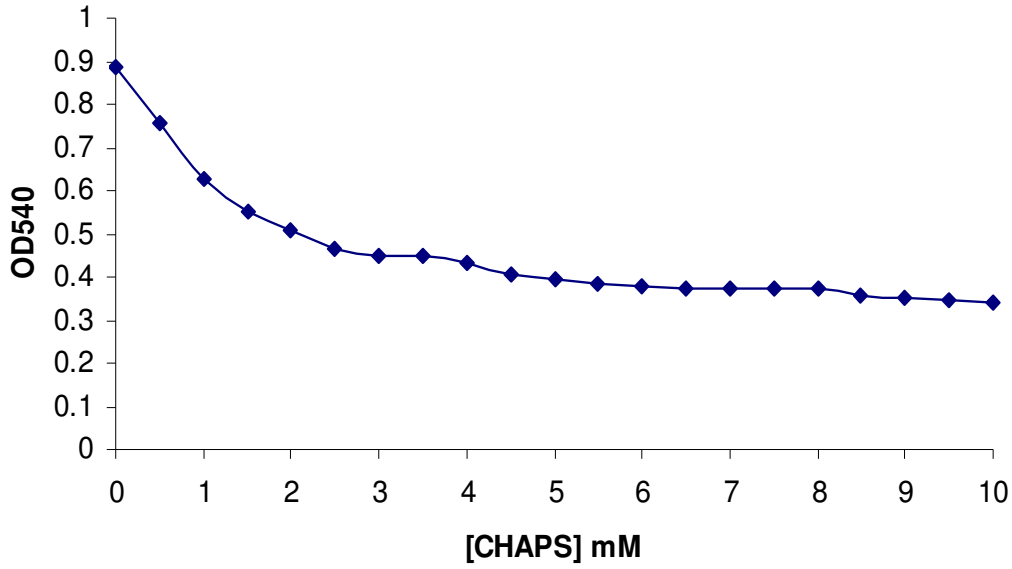

Figure 3.17 - Turbidity dependence for BPLs titrated with CHAPS

The concentration of CHAPS in the NTS1-A solution is 7 mM, falling clearly into the concentration range of stage III in the graph above (Figure 3.16) and the solubilized condition. With the DDM concentration in the solubilized receptor solution falling below the R_{sat} condition but the CHAPS concentration being in the R_{sol} condition it would appear that it would not be possible to assist the uptake of protein into the BPL vesicles by treating with detergent to destabilise them as the concentration of the detergents in the NTS1-A solubilisation buffer (2.2.3) is too high. During these titrations it was observed that the turbidity of the solutions changes slowly over time and that an equilibrium is only achieved after a number of hours, indeed in the titration shown here the solutions were made up and then left at 4 °C for 12 hours before the optical densities were measured. As lipid and protein solutions are mixed for only 2 hours in the absence of Bio-Beads it could therefore be valid to destabilize the BPLs before hand with DDM, as this surfactant seems to have a less harsh effect on the vesicles than CHAPS.

3.5.4.2 Results of the reconstitution of NTS1-A into destabilised lipid vesicles mediated by Bio Beads

In the first instance, 0.196nM of active pure receptor protein receptor protein was added to 0.04 mg of BPLs in a total volume of 200 µl, 0.118 nM of activity was recovered, as determined by radioactive binding assay described in 3.4.4.

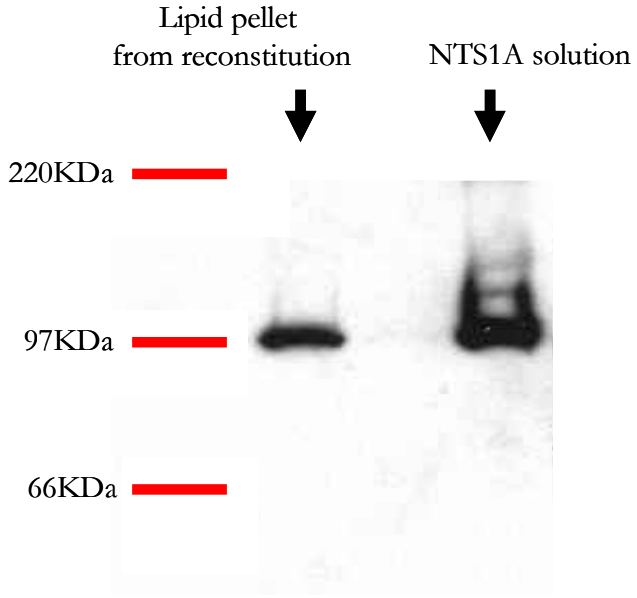

Figure 3.18 - Western blot, using an anti His-tag antibody, from a Tris-glycine SDS PAGE gel of the harvested pellet from the reconstitution of NTS1-A with NTS1-A solution loaded next to it as a control.

This level of activity corresponds to a ~60 % recovery of the protein added, the activity corresponds to 0.012 mg of protein (calculated from the activity observed) and, assuming minimal losses of lipid in the process due to the saturation of the Bio-beads with lipids before their use in the reconstitution protocol, the amount of lipid present is 0.04 mg, giving a ratio of 1:3 protein to lipid by weight. Avanti publish the composition of their total brain lipid as: 33.1 % phosphatidylethanolamine, 18.5 % phosphatidylserine, 12.6 % phosphatidylcholine, 4.1 %

phosphatidylinositol and 30.9 % other lipids. On the assumption we can ignore the other lipids in an average weight calculation as they will have a similar weight distribution as those which are quantified the average molecular weight of BPLs is 827.75 Da, giving a ratio of 360 lipid molecules per receptor.

3.5.4.3 Discussion

It is clear that the biological relevance of a membrane protein is increased by placing it back into its native membrane environment. Here reconstitution of NTS1-A into BPL has been demonstrated.

Chapter 4 Surface Plasmon Resonance studies of NTS1-A

4.1 Introduction

Surface plasmon resonance (SPR) is a spectrophotometric technique which may be used to measure the mass concentration at a surface enabling the association and dissociation of analyte and ligands to be observed and ultimately rate constants as well as equilibrium constants can be calculated. At an interface between two transparent media of different refractive index (e.g. glass and water), light coming from the side of higher refractive index is partly reflected and partly refracted Figure 4.1.

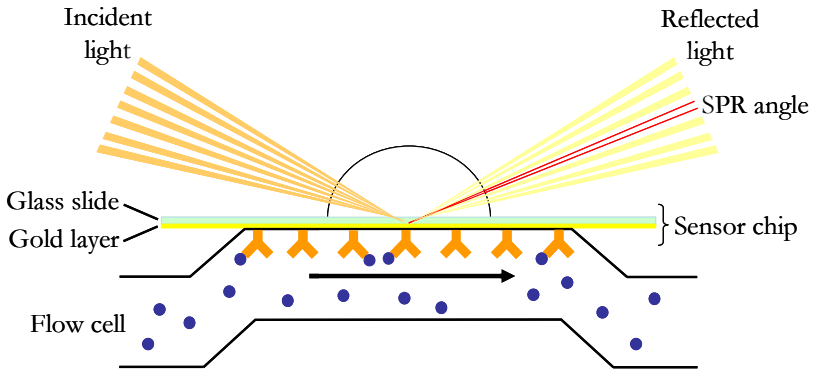

Figure 4.1 – A schematic diagram of the SPR flow cell to show the SPR principle, with ligand in orange on the chip surface and analyte in blue within the flow cell, the arrow indicates the direction of flow.

Above a certain critical angle of incidence, no light is refracted across the interface, and total internal reflection is observed at the SPR angle. While incident light is totally reflected the electromagnetic field component penetrates a short distance (tens of nanometers) into a medium of a lower refractive index creating an exponentially detenuating evanescent wave. If the interface between the media is coated with a thin layer of metal (gold), and light is monochromatic and p-polarized, the intensity of the reflected light is reduced at a specific incident angle producing a sharp shadow (called surface plasmon resonance) due to the resonance energy transfer between evanescent wave and surface plasmons. The resonance conditions are influenced by the material adsorbed onto the thin metal film. A satisfactory linear relationship is found between resonance energy and mass concentration of biochemically relevant molecules such as proteins, sugars and DNA. The SPR signal, which is expressed in resonance or response units, is therefore a measure of mass concentration at the sensor chip surface. This means that the analyte and ligand association and dissociation can be observed and ultimately rate constants, as well as equilibrium constants, can be calculated.

SPR has proved to be extremely versatile, permitting the study of analytes ranging in size from hundreds of Daltons to whole cell binding [84]. However, application to receptor-ligand interactions has largely been limited to soluble ligand-binding domains [85-87]. Detailed analysis of ligand-receptor interactions for GPCRs has proved difficult, due to problems encountered in successful overexpression, purification and stabilisation of GPCRs and, until recently, limitations in biosensor technology. Immobilisation of membrane-reconstituted rhodopsin, a GPCR, on the biosensor surface has recently been achieved, allowing the kinetics of transducin activation to be observed [88, 89]. A similar receptor immobilisation technique was applied to the chemokine receptors CXCR4 and CCR5 and active ligand binding was demonstrated, although with lower affinity than had previously been published [90]. An alternative approach, measuring direct binding of functionally active GPCR to immobilised

ligand on the SPR chip, has not been successful until now. Since responses observed in SPR are proportional to the molecular weight of bound analyte, binding of the large receptor protein gives improved sensitivity when compared with analyses in the reverse orientation.

4.2 Aims of this study

This study aims to demonstrate and quantify the specific interaction of NTS1-A with its ligand NT, in both detergent solubilized and membrane reconstituted receptor produced in Chapter 3. It also goes further to propose a model for the kinetics of this interaction in the detergent solubilised receptor.

4.3 Detergent solubilized NTS1

4.3.1 Methodology

Surface Plasmon Resonance (SPR) analysis was carried out using a Biacore 3000 biosensor instrument (Biacore AB) at 25 ^{o}C. All buffers used were de-gassed and filtered though a 0.2 μm filter (Whatman). 250 response units (RU) of biotinylated NT in HBS-EP buffer (Biacore AP) was immobilised on a streptavidin-coated chip (Biosensor SA, Biacore). 250 RU of 'scrambled sequence' biotinylated NT was immobilised in a control flow cell in the same manner. Analyte used was purified, detergent-solubilised NTS-1A, buffer-exchanged into a glycerol-free 'SPR' buffer to reduce bulk shift effects (50 mM Tris/HCl, pH 7.4, 50 mM NaCl, 0.5 % CHAPS, 0.1 % CHS, 0.1 % DDM, 1 mM EDTA). Interaction experiments were carried out at a flow rate of 20 μl.min^{-1} with sample racks maintained at a constant 5 ^{o}C throughout. Surface regeneration was achieved via two sequential 1 min injections of SPR buffer containing 1 M NaCl to dissociate bound receptor. Injection was subsequently varied between 1 min and 7 mins to test for compliance with the conformational change model. Mass transport control experiments were carried out by variation of flow rate between 15 μl.min^{-1} and 75 μl.min^{-1}.

BiaEvaluation Software v4.1 (Biacore AP) and Origin v5.0 (Microcal Software) were used for data analysis and curve fitting.

4.3.2 Results

4.3.2.1 Synthesis of Biotinylated NT and Biotinylated scrambled NT

For biotinylated NT see section 2.5.2.4. The scrambled Bio-NT (pBiotin-Leu-Tyr-Asn-Arg-Pro-Arg-Pro-Tyr-Leu-Glu-Ile-Lys-Glu-OH) this peptide was designed as a control for SPR experiments, by scrambling the sequence such that none of the terminal eight amino acids occur in the same position as in the primary sequence, so the 8-13 region responsible for receptor binding is not present, effectively destroying its activity. Biotinylation of this peptide facilitates its deposition onto avidin derivised SPR chips as with the Bio-NT. As with Bio-NT the resin was then transferred from the synthesizer, after the amino acid sequence had been formed, and deprotected in the fume hood before coupling the biotinylation reagent (Biotin OSu, Novabiochem), in the same way as with Bio-NT. The lyophilised cleavage product was then purified using HPLC Figure 4.2.

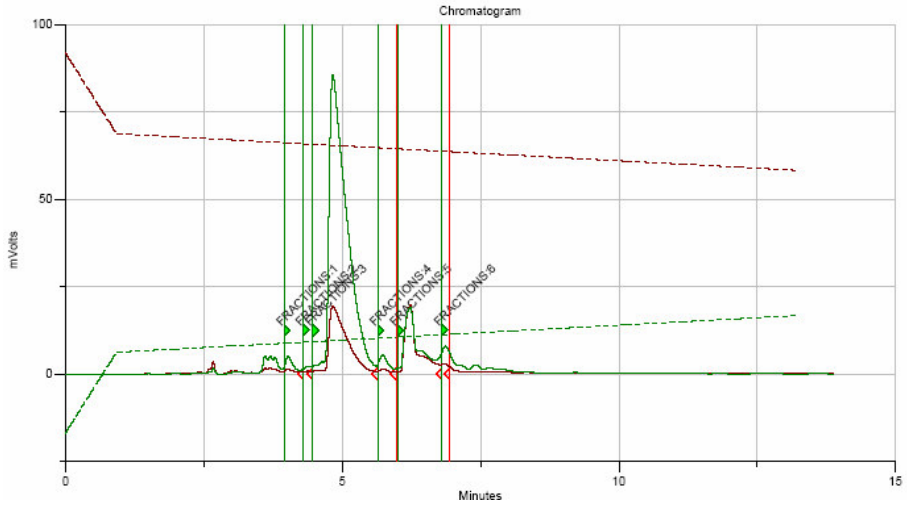

Figure 4.2 - Reverse phase HPLC trace of the lyophilised products from the solid phase synthesis of scrambled Bio-NT, with the absorption at 254 nm as a solid green line and the absorption at 280 nm as a solid red line and the percentages of H_2O and acetonitrile in dashed red and green lines respectively.

The HPLC trace shows a slightly less clean cleavage product than with the Bio-NT. Fraction 3, the dominant peak from HPLC, was identified as scrambled Bio-NT by ESI positive mass spectrometry Figure 4.3.

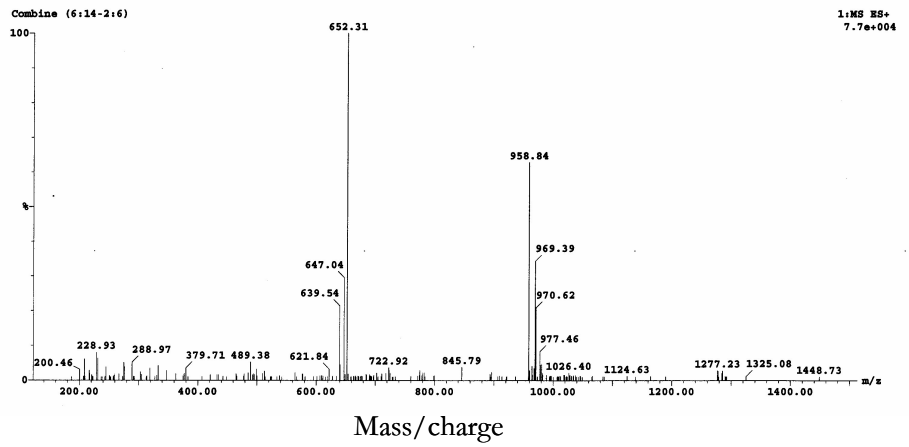

Figure 4.3 – Electro spray ionisation mass spec of the dominant peak in the HPLC purification of solid phase synthesised scrambled Bio-NT.

The mass spectrum shows two dominant peaks at 958.35, corresponding to the doubly charged ion, and 639.58, corresponding to the triply charged peptide species plus sodium, a similar profile of peaks as with Bio-NT. This synthesis was only carried out at the 0.1 mmol scale as this particular peptide was only for use in the controls of SPR experiments. With a theoretical maximum yield of 0.192 g the actual yield from one of these syntheses was 83 % of this at 0.159 g.

4.3.2.2 SPR Analysis of detergent solubilised NTS1-A

The detergent buffer, whilst being optimised for the preservation of the activity of NTS1-A in solution, is not ideal for SPR because of its viscosity, due to the high glycerol content, is likely to cause very large bulk shift effects, where the baseline is seen to rise dramatically on changing

of the buffer condition. If the glycerol is removed from the buffer, full binding activity is preserved, though the half life of the receptor in solution at 4 °C has been observed to decrease from 400 hours to 40 hours [68]. The bulk shifts were therefore analysed for NT50 buffer (2.2.3), NT50 buffer minus the glycerol and NT50 buffer minus glycerol, CHAPS and CHS (this last was tried as DDM itself in this buffer is 1.7x the critical micellar concentration (CMC) for the detergent, and it is thought that it is DDM in the mixture that it is critical for maintaining solubility and activity of NTS1-A) and the results of this are shown in Figure 4.4.

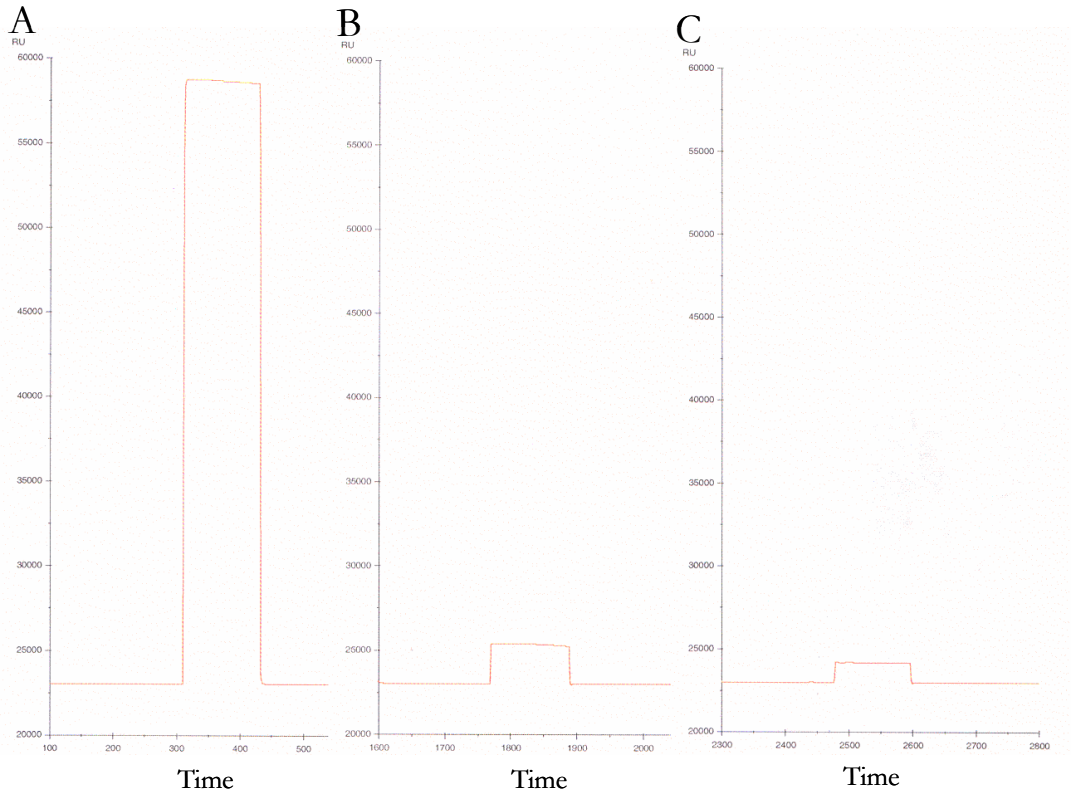

Figure 4.4 – Analysis of buffer compatibility: A = NT50 (50 mM Tris/HCl pH 7.4, 50 mM NaCl, 30 % Glycerol, 0.5 % CHAPS, 0.1 % CHS, 0.1 % DDM, 0.1 mM EDTA); B = NT50 minus the 30 % glycerol and C = NT50 minus 30 % Glycerol, 0.5 % CHAPS and 0.1 % CHS. The cell was regenerated after each injection of buffer with a buffer containing 50 mM NaOH 1M NaCl, the response changes are all compared to a base line of the SPR buffer standard HBS-EP.

Trace A of the buffer assay shows a bulk shift of nearly 37600 RU whilst trace B, with the glycerol removed, only has a shift of 2400 RU, given that the buffer with only DDM present

solublising NTS1-A has only a small 1300 RU improvement on the bulk shift effect, NT50 minus glycerol was chosen as a conservative choice for the SPR buffer for the interaction analysis of NTS1-A with NT. The new half life of the receptor in a buffer not containing glycerol can then be taken into account during the subsequent analysis of interaction.

A series of six injections, of varying concentrations, of NTS1-A were then carried out. Subtracting the response of the control flow cell, containing immobilised scrambled Bio-NT, from the flow cell containing immobilised Bio-NT shows a specific binding response from the receptor to the surface with immobilised Bio-NT Figure 4.5.

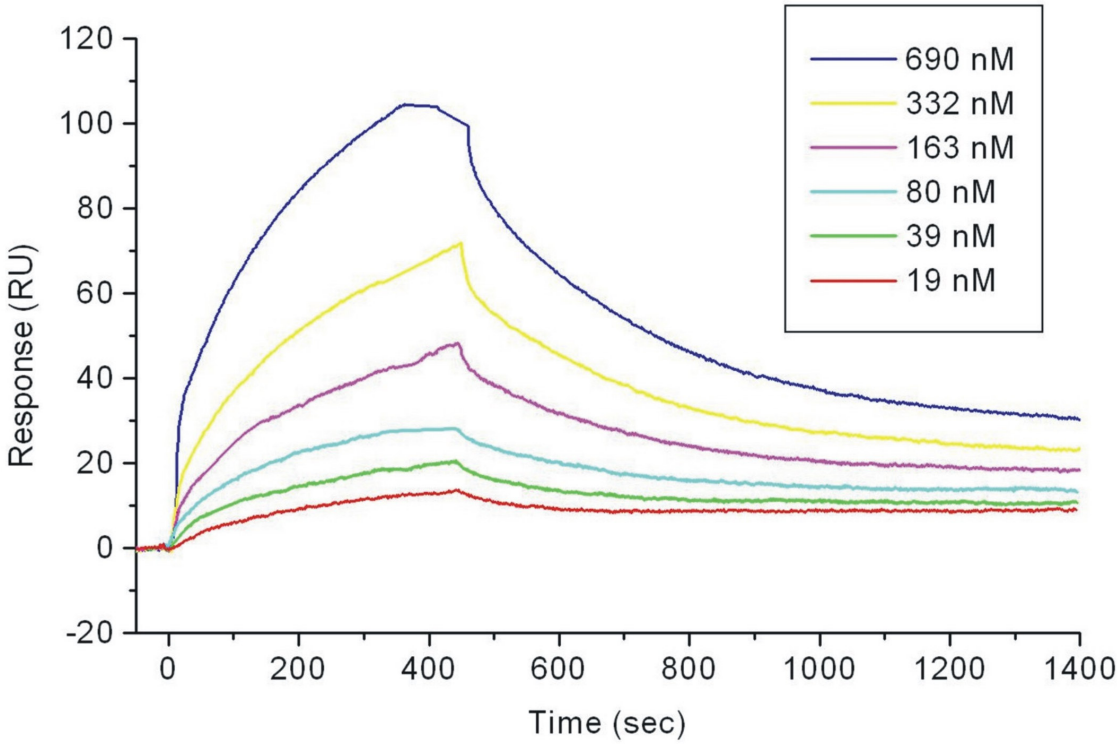

Figure 4.5 – Kinetic Analysis of the NT/NTS-1A interaction between detergent-solubilised NTS1-A and biotinylated NT. Various concentrations (shown in the key in the top right-hand corner of the figure) of NTS-1A were injected at 20 $\mu l.min^{-1}$ over 250 RU immobilised control and NT ligand. Curves shown have the control response subtracted and therefore represent specific binding of NTS-1A to immobilised NT.

The response observed in the control flow, containing immobilized scrambled Bio-NT, was not significantly different from that of a conditioned blank flow cell without any ligand bound to its surface, as shown in Figure 4.6.

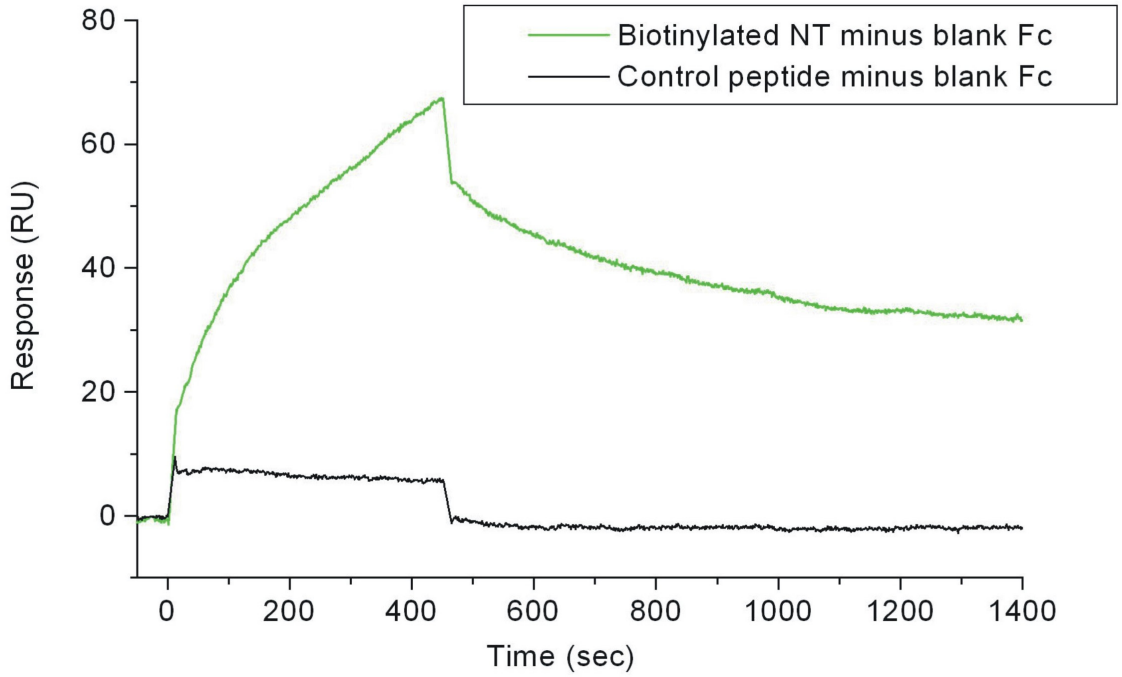

Figure 4.6 – Binding of detergent-solubilised NTS-1A to the biotinylated NT (in green) and control peptide (in dark blue) flow cells at a concentration of 175 nM. The response obtained for a blank Sensor Chip SA flow cell has been subtracted from both curves, revealing negligible non-specific binding to the control peptide surface.

The effect seen here indicates that the interaction with the immobilised Bio-NT on the surface of the chip is specific, with little if any binding to the control. The response seen in the control could in fact be due to a bulk shift effect from the presence of protein in the solution as compared to the baseline solution.

The preliminary fitting of binding curves revealed that the interaction did not follow simple monophasic Langmuir kinetics. The interaction appears to be multiphasic, suggesting that binding is occurring with at least two observable time constants attributed to a multiphasic

kinetic nature of the interaction. Subsequent fitting of exponential decay models to the dissociation phase suggests the data are biphasic since fitting of a triphasic model yielded no statistical improvement in the fit over the biphasic model. Such a deviation, from first order kinetics, can be caused not only by a complex binding mechanism, but also by experimental artifacts such as mass transport, rebinding and heterogeneity of the ligand and/or analyte [91]. Variation of flow rate between 15 $\mu l.min^{-1}$ and 75 $\mu l.min^{-1}$ showed that mass transport and rebinding effects, which can lead to an apparent biphasic response, were insignificant in this case.

Biphasic kinetics can also be caused by heterogeneity in either the immobilised ligand, in the analyte; or by a complex binding mechanism involving a ligand-induced conformational change, differentiating between these possibilities by curve fitting alone is often inconclusive [86, 92]. A decrease in the observed dissociation rate, when the sample injection time is increased, is indicative of either a conformational change or of heterogenous analyte, whereas no decrease in observed dissociation rate is indicative of heterogenous ligand and is shown in Figure 4.7.

The control experiments, carried out involving the variation of the sample injection time between 1 min and 7 min, suggested such time dependence in the dissociation phase, supporting the conformational change and heterogenous analyte models and largely excluding the heterogenous ligand possibility, which was to be expected as the ligand was not only purified to a high level by HPLC but also the biotin moiety on the ligand presents only one mode of binding to the sensor surface.

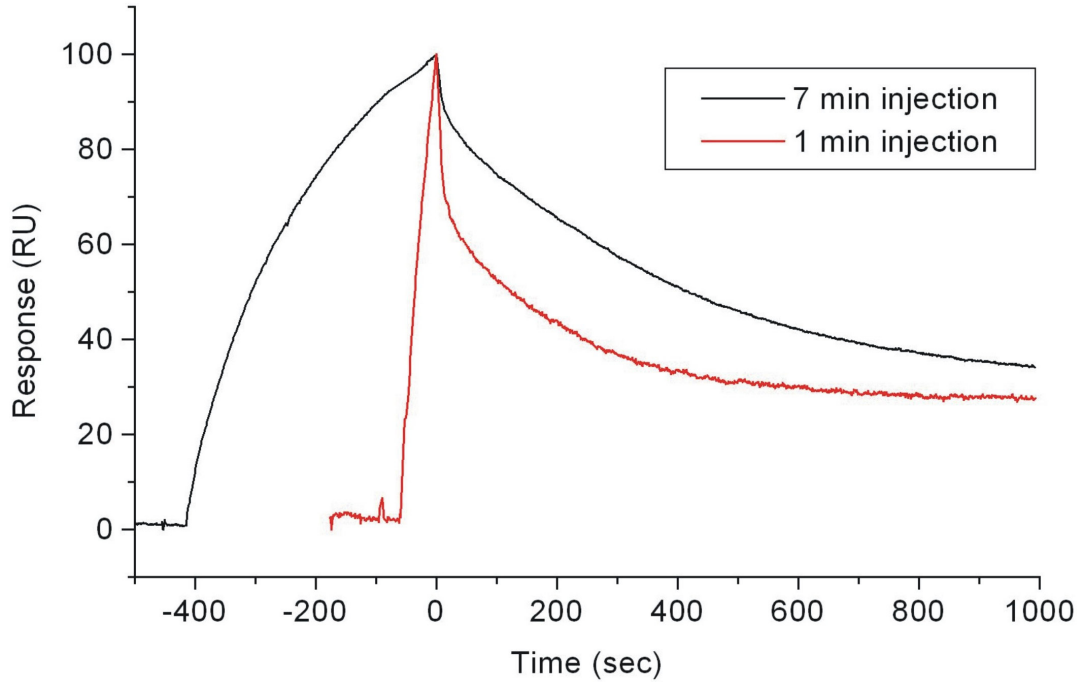

Figure 4.7 - Variation of dissociation phase with NTS-1A sample injection time (190 nM) both injections are normalised to 100 RU.

An increased contribution from the fast dissociation component is evident at short injection time. This result largely excludes heterogeneity in the ligand and supports the conformational change and heterogenous analyte models.

A conformational change of the receptor upon ligand binding is to be expected, since this is fundamental to coupling ligand binding at the cell surface to downstream signalling inside the target cell. Indeed, such conformational changes are now widely accepted as an integral part of receptor signalling, as illustrated by the Cubic Ternary Complex (CTC) receptor-occupancy model proposed by Weiss *et al* [93, 94]. Specifically, a change in conformation of the putative third intracellular loop, which has been identified as the key area of the receptor involved in coupling to phospholipase C [95], could be envisaged. A global fit of the biosensor data to a simple conformational change model was achieved (Figure 4.8). The two-state conformational

change model used for the fitting, which corresponds to the experimentally observable part of the CTC model, can be described by the following equation for the reaction shown in Equation 4.1.

$$A + B \underset{k_{off}\,1}{\overset{k_{on}\,1}{\rightleftharpoons}} AB \underset{k_{off}\,2}{\overset{k_{on}\,2}{\rightleftharpoons}} AB^{*}$$

Equation 4.1

where analyte (A) and ligand (B) interact to form the complex AB, which undergoes a conformational change into a higher affinity state AB*, where in the case of the interaction studied here A is NTS1-A and B is the Bio-NT bound to the sensor surface of the SPR chip.

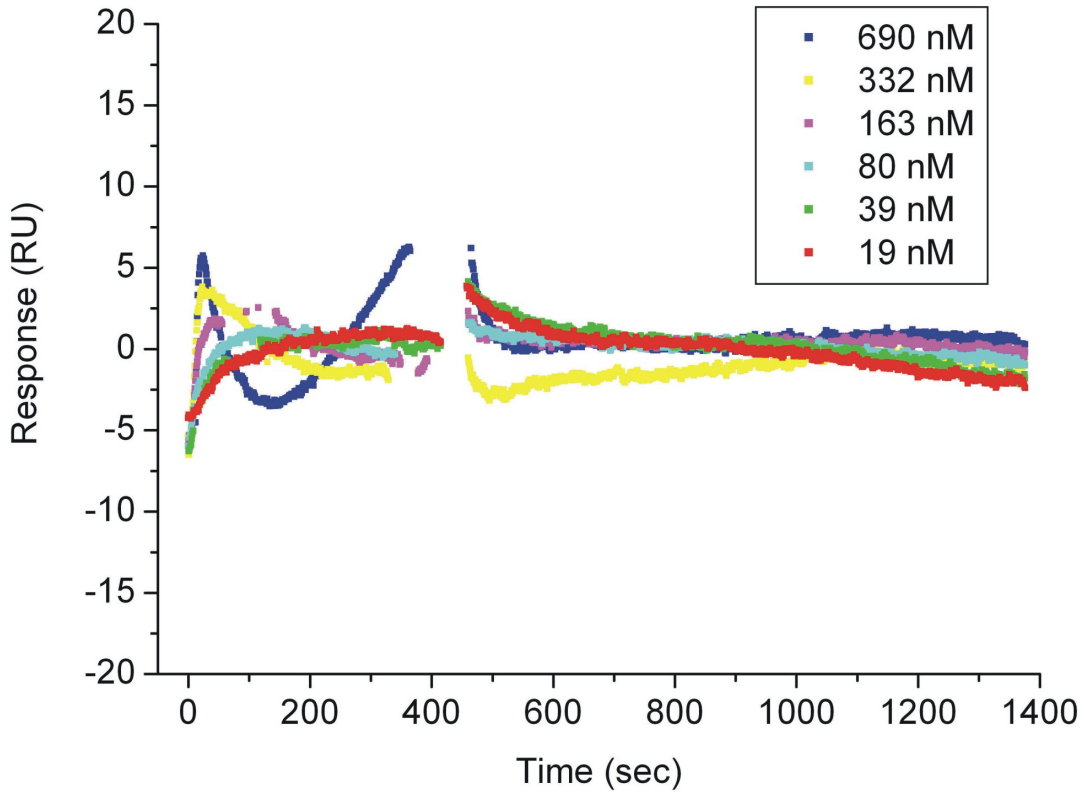

Figure 4.8 – Residuals obtained for a global fit of the NTS-1A/biotinylated NT interaction data using the two state conformational change model with drifting baseline. Residuals are the difference between calculated and experimental data points.

The fit yielded an overall apparent K_D in the nanomolar range of 37.3 ± 11.3 nM. This value is larger than the K_D of 0.4 ± 0.11 nM that was obtained for detergent-solubilised NTS-1A from saturation radioligand binding experiments [68]. However, such experiments only measure the slow component of the binding, and this therefore highlights an advantage of using SPR to study the interaction in real time. Therefore the conformational change model for ligand-activated GPCRs seems a likely explanation for the SPR data.

$k_{on}1$ ($M^{-1}s^{-1}$)	$k_{off}1$ (s^{-1})	$k_{on}2$ (s^{-1})	$k_{off}2$ (s^{-1})	K_A (M^{-1})	K_D (nM)
$(9.74 \pm 2.53) \times 10^3$	$(2.70 \pm 0.01) \times 10^{-3}$	$(3.15 \pm 0.02) \times 10^{-4}$	$(4.89 \pm 0.77) \times 10^{-5}$	$(2.68 \pm 0.81) \times 10^7$	37.3 ± 11.3

Table 4.1 - Kinetic and equilibrium constants obtained from the SPR analysis of the NTS-1A/NT Interaction using the two state conformational change model. The equilibrium constant, K_A, was calculated from the rate constants using the equation $K_A = K_A1\ (1 + K_A2)$ where $K_A1 = k_{on}1 / k_{off}1$ and $K_A2 = k_{on}2 / k_{off}2$ [96].

Variation of analyte injection time cannot differentiate between a conformational change model and heterogeneity in the analyte. However, fitting of the heterogeneous analyte model to the data does give added support to a conformational change model. The fit resulted in a high affinity and a low affinity component, both with k_{on} values of the same order of magnitude. Whilst this cannot be used as definitive evidence for the conformational change model, a fit with vastly differing k_{on} values for the two components would have argued against the conformational change hypothesis.

4.4 Reconstituted NTS1-A samples

4.4.1 Reconstituted NTS1-A in the streptavidin-coated SA sensor chip

4.4.1.1 Method

Reconstituted samples of NTS1-A were prepared as per the protocols set out in 3.5. Surface plasmon Resonance (SPR) analysis was carried out using a Biacore 2000 biosensor instrument (Biocore AB) at 25 °C. 200 RU of biotinylated NT in HBS-EP buffer (Biocore AP) was immobilized on a streptavidin-coated chip (Biosensor SA, Biacore), with 200 RU of biotinylated 'scrambled' NT immobilized in the same manner to a control flow cell. Analyte was NTS1-A reconstituted into BPLs, extruded through a 100 nm membrane, in 50 mM Tris,

150 mM NaCl, 1 mM EDTA, pH 7.4. Interaction experiments were carried out at a flow rate of 5 $\mu l.min^{-1}$, with the sample racks maintained at 5 °C throughout, the baseline buffer was the same as that in which the reconstituted NTS1-A vesicles were contained.

4.4.1.2 Results

The concentration of NaCl was investigated to determine whether increasing ionic strength of the solution would reduce the non-specific interaction of the lipid with the surface. A series of injections were made of three different concentrations of blank liposomes, not containing NTS1-A in buffer containing 50 mM NaCl (Figure 4.9).

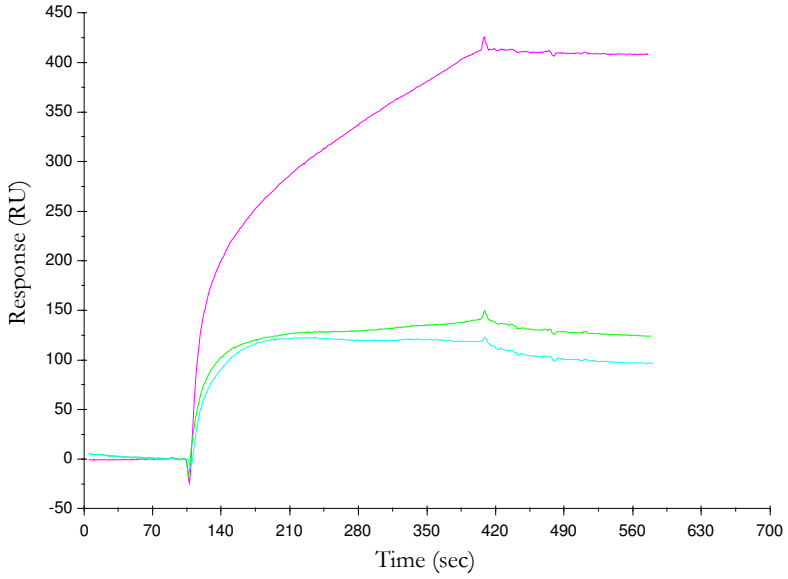

Figure 4.9 – Analysis of how the sensor chip SA interacts with lipid vesicles in buffer containing 50 mM NaCl at three different concentration: in Pink 0.4 $mg.ml^{-1}$; in Green 0.2 $mg.ml^{-1}$ and in Cyan 0.1 $mg.ml^{-1}$.

The same experiment was also carried out in buffer containing 150 mM NaCl (Figure 4.10).

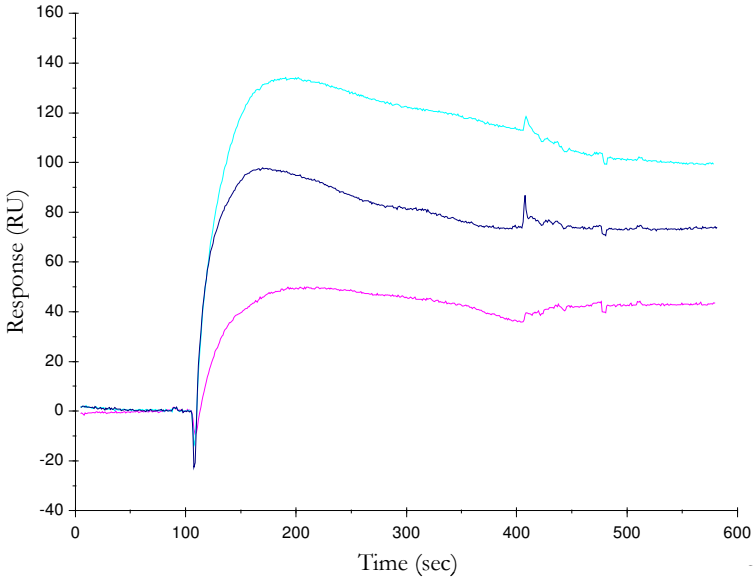

Figure 4.10 - Analysis of how the sensor chip SA interacts with lipid vesicles in buffer containing 150 mM NaCl at three different concentration: in Cyan 0.4 mg.ml^{-1}; in Blue 0.2 mg.ml^{-1} and in Pink 0.1 mg.ml^{-1}.

These two SPR traces show that there is a significant reduction in the non-specific interaction with the surface of immobilised Bio-NT on increasing the NaCl concentration to 150 mM from the 50 mM which is the final concentration of salt in the detergent solubilised NTS1-A and indeed after reconstitution. The response seen at the highest concentration, 0.4 mg.ml^{-1} of BPLs, is nearly three times less in 150 mM NaCl buffer than in the buffer with 50 mM NaCl and is lower throughout the concentration range. 150 mM NaCl is a more physiologically relevant concentration and the added ionic strength is clearly helping to discourage non-specific interactions of the liposomes which is highly desired in an SPR experiment. Samples were exchanged into a higher salt concentration by centrifugation of the proteoliposomes and resuspension in buffer containing the desired concentration.

The sensor chip SA has a dextran matrix bound to the surface with the streptavidin coating it in order to increase the surface area over which the interaction can occur, increasing the level

of response which one can see from any given sample. This benefit though has been designed for use with smaller globular proteins and certainly not for structures the size of lipid vesicles to interact with. After reconstitution the state of the lipid structures in the sample are of an unknown vesicular size, though this can be changed by extrusion of the suspension. To assess how vesicular size could effect the analysis of reconstituted NTS1-A, blank liposomes were passed over the sensor surface at the same concentration (0.4 $mg.ml^{-1}$) but with two different average vesicular sizes; the results are shown in Figure 4.11.

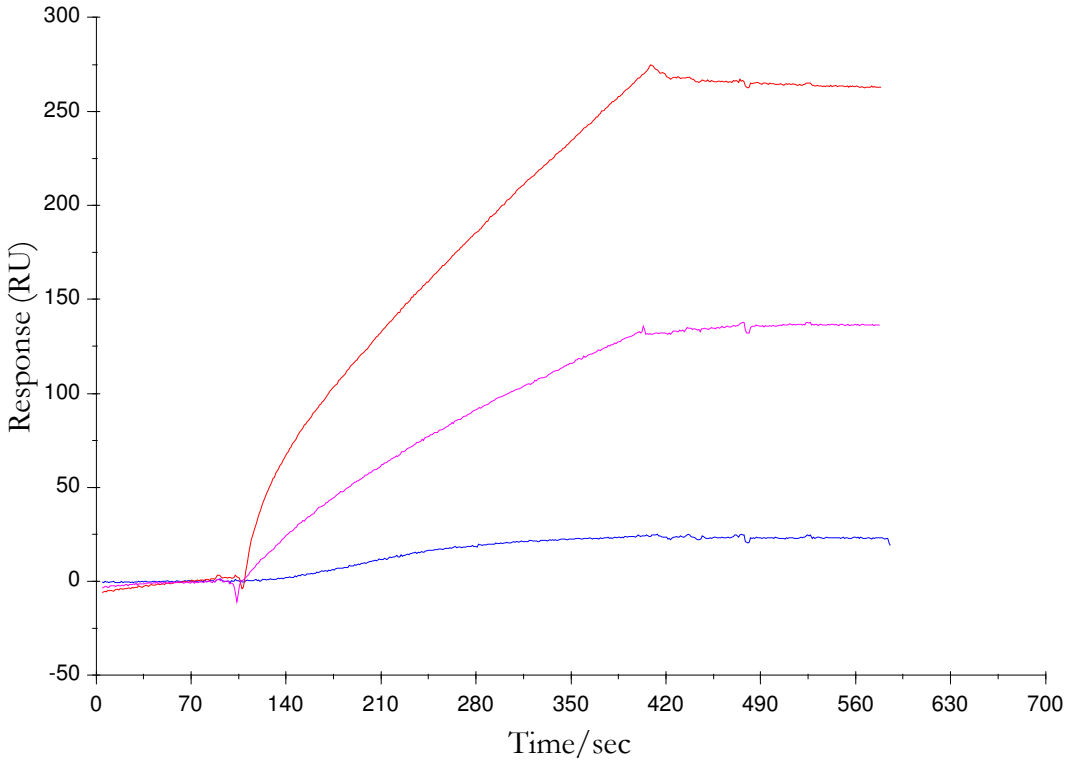

Figure 4.11 – Analysis of how the sensor chip SA interacts with lipid vesicles of two different sizes and two different immobilisation levels. Samples were injected at 5 $\mu l.min^{-1}$ in the buffer in 4.4.1.: in Red are BPLs extruded through a 0.4 μm membrane passed over 250 RU of immobilised Bio-NT; in Pink are BPLs extruded through a 0.4 μm membrane passed over 100 RU of immobilised Bio-NT and in Blue are BPLs extruded through a 0.1 μm membrane passed over 250 RU of immobilised Bio-NT.

It is clear from Figure 4.11 that the smaller vesicular size causes much less of a non-specific response to the immobilised Bio-NT surface, even compared to the 400 nm size over half the immobilised ligand; as average vesicular size of 100 nm gave less than 25 RU of non-specific interaction. It was therefore decided to extrude the reconstituted proteoliposomes through a 0.1 μm membrane before assessing the interaction with this SPR surface.

A series of eight injections, of NTS1-A reconstituted into BPLs of four different concentrations, were made starting with the lowest up to the highest, which is repeated, and then back to the lowest concentration again. As in 4.3 there was a control surface with scrambled Bio-NT and a experimental surface with Bio-NT, which the solutions were injected over, the results are shown in Figure 4.12.

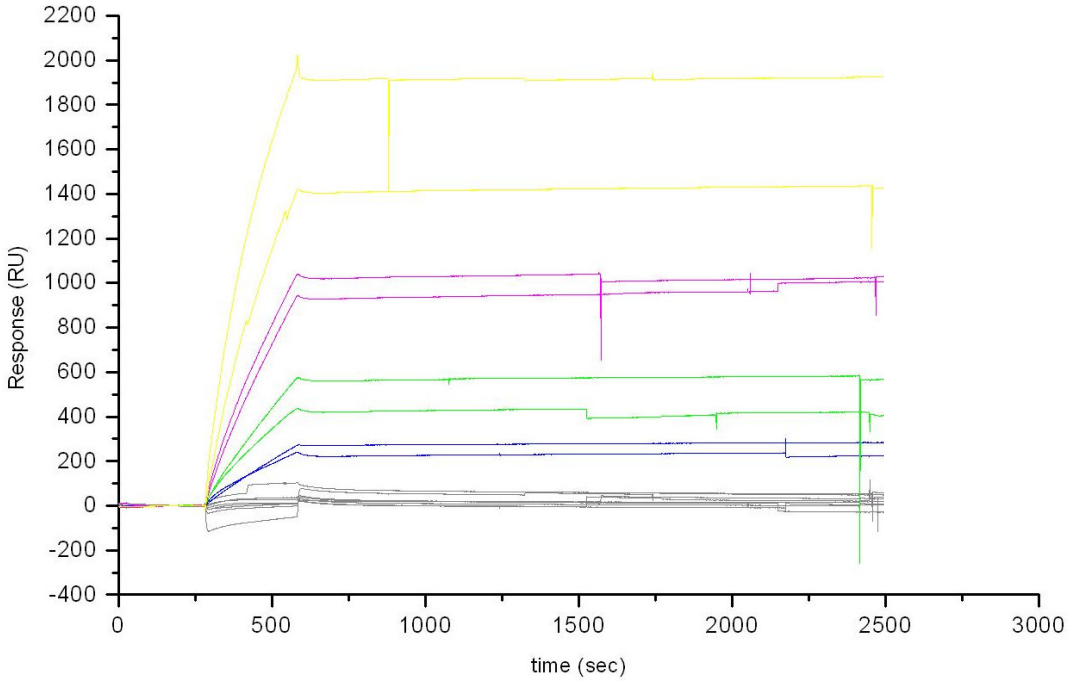

Figure 4.12 – Kinetic analysis of the NT/ NTS1-A interaction. Data for the interaction between reconstituted NTS1-A in lipid vesicles of an average diameter of 100 nm across and Bio-NT. Various concentrations of NTS1-A activity were injected at 5 $\mu l.min^{-1}$: in yellow 75 nM, in pink 38 nM, in green 19 nM and in blue 9 nM. The curves shown have the non-specific interaction with a flow cell containing scrambled Bio-NT subtracted from them, but this interaction level is also shown in grey on the graph as well to show it is minimal.

The first observation from this graph is that there was a specific, concentration dependent, response from the analyte, proteoliposomes, interaction with the ligand, Bio-NT. This constitutes direct evidence for a specific interaction between NTS1-A, reconstituted into BPLs, and its ligand NT supporting the evidence, from radio activity assay, of this found in 3.5. The second observation is that the response does not decay to any significant degree, as seen in the detergent interaction (Figure 4.5), precluding any kinetic modelling of the interaction from these data.

The results indicate that a specific interaction is forming, i.e. lipid bound NTS1-A is associating with the Bio-NT, on the surface of the sensor chip, but then this interaction is somehow held in place. The dextran matrix present on the sensor chip SA, a "sponge" or "course brush" of polysaccharides designed to increase the amount of ligand immobilization possible, in this instance though, the matrix could be hindering dissociation. Proteoliposomes associate with ligand and are tethered into the matrix of dextran for the duration of this interaction and it appears that they are "popping" and depositing themselves onto the sensor surface. Which could be described as a ligand mediated deposition of proteoliposomes onto the senor surface over the course of the injection time, preventing dissociation in terms of the NTS1-A/NT interaction.

In order to obtain kinetic data from this system a competition experiment was preformed where NT was added into the samples, all with the same concentration of NTS1-A in BPLs, before injection in varying concentration of NT to produce a plot similar to a Scatchard analysis, using the level of specific response observed. This experiment failed due to a huge baseline drift across its time course highlighting a poor regeneration condition (Figure 4.13).

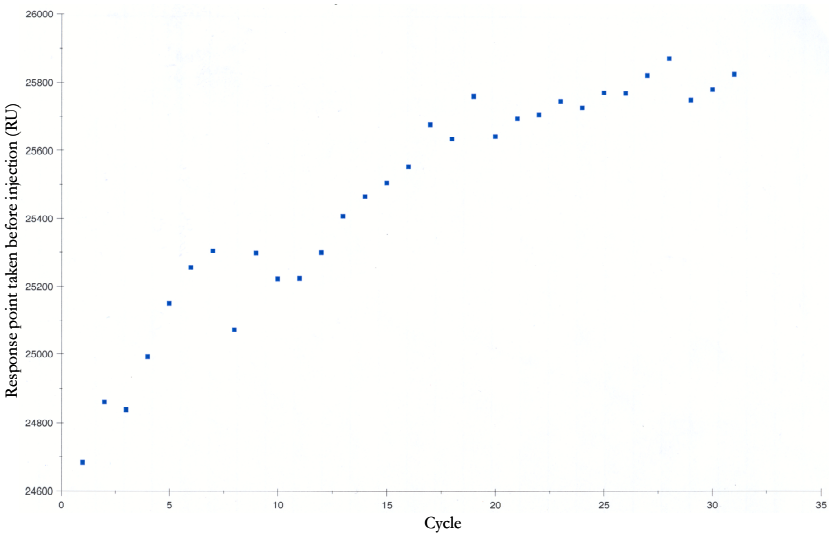

Figure 4.13 – A graphic to show baseline drift across 32 injection cycles of 19 nM of NTS1-A in proteoliposomes.

Path-finding a new regeneration condition with a variety of solvents, detergents, acids, bases and ionic strengths results in either a similar unsatisfactory baseline recovery or in the removal of Bio-NT and scrambled Bio-NT from the sensor surface. It was therefore decided to use a chip that would remove the two problems observed with the streptavidin-coated chip Biosensor SA by going to a planar surface, which removes the dextran matrix from causing possible disruptions to the proteoliposomes, and a covalent interaction with the sensor surface for the ligand in the form of thiol-coupling to the C1 sensor chip.

4.4.2 Reconstituted NTS1-A in the thiol-coupled C1 sensor chip

4.4.2.1 Methods

Reconstituted samples of NTS1-A were prepared as per the protocols set out in 3.5. Surface plasmon Resonance (SPR) analysis was carried out using a Biacore 2000 biosensor instrument (Biocore AB) at 25 °C. 100 RU of cystinylated NT (Biocore AP) was immobilized on a chip (Biosensor C1, Biacore), with 100 RU of cystinylated 'scrambled' NT immobilized in the same manner to a control flow cell. Analyte was NTS1-A reconstituted into BPLs, extruded

through a 100 nm membrane, in 50 mM Tris, 150 mM NaCl, 1 mM EDTA, pH 7.4. Interaction experiments were carried out at a flow rate of 5 $\mu l.min^{-1}$, with the sample racks maintained at 5 °C throughout; the baseline buffer was the same as that in which the reconstituted NTS1-A vesicles were contained.

4.4.2.2 Results

4.4.2.2.1 Synthesis of Cystinylated NT and Cystinylated scrambled NT

Here a cystine was added to the N-terminus of NT to produce Cys-NT (pCys-Glu-Leu-Tyr-Glu-Asn-Lys-Pro-Arg-Arg-Pro-Try-Ile-Leu-OH) in order to facilitate thiol linkage to planar SPR chip surfaces and spin labels, again using the same theory as with the biotin moieties with the modification from wild type NT being away from the 8-13 region, will have little, if any, effect on the activity of the ligand. The synthesis was carried out at the 0.2 mmol scale with a theoretical maximum yield of 0.359 g. A milder cleavage reaction was used to remove the peptide from the resin and its side chain protection; 82.5% TFA, 5% phenol, 5% H_2O, 5% thioanisole and 2.5% EDT left on the resin over night before a work up in the same manner as the other synthesis. The HPLC analysis of the lyophilised cleavage product was carried out in the presence of dithiotheritol (DTT) to maintain the reduced state of the cysteine side chain, the results of which are shown in Figure 4.14.

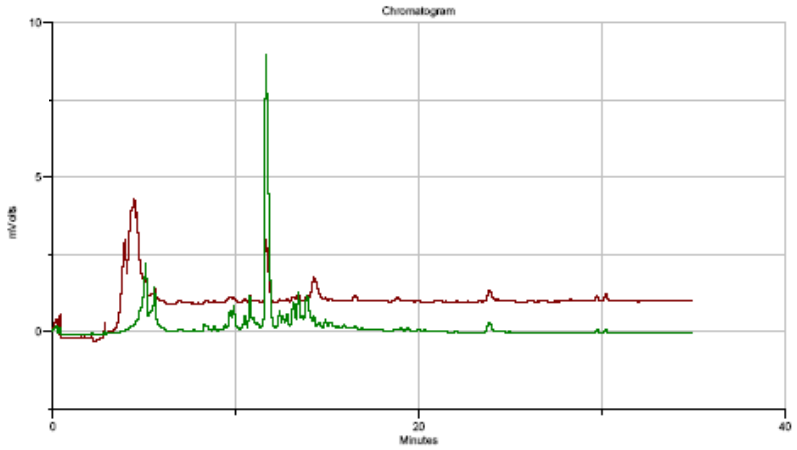

Figure 4.14 – Reverse phase HPLC trace of the lyophilised products from the solid phase synthesis of cys-NT, with the absorption at 254 nm as a green line and the absorption at 280 nm as a red line.

The HPLC trace shows multiple peaks from the lyophilised cleaved product from this synthesis; this is why the fractionation markings have been removed from this trace. The largest peak at approximately 12 minutes into the run was mass spectrographed using ESI positive, the results of which can be seen in Figure 4.15

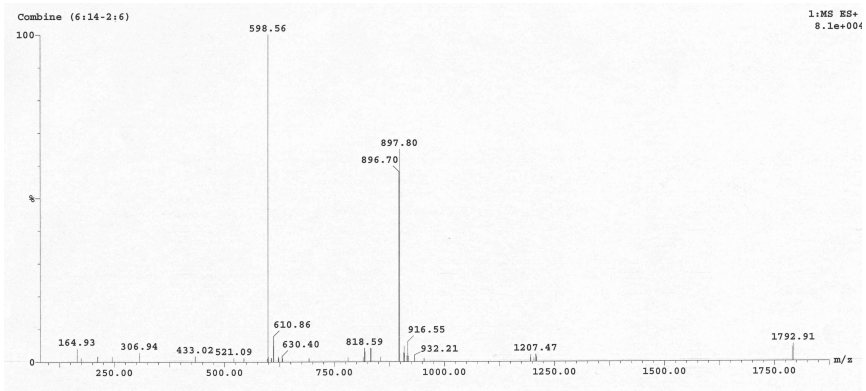

Figure 4.15 - Electro spray ionisation mass spectrum of the dominant peak in the HPLC purification of solid phase synthesised Cys-NT.

The mass spectrum of this peptide shows the two dominant peaks common to NT derivative peptides, the doubly charged ionic species at 897.8 and the triply charged species at 598.56 of Cys-NT, though this mass spectrum unusually shows the parent ion at 1792.91 as well. The yield from one of these syntheses was 91% of the theoretical maximum 0.325g.

Scrambled Cys-NT (pCys--Leu-Tyr-Asn-Arg-Pro-Arg-Pro-Tyr-Leu-Glu-Ile-Lys-Glu-OH) was produced in the same reasons as Scrambled Bio-NT, as a control peptide for SPR chips where the ligands are deposited onto the sensor surface by means of a thiol linkage. The peptide was treated in exactly the same manner as Cys-NT. This synthesis was carried out at the 0.1 mmol scale, as with the scrambled Bio-NT this peptide is only used as a control in SPR experiments, giving a theoretically maximum yield of 0.179 g. The HPLC purification trace of the lyophilised resin cleavage product is shown in Figure 4.16.

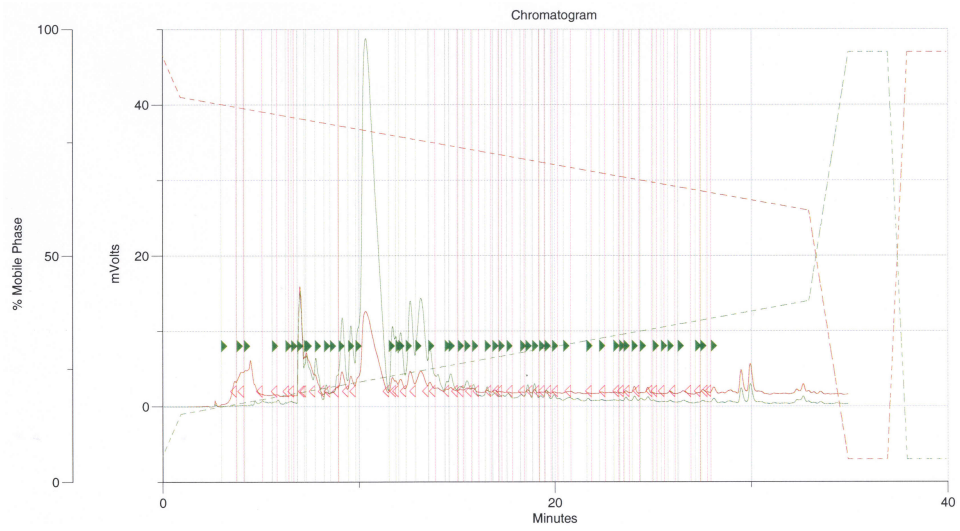

Figure 4.16 - Reverse phase HPLC trace of the lyophilised products from the solid phase synthesis of scrambled Cys-NT, with the absorption at 254 nm as a solid green line and the absorption at 280 nm as a solid red line and the percentages of H_2O and acetonitrile in dashed red and green lines respectively.

The HPLC trace shows multiple peaks from the lyophilised cleaved product from this synthesis. The highest peak at approximately 12 minutes into the run, fraction 14, was

analysed using a mass spectrometer (ESI positive), the results of which can be seen in Figure 4.17.

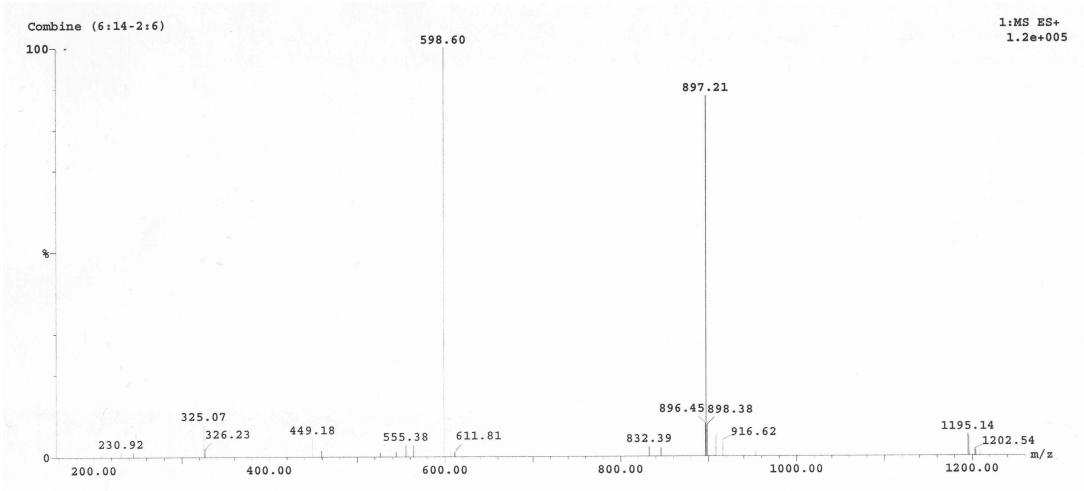

Figure 4.17 – Electro spray ionisation mass spectrum of the dominant peak in the HPLC purification of solid phase synthesised Cys-NT.

The mass spectrum of this peptide shows the two dominant peaks, common to NT derivative peptides, the doubly charged ionic species at 897.8 and the triply charged species at 598.56 of scrambled Cys-NT. The yield from one of these syntheses was 93 % of the theoretical maximum 0.167 g.

4.4.2.2.2 Analysis of the interaction of reconstituted NTS1-A's with thiol coupled C1 sensor chips

A series of eight injections, of NTS1-A reconstituted into BPLs of four different concentrations, were made starting with the lowest up to the highest, which is repeated, and then back to the lowest concentration again; the results are shown in Figure 4.18

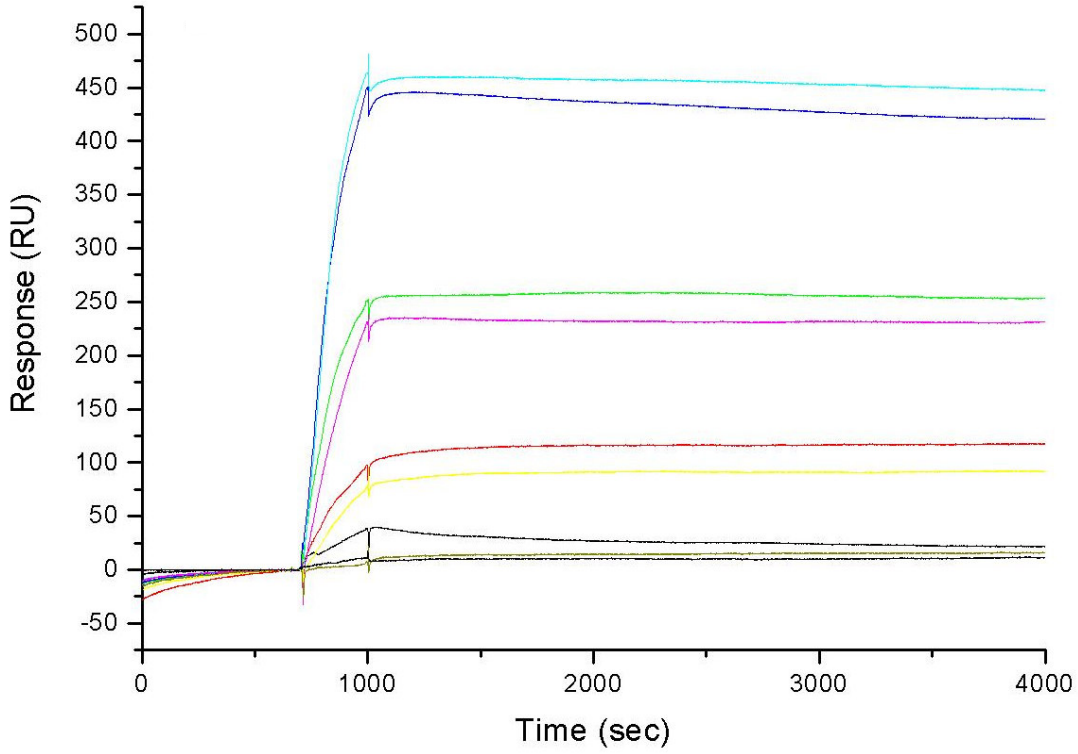

Figure 4.18 – Kinetic analysis of the NT/ NTS1-A interaction, data for the interaction between reconstituted NTS1-A in lipid vesicles of an average size of 100 nm across and Cys-NT. Various concentration of NTS1-A were injected at 5 $\mu l.min^{-1}$: (with first across the chip then 2nd at each concentration respectively) in Blue and Cyan 38 nM, in Pink and Green 19 nM, in Brown and Yellow 9 nM and in Grey and Black 5 nM. The curves shown have the non-specific interaction with a flow cell containing scrambled Cys-NT subtracted from them.

Again a specific binding response was seen using the C1 chip and Cystinylated ligand and control ligand for SPR analysis of NTS1-A proteoliposomes. The response is less than on the SA chips but this is expected as less ligand is immobilised on the planar surface than can be immobilised on the dexran matrix of SA chips. This experiment included a long, 50 minute, dissociation phase in the hope to obtain kinetic information from the reconstituted receptor, and in some instances it does appear that the interaction level is decreasing but certainly not in every case and it would be difficult to determine the average weight of the interacting body in any case.

The real bonus of using this chip for studying an interaction with proteoliposomes is the covalent linkage of the ligand to the surface, thus allowing the use of relatively harsh

regeneration conditions without the worry of removing immobilised ligand as with the SA chip, and baseline drift over the course of the experiment was within acceptable limits for the hardware (Figure 4.19).

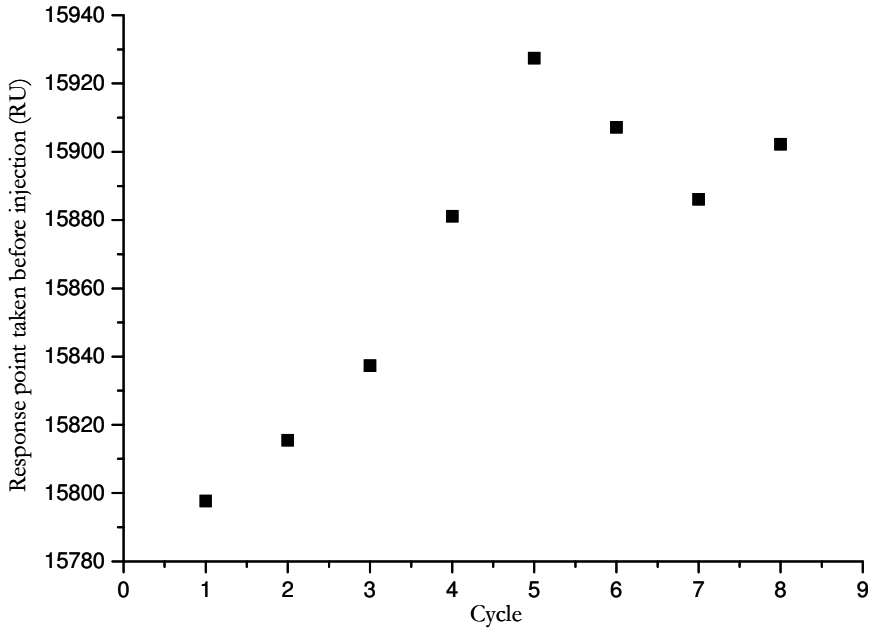

Figure 4.19 – A graphic to show baseline drift across 8 injection cycles of NTS1-A in proteoliposomes from the above experiment.

Therefore this sensor surface would allow for the long competition experiments, if there are still problems seen with the dissociation of the interaction observed in this case. Though not as marked as in the chips containing a dextran matrix, the proteoliposomes seem to still deposit on the surface, after association with immobilised ligand, in a manner that simple flow of baseline buffer over the surface of the chip will not remove to any significant degree.

4.5 Discussion

This study has yielded the first SPR kinetic data for a full length, detergent-solubilised ligand-binding GPCR. Using the large receptor molecule as the analyte overcomes the problem of

the small responses encountered in the reverse orientation. This technique will have useful applications to other suitable GPCR systems, not only providing insights into the kinetics and binding mechanisms involved in ligand binding, but also in the search for novel ligands and in the more rigorous optimisation of detergent solubilisation procedures than is currently possible using conventional techniques. Study of possible conformational changes which occur upon ligand binding to NT receptors and other GPCRs will be crucial if we are to gain an understanding of how ligand binding at the cell surface is coupled to downstream signalling events.

Chapter 5 Electron Spin Resonance studies to investigate the mobility of NT at its binding site on NTS1-A

5.1 Introduction

Electron spin resonance (ESR), like NMR, relies on the Zeeman Effect caused by the interaction of unpaired electrons with an external magnetic field. In both ESR and NMR, the sample material is placed in a strong static magnetic field, B_0, for excitation and exposed to an orthogonal low- amplitude high-frequency field for detection. ESR usually requires microwave-frequency radiation (GHz), while NMR is observed at lower radio frequencies (MHz). With ESR, energy is absorbed by the sample when the frequency of the radiation is appropriate to the energy difference between two spin states of the electrons in the sample, but only if the transition satisfies the appropriate selection rules. Most materials are diamagnetic and have net zero electronic spin and, thus, are ESR silent, but some are paramagnetic and can provide an ESR signal under the correct conditions.

As the electron has a magnetic moment, μ, it will have a state of lowest and highest energy when μ is aligned against the magnetic field. The two states are labelled by the projection of the electron spin, M_s, on the direction of the magnetic field, because the electron has a spin ½;

the parallel state is designated as M_s = - ½ and the antiparallel state is designated as M_s = + ½. From this we obtain the most basic equation of ESR:

$$\begin{aligned}\Delta E &= g\mu_B B_0 M_s \\ &= \pm\tfrac{1}{2} g\mu_B B_0\end{aligned}$$

Equation 5.1

And so:

$$\begin{aligned}\Delta E &= h\nu \\ &= g\mu_B B_0\end{aligned}$$

Equation 5.2

where g is the g-factor which is a proportionality constant approximately equal to 2.0023 for the free electron, but varies (between 1 and ~5) depending on the electronic configuration of the radical or ion. μ_B is the Bohr magneton, which is the natural unit of electronic magnetic moment equal to 9.2741 x 10^{-24}A.m^2. These equations lead to two conclusions: the two spin states have the same energy in the absence of a magnetic field, and the energies of the spin states diverge linearly as the field strength increases. By applying a constant field and scanning the frequency of electromagnetic radiation, or the reverse by keeping the frequency of the electromagnetic radiation constant and scanning the magnetic field, an absorption spectrum can be obtained. A peak in the absorption will occur when the magnetic field satisfies equation Equation 5.2 and the energy difference matches the energy of the applied radiation.

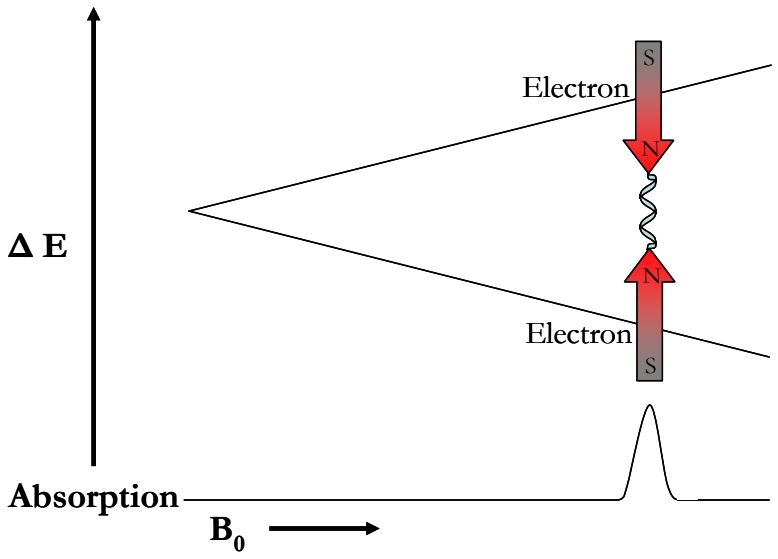

Figure 5.1 - Variation of the spin energies as a function of the applied magnetic field.

The tuning event is called the field of resonance, and is not a unique "fingerprint" for identification of a compound because spectra can be acquired at several different frequencies. The g-factor, being independent of microwave frequency, is much better for that purpose (Equation 5.3).

$$g = h\nu / \mu_B B_0$$

Equation 5.3

Molecular motion of a nitroxide spin-labelled molecule is related quantitatively in ESR to the rotational correlation time (τ_C), the derivation of expressions for which, for fast (μs-ps) motion, were given by McConnell [97]:

$$\tau_C = \pi\sqrt{3}W_0 \Big/ b \left[4\Delta\gamma H \Big/ 15 + b \Big/ 8 \right]^{-1} \left[W_{-1} \Big/ W_0 - 1 \right]$$

Equation 5.4

Here $\Delta\gamma$ is a constant that depends on the anisotropic g values of the nitroxide, b is a constant that depends on the anisotropic nitrogen hyperfine couplings (A^N), H is the laboratory magnetic field, and W_0 and W_{-1} are the widths of the mid- and high-field lines. When using the simplified parameters of Griffith *et al.* [98] for b and $\Delta\gamma$ with H maintained at 3400 gauss, W_{-1}/W_0 can be replaced with $(h_0/h_{-1})^{1/2}$, where h_0 and h_{-1} are the mid-field line height and the high-field line height of the first derivative absorption spectrum, respectively (Figure 5.2).

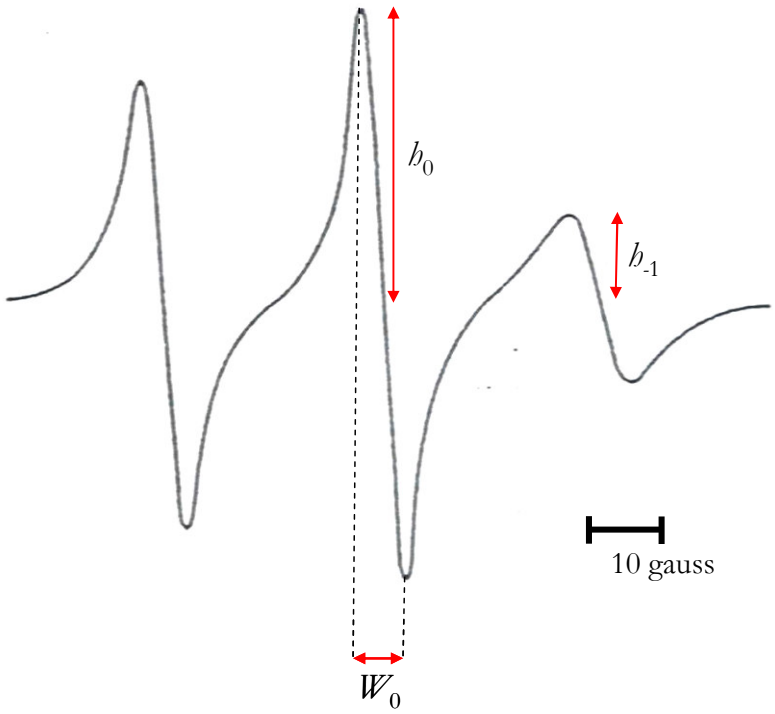

Figure 5.2 – ESR spectrum to illustrate the measurement used in Equation 5.5 for the determination of τ_c.

For a simple nitroxide in the fast motional regime, for which the g and A values are known, the expression reduces to:

$$\tau_C = 6.5 * 10^{-10} W_0 [(h_0 / h_{-1})^{1/2} - 1]$$

Equation 5.5

The expression exploits line broadening due to motion, assuming isotropic motion, where the ESR spectra reflect partial immobilization and the axial symmetry parameter of the spin label is not equal to one, as seen in the majority of the spectra in biological spin label ESR. The net motion is almost certainly somewhat anisotropic however, and therefore results in inaccuracies in the absolute calculation of τ_C. As a consequence of this, the numerical values may be off by as much as a factor of 2, but the relative values for the purposes of comparison are still very useful.

Electron spin resonance is a powerful technique for determining rotational freedoms of spin-labelled molecules and has found particular application to biological membrane systems. The method has been successfully employed to identify, amongst other things, the preferential immobilisation of lipids by rhodopsin in bovine rod outer segment membranes [99], the depth of penetration of hapten in Fv [100] and to determine the rotational mobility of a membrane-integral transport protein [101].

Understanding the structure-activity relationship between activating ligand and target protein is particularly desirable in advancing the process of understanding receptor activation and rational drug design. NT, which is endogenous as a 13-amino acid peptide, has been found to require only its C-terminal hexapeptide sequence to bind its receptor proteins [95]. This truncated peptide, termed $NT_{(8-13)}$, binds with a higher affinity than the native ligand, and has

subsequently provided the focus for design of NT receptor antagonists for treatment of, amongst other conditions, pain [33, 34], obesity [39, 40], schizophrenia [37, 38], and cancer [41]. Whereas the structure of $NT_{(8-13)}$ is highly flexible, the structure of the non-peptide antagonist SR 48692 is rigid in solution (Quere 1996). Although the role of the N-terminal heptapeptide is unclear, it is of interest to assess the influence of this reportedly-redundant portion of the peptide in stabilisation of ligand secondary structure and dynamics in the receptor binding site, here nitroxide spin-label studies could be informative as explored here.

5.2 Aims of this Study

In this study, spin-labelled full-length NT analogues and NTS1-A were observed by conventional ESR methods in order to compare the relative mobility of the N-terminal seven amino acids of NT to gain an insight into the binding of this important neuropeptide to its GPCR.

5.3 Methodology

5.3.1 Production of spin labelled NT

The method for spin labelling NT is shown in 2.7.1. the reaction is shown below (Figure 5.3).

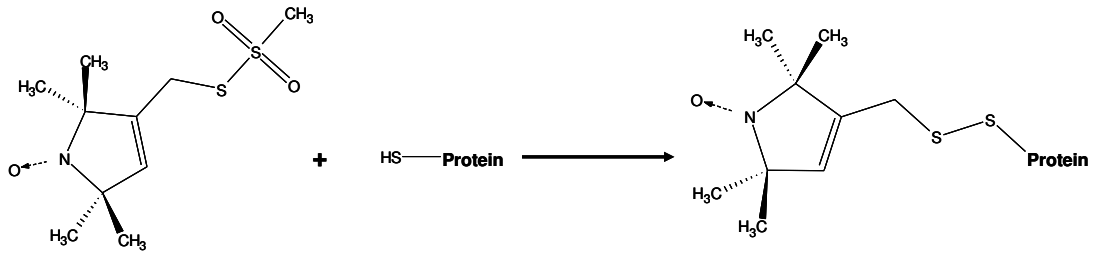

Figure 5.3 – Reaction of a spin label, a methanethiosulphonate derivative, to generate a nitroxide side chain.

Two peptides were synthesized with a nitroxide spin label within the N-terminal seven amino acids of NT in order to investigate the dynamics of this region. The first, NTspin0, is Cys-NT (4.4.2.2.1) modified with methanethiosulphonate as shown in Figure 5.4. NTspin0 will provide an insight into the motional characteristics of the N-terminus of NT whilst it is bound to the receptor, whether it is, for instance, uninvolved with binding and remains unattached to the receptor and largely mobile, if it sits in a channel or grove in the receptor surface which confers slight motional restriction or if the N-terminus is bound to the receptor directly in some manner inhibiting any large motion of the spin label.

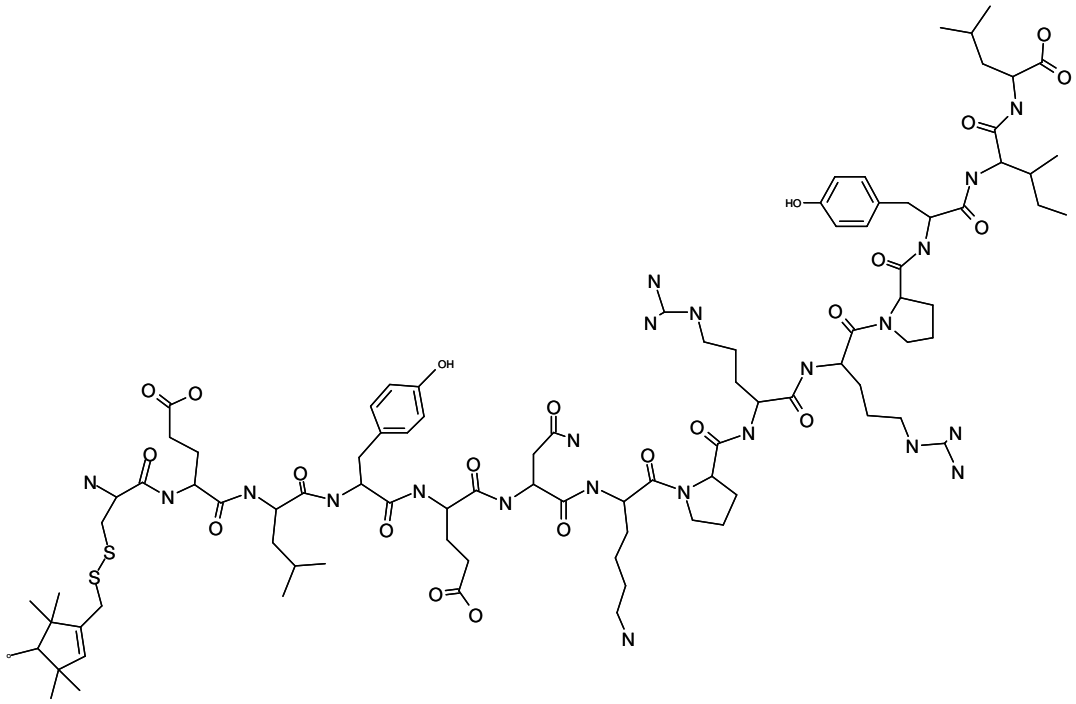

SlCys-Glu-Leu-Tyr-Glu-Asn-leu-Pro-Arg-Arg-Pro-Try-Ile-Leu

Figure 5.4 – The chemical structure of NTspin0.

Placing the spin label here is unlikely to affect the binding of NT to its receptor as has been seen in 3.3.3 where receptor binds to biotinylated NT bound to a chromatography resin and Chapter 4 where NTS1-A binds to NT immobilized on the surface of SPR chips.

The second nitroxide spin labelled peptide NTspin6 has this sixth amino acid, lysine in the native NT sequence, substituted for a cysteine reside which was then modified with methanethiosulphonate as shown in Figure 5.5.

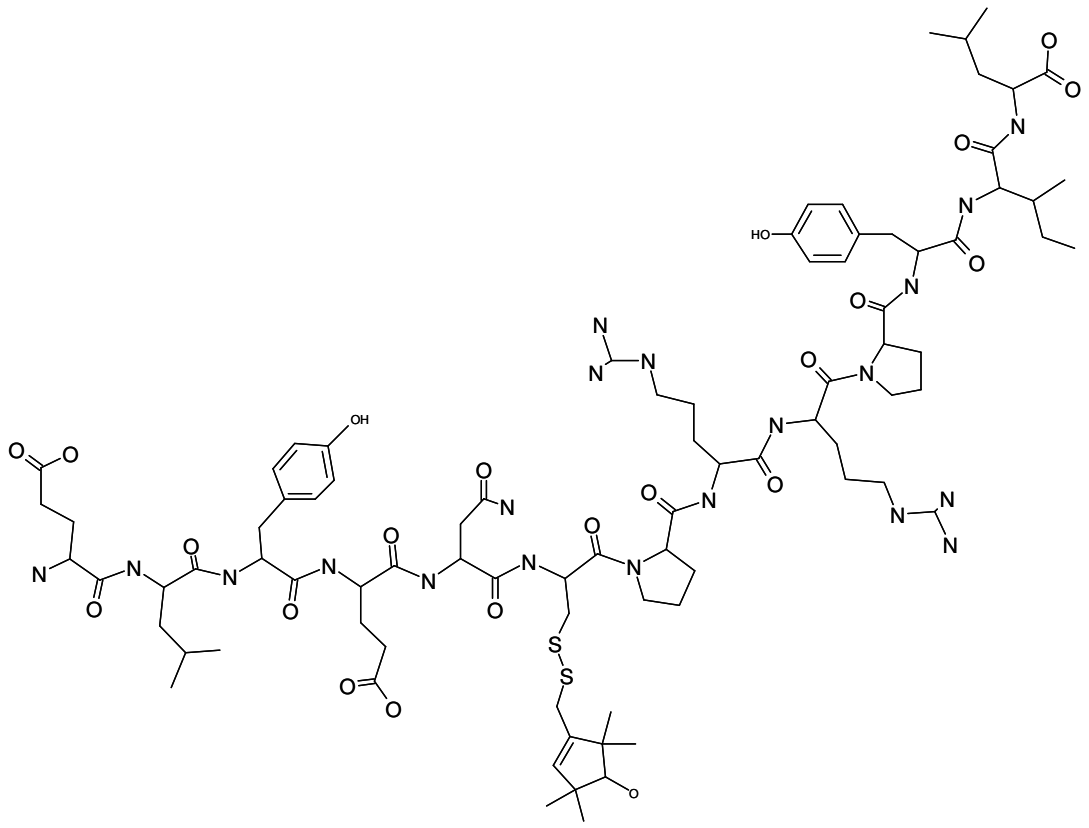

Glu-Leu-Tyr-Glu-Asn-SlCys-Pro-Arg-Arg-Pro-Try-Ile-Leu

Figure 5.5 – The chemical structure of NTspin6.

NTspin6 was synthesized using the methods from 2.5.2 and the spin label modification was carried out using the methods in 2.7.1 as above. This peptide was synthesized to investigate the opposite end of the 1-7 region of NT to NTspin0. The spin label in this peptide occurs just before the first proline residue in the sequence, which in solution were found to be the only constant structural element exhibiting *cis/trans* isomerisation [43, 102]. This second spin labelled NT analogue will give an indication, when compared with NTspin0, of the overall motion of the 1-7 region and whether the first proline is behaving as a flexible hinge attached to the rigidly bound 8-13 region or if it is held bound to the receptor. The substitution of a

lysine residue with spin labelled cysteine, is not a conservative change to NT and although this change has been made outside the 8-13 region, critical for ligand binding, the added steric bulk of the spin label could interfere with binding interactions within the 8-13 to the receptor.

5.4 Results

5.4.1 Production of Spin labelled Peptide

NTspin0, the full length native neuropeptide with an additional, spin labelled, cystine residue on the N-terminus, exactly the same as Cys-NT produced above (4.4.2.2.1) with the addition of the spin label has been synthesized. After spin labelling it is passed down a G10 resin (Amersham) size exclusion column to separate free spin label form spin labelled peptide, the trace for which is shown in Figure 5.6.

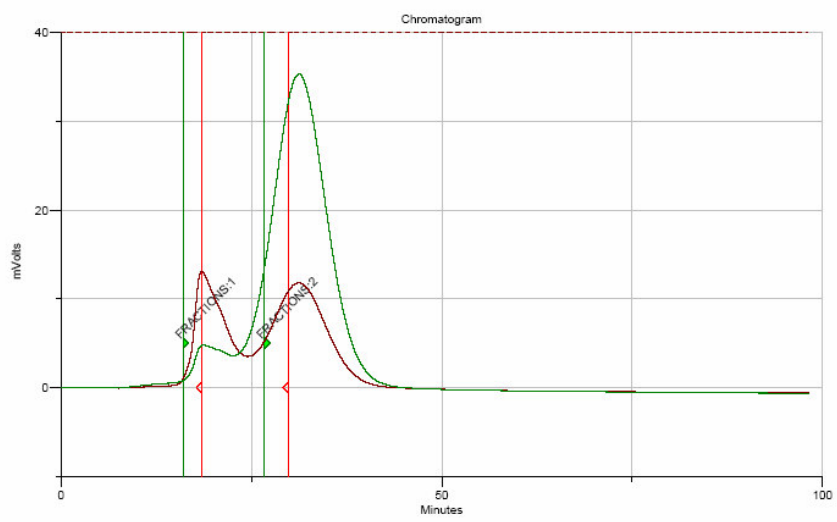

Figure 5.6 – FPLC trace for the G10 column separation of NTspin0 from free spin label, run in 20 % ethanol in Milli Q water, detecting at 254 nm in red and 280 nm in green.

The first peak corresponds to NTspin0 and was verified by electro-spray mass spectrum shown in Figure 5.7.

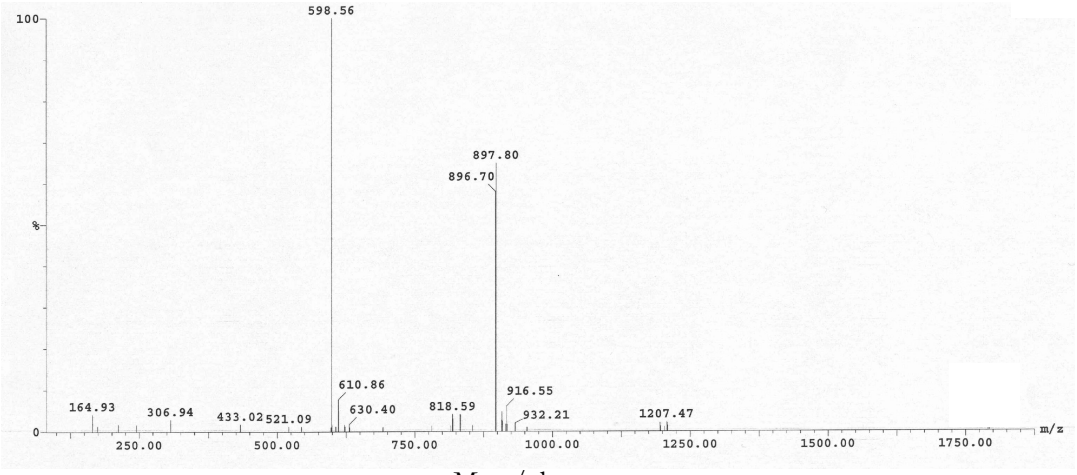

Figure 5.7 – Electro spray positive ionisation mass spectrum of the first peak from the FPLC purification of NTspin0 after the spin labelling reaction.

The mass spectrum of this peptide shows the two dominant peaks attributed to Cys-NT derivative peptide as the electro-spray ionisation appears to strip off the spin label, the doubly charged ionic species at 897.8 and the triply charged species at 598.56 of Cys-NT, with the mass of the parent ion of Cys-NT being 1792.9. Subsequent use of this peptide in ESR experiments shows that a spin labelled species is present as it produces an ESR spectrum (Figure 5.10 below).

NTspin0 was tested for binding activity with NTS1-A by using it as a competitor in the activity assay 3.4.4, replacing unlabeled native NT and was found to compete off the specific activity. This result was to be expected as it has already been seen that attaching streptavidin resin and an SPR chip at the N-terminus of this peptide does not preclude binding of NTS1-A (3.3.3 and Chapter 4 respectively).

NTspin6 was produced in a similar manner to NTspin0 and the FPLC trace for the G10 column separation of Ntspin6 from free spin label is shown below in Figure 5.8.

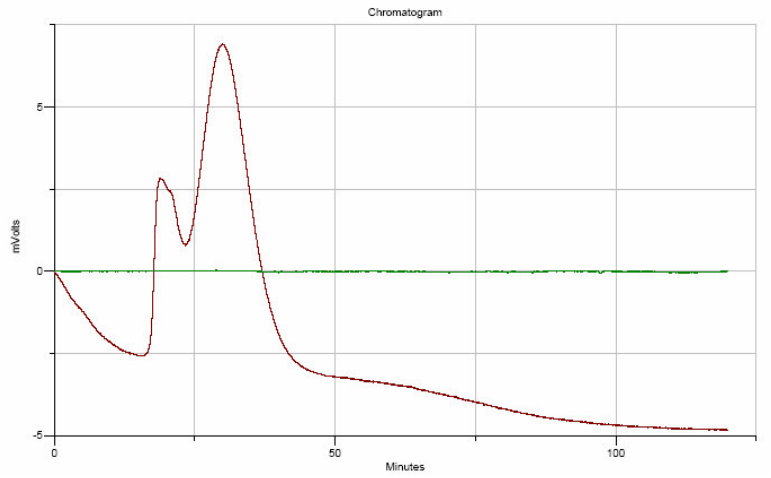

Figure 5.8 - FPLC trace for the G10 column separation of NTspin6 from free spin label run, in 20 % ethanol in Milli Q water, detecting at 254 nm in red the green line denotes a detector channel which is off.

As with the size exclusion chromatography of NTspin0, the first peak corresponds to NTspin6 and this was verified by electro-spray mass spectrometry (Figure 5.9).

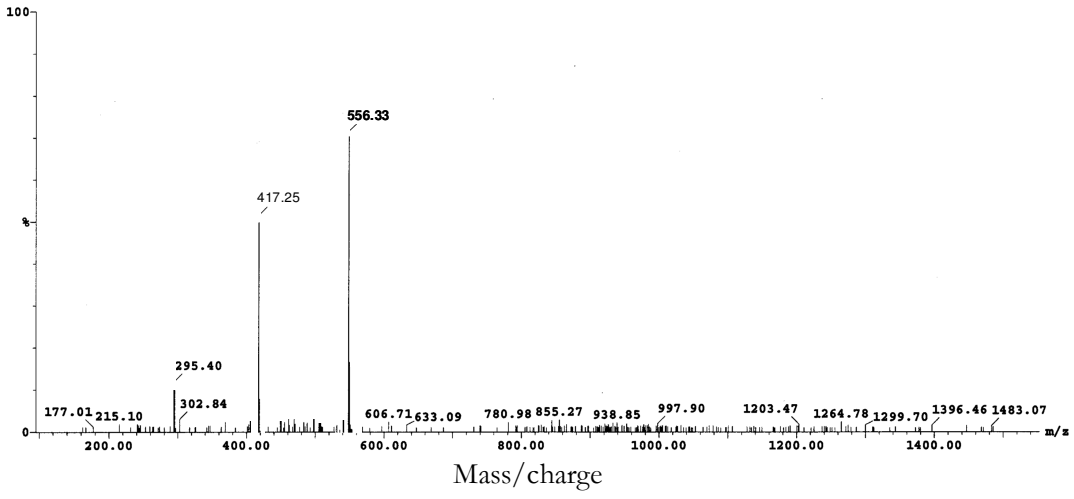

Figure 5.9 – Electro spray positive ionisation mass spectrum of the first peak from the FPLC purification of NTspin6 after the spin labelling reaction.

The mass spectrum of this peptide show the two peaks attributed to NT with the sixth amino acid substituted cystine; as with NTspin0 the electro-spray ionisation appears to strip off the

spin label, the triple charged ionic species at 556.33 and the quadrupally charged species at 417.25 of Cys-NT, with the mass of the parent ion being 1669. Subsequent use of this peptide in ESR experiments show that a spin labelled species is present, since it produces an ESR spectrum (Figure 5.13).

NTspin6 was used, as with NTspin0, in the activity assay in place of native NT used to determine the non-specific activity by competing off the specific binding radio labelled ligand (3.4.4) and was found not to compete for the binding sites with native NT. The steric bulk of the spin label so close to the 8-13 region, critical for activity, appears to prevent NTspin6 binding to the receptor, this peptide was therefore used as a control to see how a non-binding spin labelled peptide of similar properties reacts to the experimental conditions used.

5.4.2 ESR measurements of NTspin0 in the presence and absence of NTS1-A

Figure 5.10 shows the ESR spectra of NTspin0 in the absence (A) and presence (B) of detergent solubilized NTS1-A. Figure 5.10 (A), 2 nM NTspin0 in NT50 buffer (2.2.3), shows a degree of motional restriction (τ_c = 1.9 ns (Table 5.1)), approximately an order of magnitude slower than TEMPO in water (τ_c ~ 0.1 ns), of the spin label characterised by the decrease in size and broadening of the high field line in the spectrum, as in Equation 5.5 the ratio of the heights of the mid and high field lines, h_0 and h_{-1} respectively, will effect the τ_C.

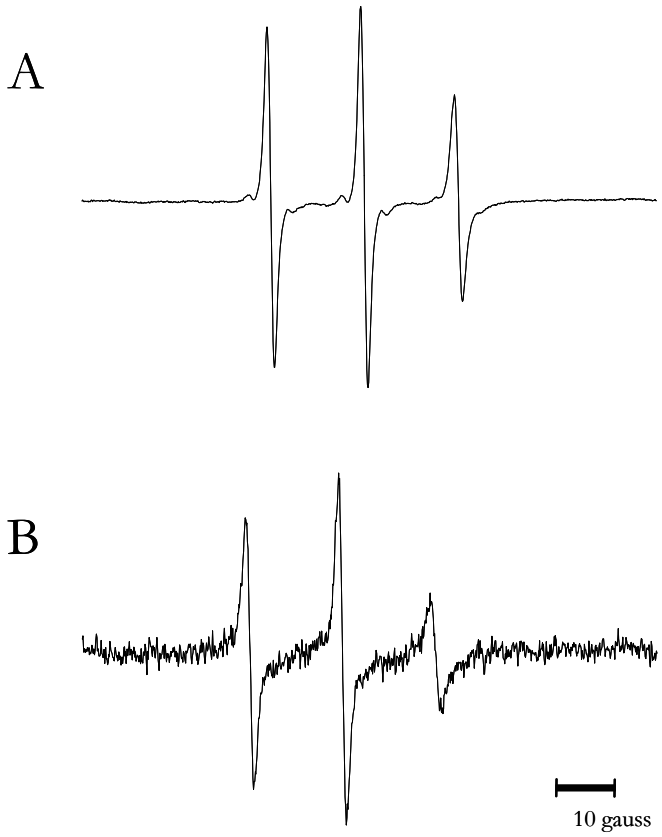

Figure 5.10 – ESR spectra of NTspin0: (A) 2 nM of NTspin0 in detergent buffer NT50 (2.2.3) and (B) 0.5 nM of NTspin0 in the presence of 1 nM NTS1-A in NT50 buffer, 16 acquisitions (40 s each acquisition).

The motional restriction of NTspin0 in the detergent buffer is very likely due to the glycerol in the NT50 buffer affecting the nitroxide spin labels motion, a well known side effect of glycerol in the presence of nitroxide spin labels [103], as it has been demonstrated, by ROSEY solution NMR, that the peptide has no structure in solution other than *cis/trans* isomerisation around the prolines [43, 102].

Figure 5.10 (B), 0.5 nM NTspin0 with 1 nM NTS1-A in NT50 buffer, shows that the presence of the receptor has an effect on the motion of the spin label (τ_c = 11.4 ns (Table 5.1)), with increased broadening of mid field and high field lines of the spectrum and a marked decrease in the intensity of the high field peak from Figure 5.10 (A). The broadened nature of this spectrum of NTspin0 bound to NTS1-A suggests that it is possible the spectrum has two contributing components, a more mobile sharper component akin to Figure 5.10 (A) and a broad motionally restricted element.

The same experiments were repeated with NTS1-A reconstituted into BPLs produced using the methods in (2.4.3), extruded through a 0.1 μm membrane before incubation with the spin labelled ligand (as in 4.4), with the control being BPL liposomes extruded through a 0.1 μm. Extrusion was carried out before the titration of spin labelled ligand into the sample in order to produce a uniform proteoliposomes/liposomes size and attempted to free any receptor occluded by possible stacking of membrane structures. The ESR spectra for these samples are shown in Figure 5.11.

The first spectrum, (Figure 5.11 (A)), NTspin0 with 0.1 μm diameter BPL liposomes, shows a similar profile to that of NTspin0 in NT50. There is motional restriction (τ_c = 2.4 ns (Table 5.1)), twice that seen from the presence of glycerol in buffer solution (Figure 5.10 (A)), indicated again by the broadening and decrease in intensity of the high field peak in relation to the spectra of the free nitroxide spin label. This motional restriction may be explained by the

observation that NT has been shown to associate in a non-specific manner with the membrane mimetic SDS [43]. This interaction, in turn, could cause a restriction in the movement of the spin label.

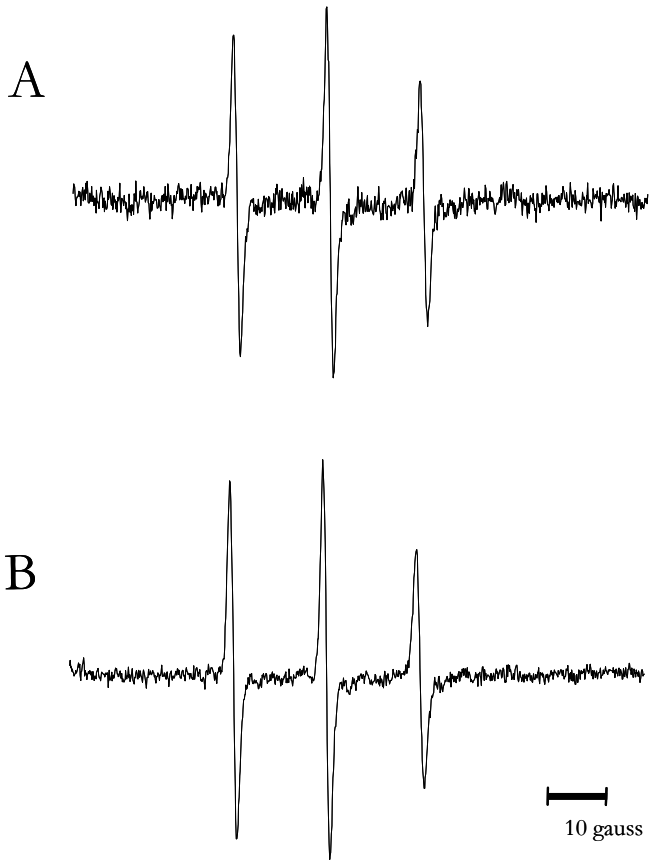

Figure 5.11 – ESR spectra of NTspin0: (A) 2 nM of NTspin0 with BPL liposomes in 50 Tris HCl 50 mM NaCl pH 7.4 buffer and (B) 0.5 nM of NTspin0 in the presence of 1 nM NTS1-A in BPL proteoliposomes in 50 mM Tris HCL, 50 mM NaCl pH 7.4 buffer, 16 acquisitions (40 s each acquisition).

The spectra in Figure 5.11 (B), NTspin0 in with NTS1-A in BPL proteoliposomes, shows a further motional (τ_c = 6.8 ns (Table 5.1)), restriction from the control spectra in Figure 5.11 (A), though this change is not nearly as marked as that which was seen in the detergent samples. This could be due to occlusion of the sites by the lipids, if less NTspin0 was able to bind to NTS1-A and the spectra was indeed two component, as it appears to be in the spectra

in Figure 5.10 (A), then there would be less contribution from the broad component and therefore the spectra as a whole would look as if the ligand was more mobile.

The correlation times for the samples containing NTspin0 were measured and are shown in the table in below (Table 5.1).

Sample	W_0	h_0	h_{-1}	τ_c (ns)
NTspin0 in NT50 buffer	1.0752	1	0.61797	1.9
NTspin0 in 50 mM Tris 50 mM NaCl with BPLs	1.173	1	0.58414	2.4
NTspin0 in 50 mM Tris 50 mM NaCl with NTS1-A in BPLs	1.3685	1	0.32156	6.8
NTspin0 in NT50 buffer with NTS1-A	1.56387	1	0.22239	11.4

Table 5.1 – Rotational correlation times (τ_c) of the NTspin0 ligand in both a detergent and lipid environment in the presence and absence of NTS1-A.

The table, of calculated values, clearly supports the conclusions made on the mobility level of the samples measured above. Curiously the presence of the BPL liposomes had more of an effect on the motion of the spin label than the presence of 30 % glycerol on the NT50 buffer (2.2.3) though as stated above, NT does associate with lipid memetics [43] and lipids (4.4).

To investigate whether there are indeed two components to the spectra where NTS1-A is present, the detergent samples were measured again, acquiring spectra with more scans (64) and a longer scan time (180 s) in order to improve the signal to noise ratio (Figure 5.12). Figure 5.12 (A) and (B) are longer acquisition equilivants of Figure 5.10 (A) and (B) with Figure 5.12 (C) showing a subtraction of (A) from (B), this broad difference spectrum appears to be two component and is indicative of the spin label being in two possible states: highly immobilised ($\tau_c \sim 300$ ns), motional restricted ($\tau_c \sim 2$ ns).

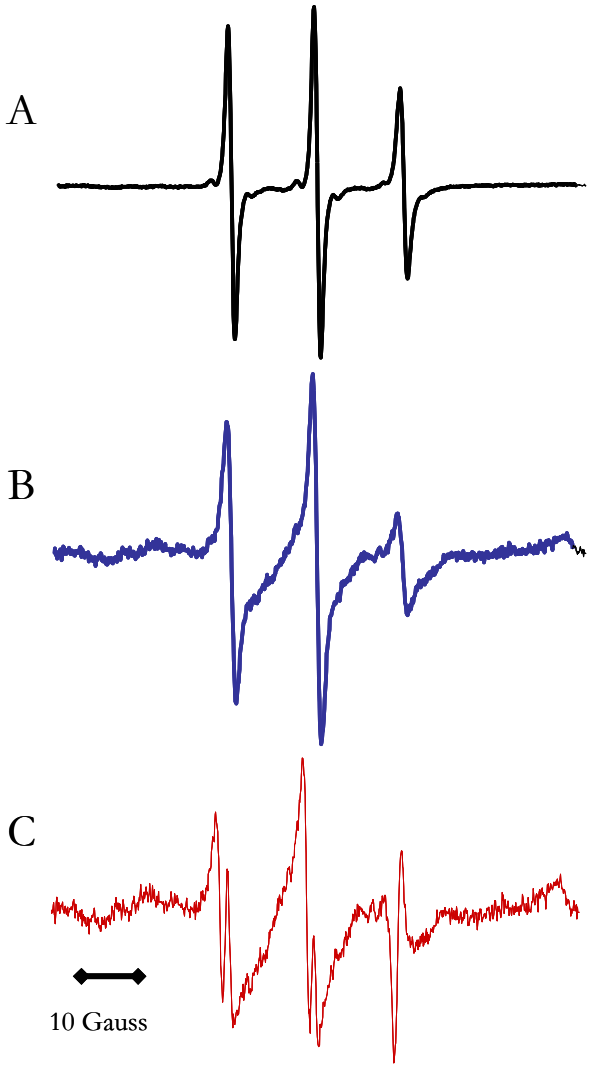

Figure 5.12 - ESR spectra of NTspin0: (A) in black 2 nM of NTspin0 in detergent buffer NT50 (2.2.3), (B) in blue 0.5 nM of NTspin0 in the presence of 1 nM NTS1-A in NT50 buffer and (C) in red a difference spectrum of A from B, spectra where obtained over 64 acquisitions of 180 s each.

A two component spectrum clearly arises from two conformational species of spin labelled ligand being present; this could arise for a number of reasons. It could be that there are two heterogeneous spin labelled species present, one spectrum which results from NTspin0 which does not bind to NTS1-A and one where the ligand does. This is unlikely as the mass spectral analysis of the purified NTspin0 does not show any significant peaks that could be attributed

to impurities, though this does not exclude the presence of free spin label as its mass is out of the molecular weight range the mass spectrometry was measured in.

Two components can also arise from there being two homogeneous ($\nu_{ex} \leq \mu s$) spin labelled species present which are exchanging between being bound to NTS1-A and free in solution. This situation is possible if there were errors in the calculation of the quantity of active NST1-A present in the samples, there is slow exchange on the ESR timescale at these concentrations of ligand and receptor or if the activity was decaying over the duration of the experiment, though the likelihood of this situation arising was reduced by using 50 % of the maximum stoichiometric NTspin0 that could bind to the active quantity of NTS1-A in each sample and the ligand was incubated with each sample for it to reach a steady state before measurement. The time taken to measure the samples discounts the possibility that the activity of the receptor is decaying over the course of the experiment. All measurements were made at 4 °C and it has been shown that the half life of NTS1-A at this temperature is 400 hours [68], with a maximum measurement time of three hours the experiment is well within the decay window especially with the use of only 50 % of the binding sites available in each sample.

The third possibility is that there is again homogeneous ligand, but in this case it is bound in two different conformations to NTS1-A, one in which the N-terminus is free to move and a second where the motion of the N-terminus becomes more restricted. This situation could arise if there was a two stage kinetic to the binding of the NT to NTS1-A that occurred on the ESR time scale where there is a conformational change induced in the receptor on binding of the ligand, which causes a complementary change in structure in the ligand, this hypothesis is supported by the kinetic model proposed in 4.3.2.2.

5.4.3 ESR measurements of NTspin6 in the presence and absence of NTS1-A

Figure 5.13 shows the ESR spectra of NTspin6 in the absence and presence of detergent solubilized NTS1-A. Figure 5.13 (A), 2 nM NTspin6 in NT50 buffer (2.2.3), shows the three peak spectrum of a motionally free nitroxide spin label with a slight motional restriction in the high field line. It could, therefore, be possible that NTspin0 in the same conditions as this spectrum seen in Figure 5.10 has an innate motional restriction in it and that its spectrum is not entirely due to the presence of glycerol as the same level of restriction is not seen here.

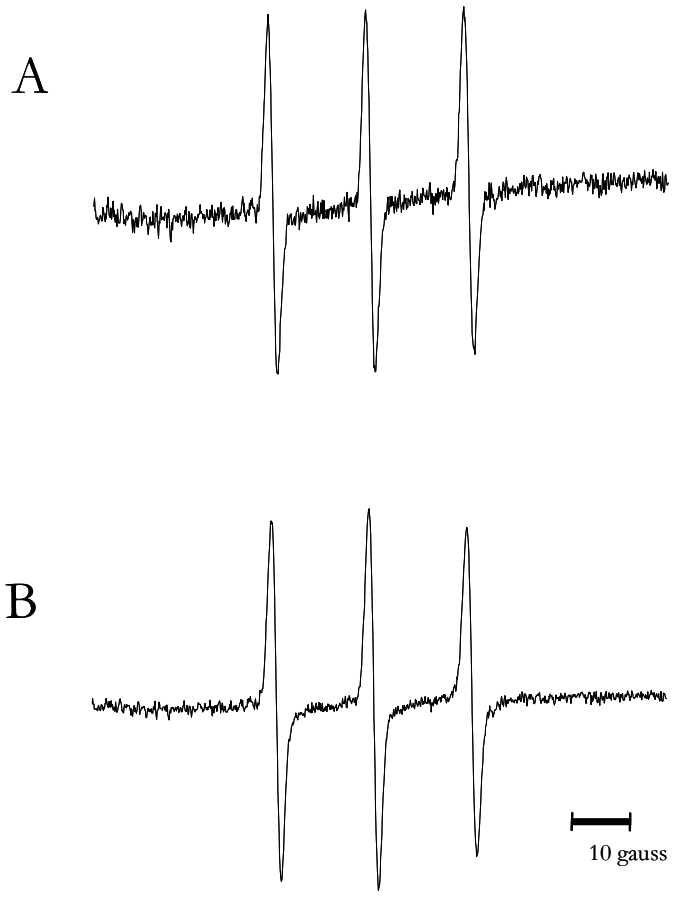

Figure 5.13 – ESR spectra of NTspin6: (A) 2 nM of NTspin6 in detergent buffer NT50 (2.2.3) and (B) 0.5 nM of NTspin0 in the presence of 1 nM NTS1-A in NT50 buffer, 16 acquisitions (40 s each acquisition).

Figure 5.13 (B), 0.5 nM NTspin6 with 1 nM NTS1-A in NT50 buffer, shows that the presence of the receptor does have an effect on the spin labelled peptide, but that as NTspin6 does not bind to the receptor NTS1-A the effect is nowhere near as marked as with NTspin0 in the same environment Figure 5.10. This could be caused by a non-specific interaction of the ligand with the detergent protein micelle, as discussed above.

The spectra in Figure 5.14, show the effects of the liposomes (A) and proteoliposomes (B) on the motion of NTspin6.

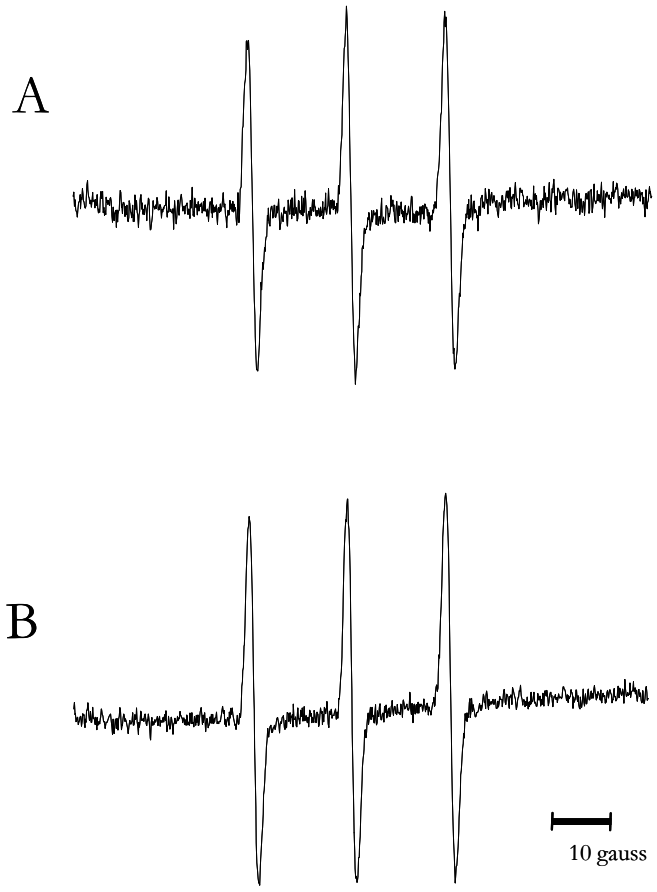

Figure 5.14 – ESR spectra of NTspin6: (A) 2 nM of NTspin6 with BPL liposomes in 50 Tris HCl 50mM NaCl pH 7.4 buffer and (B) 0.5 nM of NTspin0 in the presence of 1 nM NTS1-A in BPL proteoliposomes in 50mM Tris HCL, 50 mM NaCl pH 7.4 buffer, 16 acquisitions (40 s each acquisition).

As with NTspin0 there is less effect on the motions seen in this system and the spectra acquired demonstrate a motionally free spin label.

5.5 Discussion

To date, the majority of studies made on NT and NTSs have focused on the interaction of $NT_{(8-13)}$ with NT receptors, due to the fact that this is the only part of NT required for receptor activity, and indeed the ease of production and working with a smaller ligand simplifying experimentation. It has been so engrained in the field that statement likes "$NT_{(8-13)}$ is a peptide fragment of neurotensin (NT) and is more biologically relevant than the parent peptide" [50] start to arise in the literature, but is this misguided?

Like all neuropeptides, NT is synthesized *in vivo* as part of a larger precursor which also contains neuromedin N (NN), a six amino acid neurotensin-like peptide (Figure 5.15). NT and NN are located in the C-terminal domain of the precursor (pro-NT/NN), where they are flanked and separated by three Lys-Arg sequences [104].

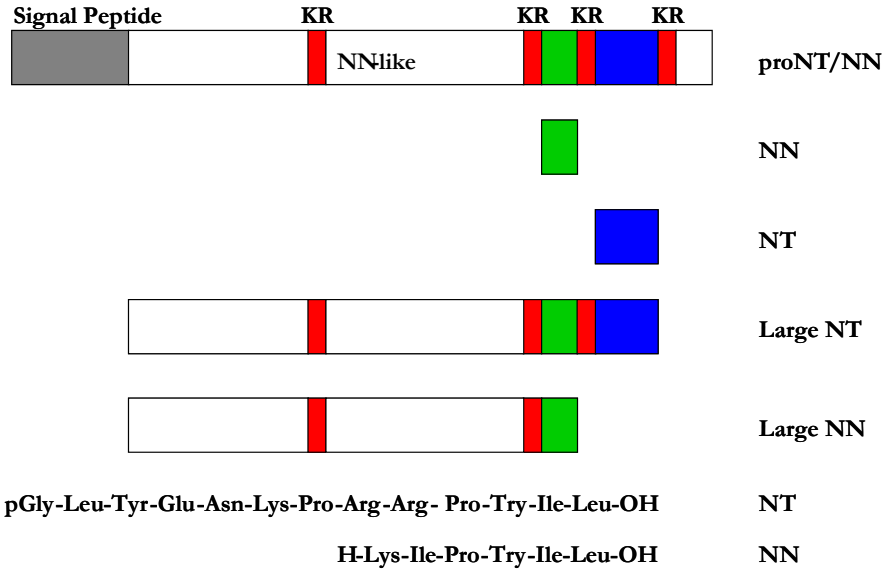

Figure 5.15 – Illustration of the NT/NN pro-protein and its cleavage products with protease sites in red, NN in green and NT in blue.

A fourth dibasic sequence preceding an NN-like sequence is present in the N-terminal domain. Dibasics are the consensus sites recognised and cleaved by processing endoproteases that belong to the family of proprotein convertases. In tissues that express pro-NT/NN, the three C-terminal Lys-Arg sites are differentially processed, whereas the dibasic sites upstream of the NN-like sequence is not cleaved. In the brain, pro-NT/NN processing gives rise to NT and NN. In the gut, processing leads mainly to the formation of NT and a large peptide ending in the NN sequence at its C-terminus (dubbed large NN). In the adrenal glands, NT, large NN and a large peptide ending with the NT sequence (large NT) are the major products [105].

The mechanisms by which extracellular NT and NN are degraded have been elucidated [104]. NN is rapidly inactivated by aminopeptidases, whereas NT is somewhat more slowly inactivated by metalloendopeptidases that cleave the peptide in its C-terminal domain within the 8-13 region crucial for binding to its receptors, a clear biological necessity for the removal of the stimulus of NT. Thus $NT_{(8-13)}$ never occurs *in vivo* and thus how can its study be "more biologically relevant" that than of the parent peptide?

In this chapter it has been demonstrated that there is an induced restriction of motion in the N-terminus of NT upon binding to NTS1-A, with the correlation time increasing at least approximately by an order of magnitude (1.9 ns to 11.4 ns) in the presences of excess receptor binding sites. If the K_d determined by SPR above (4.3) is the case then further studies would need to be carried out using more spin labelled ligand in order to be sure ligand was associating with receptor. If the values for the K_d of NTS1 from the literature are taken then the observations made here will likely be of ligand bound to receptor. The extent of the motional restriction observed could be attributed to the binding of the spin labelled ligand to the 100kDa receptor contruct which would clearly have an effect on the motions of the spin label in solution. Also the K_d of the NTS1-A construct could have having an effect here.

Thus the 1-7 region of NT is associating with the receptor on binding and although it is not responsible for inducing communication through the NTS1 to G-proteins, as the 8-13 region alone can accomplish this, it could have a role other than inducing the conformational change which communicates the signal into the cell. Since $NT_{(8-13)}$ does not occur *in vivo* and given the observations in this chapter, it clearly is biologically relevant to study the native ligand NT. Clearly this initial study now opens up the way for more similar studies to elucidate these possibilities.

Chapter 6 Nuclear magnetic resonance (NMR) studies of the NT agonist analogue $NT_{(8-13)}$

6.1 Introduction

6.2 NMR

6.2.1 Basic Principles

The NMR spectrum results from the interactions of nuclear spins with a large external magnetic field (B_0) and is described by a nuclear spin Hamiltonian, where H_{TOTAL} in a generalized form is given by:

$$H_{TOTAL} = H_Z + H_{CS} + H_J + H_D + H_Q$$

Equation 6.1

where all components have anisotropic interactions with the applied field. A spin I present in a static magnetic field B_0 will be in one of $2I+1$ energy levels, which are characterised by the magnetic moment of the nucleus and the strength of the magnetic field. This interaction of the spins with the static magnetic field B_0 is called the Zeeman interaction. The Zeeman term of the spin Hamiltonian H_Z:

$$H_Z = \gamma B_0 I_Z$$

Equation 6.2

Where γ is the gyromagnetic ratio and I_Z is the z-component of the spin operator *I*. Chemical shift is a chemical shielding interaction arising through the interaction of the nuclear spin with its surrounding electrons, i.e. the chemical shift is a reflection of how the nuclear spin is affected by its electronic environment. In terms of a Hamiltonian, the chemical shift is given by:

$$H_{CS} = \gamma I \sigma B_0 = \gamma (I_X \sigma_{xx} + I_Y \sigma_{yy} + I_Z \sigma_{zz}) B_0$$

Equation 6.3

In the principle axis frame of reference (PAS), the chemical shift is an anisotropic parameter (i.e. it has a directional dependence) which is characterised by a tensor, which is illustrated below (Figure 6.1). Important parameters arising from this illustration are the isotropic chemical shift, σ_{iso}, given by:

$$\sigma_{iso} = \sigma_{11} + \sigma_{22} + \sigma_{33} \Big/ 3$$

Equation 6.4

And the anisotropy parameter, η, given by:

$$\eta = \sigma_{yy} - \sigma_{xx} \Big/ \sigma_{zz} - \sigma_{iso}$$

Equation 6.5

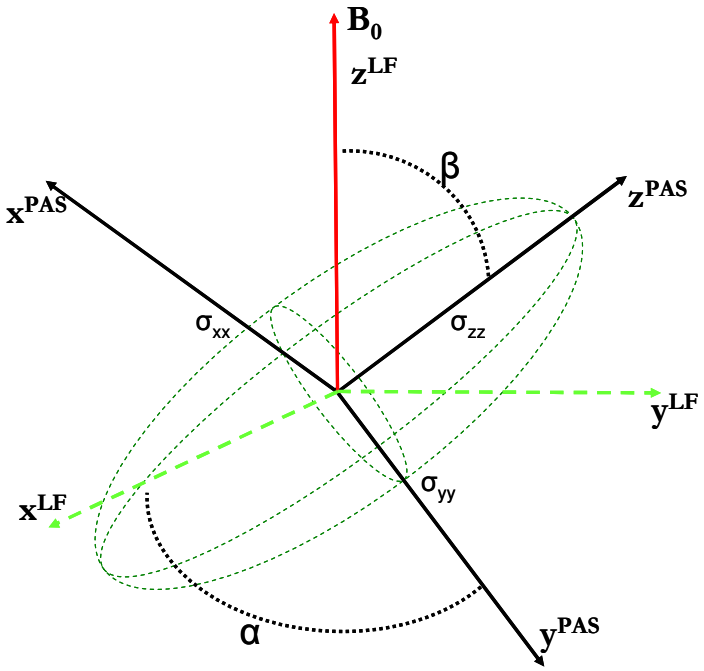

Figure 6.1 – The description of the chemical shift tensor, shown as an ellipsoids and is defined by the principle axis components σ_{xx}, σ_{yy}, σ_{zz} and the angles α and β, which are the angle between the long axis of the electric field gradient and the reference axis.

The two equations are defined once in terms of σ_{xx}, σ_{yy}, and σ_{zz} and once with σ_{11}, σ_{22}, and σ_{33}; these notations are not interchangeable.

From the reference frame of the tensor, the overall chemical shift in the PAS is given by:

$$\delta = \sigma_{xx}^{PAS} + \sigma_{yy}^{PAS} + \sigma_{zz}^{PAS}$$

Equation 6.6

However, it is more convenient to define chemical shift anisotropy with respect to the laboratory frame of reference (LF), i.e. the frame of reference where the static magnetic field B_0 is along the z-direction. In this case the overall chemical shift is given by:

$$\delta = \sigma_{xx}^{PAS}(\cos\alpha\sin\beta)^2 + \sigma_{yy}^{PAS}(\sin\alpha\sin\beta)^2 + \sigma_{zz}^{PAS}(\cos\beta)^2$$

Equation 6.7

An diagrammatic example of the ^{15}N chemical shift tensor in a peptide plane is shown in Figure 6.2.

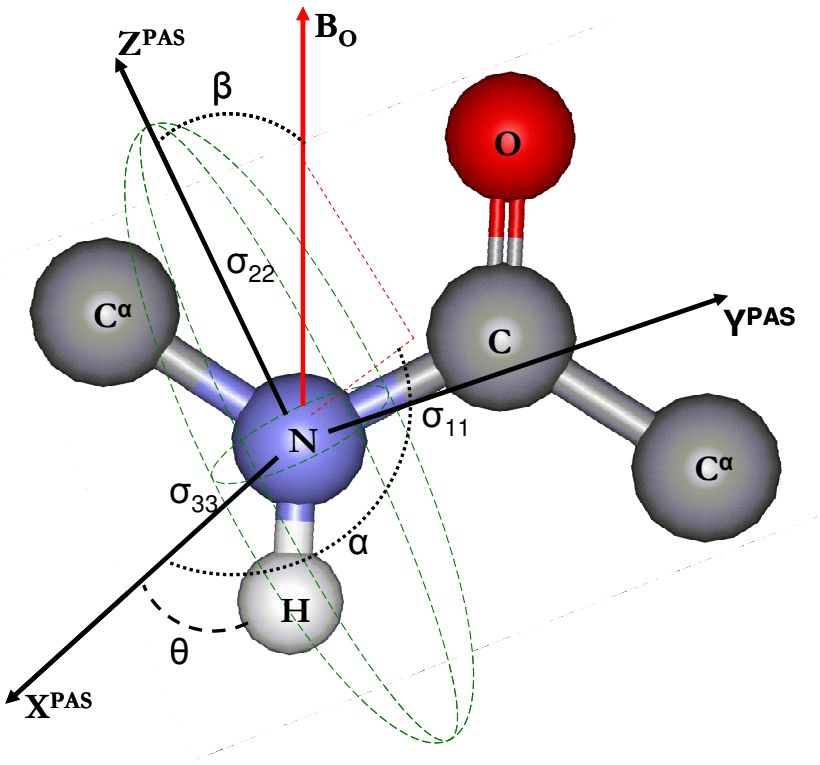

Figure 6.2 - The shape of the chemical shift tensor. The shape of the three-dimensional ellipsoids is defined by the principle axis components σ_{11}, σ_{22}, σ_{33} and the angles α and β, which are the angle between the long axis of the ellipse and the reference bond.

For the example in Figure 6.2, the ^{15}N chemical shift tensor is given by:

$$\delta = \sigma_{11}\sin^2(\alpha-\theta)\sin^2(\beta) + \sigma_{22}\cos^2(\beta) + \sigma_{33}\cos^2(\alpha-\theta)\sin^2(\beta)$$

Equation 6.8

As mentioned above there are two sets of notations for the principal components of the chemical shift tensors: σ_{xx}, σ_{yy}, σ_{zz}, or σ_{11}, σ_{22}, σ_{33}. For σ_{xx}, σ_{yy}, σ_{zz} the following definition applies:

$$\left|\sigma_{zz} - \sigma_{iso}\right| \geq \left|\sigma_{xx} - \sigma_{iso}\right| \geq \left|\sigma_{yy} - \sigma_{iso}\right|$$

Equation 6.9

For the σ_{11}, σ_{22}, σ_{33} version, the following definition applies:

$$\sigma_{11} \leq \sigma_{22} \leq \sigma_{33}$$

Equation 6.10

The relationship between both notations is:

$$\begin{aligned}\sigma_{xx} &= \sigma_{iso} - \sigma_{11},\\ \sigma_{yy} &= \sigma_{iso} - \sigma_{22},\\ \sigma_{zz} &= \sigma_{iso} - \sigma_{33}.\end{aligned}$$

Equation 6.11

And thus

$$\sigma_{xx} + \sigma_{yy} + \sigma_{zz} = 0$$

Equation 6.12

The methods used to measure the chemical shift anisotropy of a particular nucleus depend primarily on the state of the sample, i.e. whether the solid is a powder, a microcrystalline sample, or a single crystal. In the case of powdered samples, the molecules have a statistical distribution of possible orientations with respect to the magnetic field B_0. For a single oriented crystal, on the other hand, all the molecules are aligned in the same direction in a crystal lattice.

Thus for a given crystal orientation, the molecules will have a particular alignment in the magnetic field B_0.

In Figure 6.3 (a), a broad "powder pattern" is shown, which is typical of the functional groups that have very asymmetric electronic environments, such as, for example, the carbonyl group (C=O).

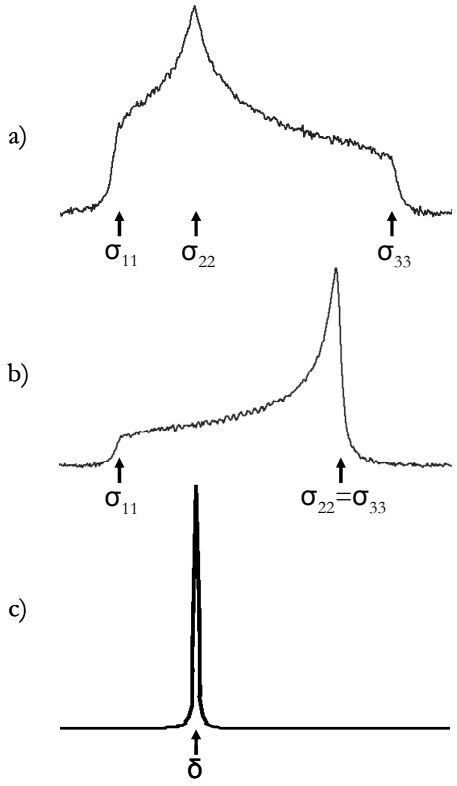

Figure 6.3 – Illustration of the spectra one would obtain for: a) a powder sample with $\sigma_{11} \neq \sigma_{22} \neq \sigma_{33}$; b) a powder sample with axial symmetry in σ, with σ_{11}, and $\sigma_{22} = \sigma_{33}$ and c) a single crystal in a specific orientation with respect to the magnetic field.

The spectrum (b) illustrates the case of an axially symmetric tensor, with two of the three components being equal. This occurs for moieties where there is a threefold symmetry axis through the nucleus, such as for N in NH_3 groups. Note that in the case of nuclei with symmetric electronic environments, such as C in methane, all the tensors components are

equal and the spectrum collapses to a single peak at the isotropic position σ_{iso} which is also seen in solution. The spectrum in (c) displays the chemical shift for a particular crystallite orientated in the magnetic field. If there are a number of inequivalent sites in the crystal, these would be reflected in the spectra in that there would be one line for each crystallographic inequivalence. The particular chemical shift measured depends on the orientation and thus by changing the orientation of the crystal, one gets a new measurement for the chemical shift, within the anisotropy range.

For dipolar interactions a nucleus with spin $I \geq ½$ has a magnetic moment, μ, associated with it given by:

$$\mu = \gamma L$$

Equation 6.13

If two different nuclear spins, I_1 and I_2 are separated by a distance r (Figure 6.4),

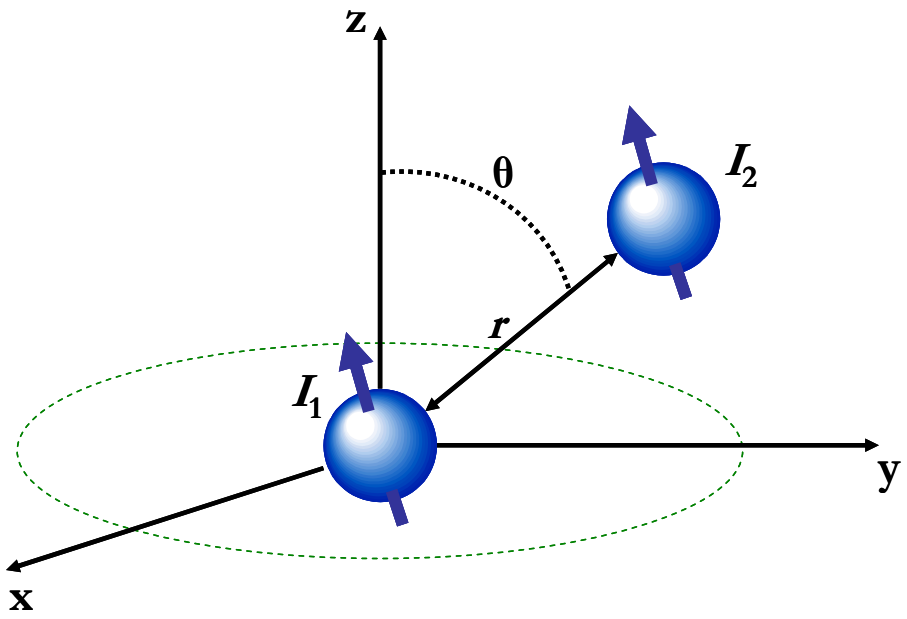

Figure 6.4 – Diagramatic representation of a two spin system in the principle access frame

then the energy of the interaction between the two magnetic dipoles, μ_1 and μ_2 is given by:

$$E = \frac{\mu_0}{4\pi}\left[(\mu_1 \cdot \mu_2)r^{-3} - 3(\mu_1 \cdot r)(\mu_2 \cdot r)r^{-5}\right]$$

Equation 6.14

Where μ_0 is the permeability constant and is equal to $4\pi \times 10^{-7}$ kg.m.s^{-2}.A^{-2}. If the two dipoles have the same orientation with respect to *r*, then:

$$(\mu_1 \cdot r)(\mu_2 \cdot r) = (\mu_1 \cdot \mu_2)r^2 \cos^2\theta$$

Equation 6.15

And thus,

$$E = \frac{\mu_0}{4\pi}(\mu_1 \cdot \mu_2)r^{-3}\left[1 - 3\cos^2\theta\right]$$

Equation 6.16

The Hamiltonian is then given by replacing the vectors μ_1 and μ_2 by their corresponding operators in Equation 6.14 above:

$$H_D = \frac{\mu_0\gamma_1\gamma_2h^2}{16\pi^3}\left[(I_1 \cdot I_2)r^{-3} - 3(I_1 \cdot r)(I_2 \cdot r)r^{-5}\right]$$

Equation 6.17

This equation represents the full dipolar Hamiltonian. In the presence of an external magnetic field B_0, however, many of the higher order terms can be neglected, i.e. if the following condition is valid:

$$|\omega_{01} - \omega_{02}| >> \frac{\mu_0\gamma_1\gamma_2h^2}{16\pi^3r^3}$$

Equation 6.18

This approximation is called a secular approximation. Thus the Hamiltonian in the case of homonuclear coupling (between like spins) is:

$$H_D = \frac{\mu_0 \gamma_1 \gamma_2 h^2}{16\pi^3 r^3} \frac{1}{2}\left(3\cos^2\theta - 1\right)\left[3I_{1z}I_{2z} - I_1 \cdot I_2\right]$$

Equation 6.19

Whereas in the case of heteronuclear coupling, H_D is given by:

$$H_D = \frac{-\mu_0 \gamma_1 \gamma_2 h^2}{16\pi^3 r^3}\left(3\cos^2\theta - 1\right)I_{1z}I_{2z}$$

Equation 6.20

The constant terms in front of Equation 6.19 and Equation 6.20 are the homonuclear and heteronuclear dipolar coupling constants, respectively. Typical values for ^{1}H, ^{13}C, and ^{15}N are:

$$d_{IS} = \frac{\mu_0 \gamma_I \gamma_S h}{4\pi r_{IS}^{\ 3}}\left(Hz\right)$$

Equation 6.21

With

$$\gamma^1 H = 42.5759 * 10^6\, Hz.T^{-1}$$
$$\gamma^{13} C = 10.7054 * 10^6\, Hz.T^{-1}$$
$$\gamma^{15} N = 4.3142 * 10^6\, Hz.T^{-1}$$
$$\mu_0 = 4\pi * 10^{-7}\, N.A^{-2}$$
$$h = 1.0546 * 10^{-34}\, J.s$$

Equation 6.22

Thus

$$d_{HH}.r^3 = 120000 \text{ Hz.Å}^3$$

$$d_{CC}.r^3 = 7500 \text{ Hz.Å}^3$$

$$d_{NN}.r^3 = 1200 \text{ Hz.Å}^3$$

$$d_{HC}.r^3 = 30000 \text{ Hz.Å}^3$$

$$d_{HN}.r^3 = 12000 \text{ Hz.Å}^3$$

$$d_{CN}.r^3 = 3000 \text{ Hz.Å}^3$$

Note that since the static magnetic field lies along the z-axis in Figure 6.1, the dipolar interaction has an orientational dependence with respect to B_0 given by the expression $3\cos^2\theta$-1. This manifests itself by a dependence of the observed dipolar splitting on the orientation of the crystallite in a single crystal in the probe (recall the orientation dependence of the CSA for the single crystals Figure 6.3). For a powder sample, a Pake pattern, which is the sum of the spectra of individual crystallites which are randomly distributed in the sample, is observed.

The quadropolar interaction (H_Q) is an interaction between the nuclear spin $I \geq 1$ and the electric field surrounding it, created by the charges around the nucleus in question. The quadropolar interaction is a tensor quantity which depends on the electric field gradient (EFG) V

$$Q = \frac{eQV}{2I(2I-1)h}$$

Equation 6.23

Where the EFG is given by

$$V = \begin{pmatrix} V_{xx} & 0 & 0 \\ 0 & V_{yy} & 0 \\ 0 & 0 & V_{zz} \end{pmatrix}$$

Equation 6.24

in the PAS of the EFG. As with the CSA, there are a number of definitions associated with the EFG, such as

$$V_{xx} + V_{yy} + V_{zz} = 0$$

Equation 6.25

which is analogous to Equation 6.12 above.

Also,

$$|V_{zz}| \geq |V_{xx}| \geq |V_{yy}|$$

Equation 6.26

And one can define an asymmetry parameter η

$$\eta = \frac{V_{yy} - V_{xx}}{V_{zz}}$$

Equation 6.27

The quadropolar coupling constant is given by

$$\mathbf{X} = \frac{e^2 Q q_{zz}}{h}$$

Equation 6.28

where eq_{zz} corresponds to the largest principal component to the EFG, i.e. V_{zz}. As a result of the quadropolar interaction, the lines observed in spectra of quadropolar nuclei are split by $\Delta\nu_Q$

$$\Delta\nu_Q(\theta,\phi)=\frac{1}{2}\nu_Q\left[3\cos^2\theta-1-\eta\sin^2\theta\cos 2\phi\right]$$

Equation 6.29

Where

$$\nu_Q=\frac{3\chi}{2I(2I-1)}$$

Equation 6.30

And θ and ø are defined as

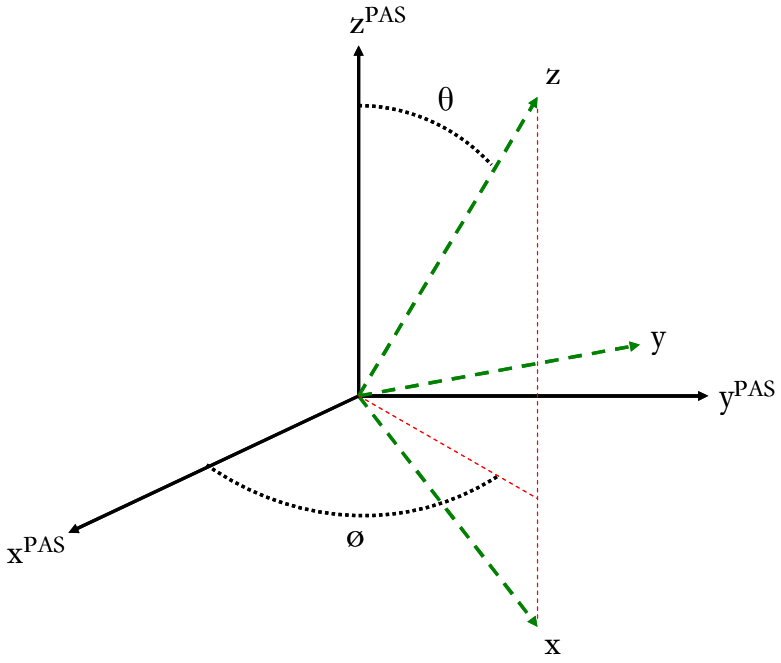

Figure 6.5 - Diagramatic representation of how θ and ø are defined in the principle access frame

The energy levels for each allowed state are given by

$$\Delta E_m=\frac{1}{4\pi}\Delta\upsilon_Q(\theta,\phi)\left[m^2-\frac{1}{3}I(I+1)\right]$$

Equation 6.31

i.e for I=1 and I=5/2, and the experimentally determined double quantum spins ΔE_m.

The Hamiltonian for the quadropolar interaction is given by

$$H_Q = \frac{2\pi eQ}{4I(2I-1)h}\left[\begin{array}{l} V_{zz}\left(3I_z{}^2 - I(I+1)\right) + \left(V_{xx} - V_{yy}\right)\left(I_x{}^2 - I_y{}^2\right) + 2V_{xy}\left(I_xI_y + I_yI_x\right) \\ + 2V_{xz}\left(I_xI_z + I_zI_x\right) + 2V_{yz}\left(I_yI_z + I_zI_y\right) \end{array}\right]$$

Equation 6.32

6.2.2 Solid-State NMR

Over the past twenty years, solid state NMR has emerged as an effective method for the study of the structure of membrane proteins; it is not hindered by the problems associated with solution NMR where fast tumbling of the species being studied is required for high resolution and can be readily applied to yield a variety of structural information. Indeed the molecular weight limit which can be studied using solid state techniques is virtually unreachable and the field has seen a number of high molecular weight proteins used in structural determination [106-114].

There have been two general approaches for obtaining high-resolution solid-state NMR spectra. The first approach relies on orienting the sample, either by mechanical means or by an external magnetic field [115]. Orientational constraints are derived from dipolar couplings, chemical shift and dipolar interactions whose values depend on how the molecule is aligned relative to the external field. These interactions are all anisotropic and have an orientational dependence which once the interactions are characterised, usually in a powder sample, a comparison of the spectra from aligned samples with simulated spectra allows determination of molecular orientation.

The second approach for obtaining "high" resolution spectra is magic angle spinning (MAS), which increases spectral resolution by mechanically rotating the sample at a specific angle (θ = 54.7°) relative to the external magnetic field $\boldsymbol{B}_0$. The dipolar interaction of a solid sample, which is averaged out in solution state NMR by molecular tumbling, is static. This leads to line broadening in all solid samples, except for single crystals, because although the sample is pure (a single species) it is present in a number of different conformations each contributing to homogenous line broadening resulting in a Pake pattern (Figure 6.3).

Some line shapes from solid spectra are sharper than others, which reflects varying levels of motion within "solid" samples, leading to the conclusion that increasing motion could lead to narrower lineshapes [116, 117]. By varying the angle of rotation of the sample with respect to the magnetic field varying degrees of line broadening were observed; rotating the sample around $\boldsymbol{B}_0$ had no effect, perpendicular rotation to $\boldsymbol{B}_0$ halved the spectral linewidth and rotation about 54.73° reduced the dipolar broadening to zero. This reduction occurs because dipolar interactions (D), indirect electron coupled interactions, chemical shift anisotropy (σ) and the quadrapolar interaction are all affected by magic angle spinning. As an example, the Hamiltonian for the dipolar interaction between two homonuclear spins is shown above (Equation 6.19), if a sample is rotated about an axis inclined to $\boldsymbol{B}_0$ at an angle β then the resulting spectrum will retain its shape but be reduced in width by the scale factor:

$$F(\beta) = \left| \frac{1}{2}\left(3\cos^2\beta - 1\right) \right|$$

Equation 6.33

Therefore, in Equation 6.3, when β = 0, 180° and 54.73° then $F(\beta)$ = 1, ½ and 0, respectively, explains the observations of Andrew *et. al.* and Lowe *et. al.* when spinning samples at these

angles with respect to the magnetic field, MAS removes the residual CSA and dipolar interactions.

Biological solid-state NMR experiments employ MAS and cross-polarisation (CP). Biologically interesting NMR sensitive nuclei ^{13}C and ^{15}N have a low gyromagnetic ratios compared to ^{1}H and so experiments employ a cross polarisation double resonance method to amplify the weaker nuclei using the stronger plentiful protons. By employing the Hartman-Hahn condition [58], with decoupling of the strong proton heteronuclear dipolar interactions, the weak signals from either ^{13}C or ^{15}N are enhanced by the proton polarisation transfer.

6.3 Aims of this study

In this study the agonist analogue of NT, $NT_{(8-13)}$, was labelled with NMR visible nuclei. This peptide was studied using solid state NMR in order to gain an insight into methods that could facilitate the assignment of the resonances arising from the ligand when bound to its target GPCR.

6.4 Methodology

Methods and pulse programs can be seen in 2.8.

6.5 Results

6.5.1 Synthesis of the NT agonist analogue $NT_{(8-13)}$

The NT agonist analogue $NT_{(8-13)}$ (pArg-Arg-Pro-Try-Ile-Leu-OH) was synthesized as a test bed for proposed labelling of this region for NMR experiments, as the region is all that is needed for NTR1 activity and shortening the length of the peptide to be synthesized improves the yields. This synthesis was carried out exclusively in the fume-hood using stoiciometric amounts of amino acid in each coupling step, with each reaction being monitored with the ninhydrin test for the presence of primary amides. The synthesis was carried out at a 0.1 mmol

scale, with a theoretical maximum yield of 0.0817 g. The HPLC trace of the purification of the lyophilised cleavage product is shown in Figure 6.6.

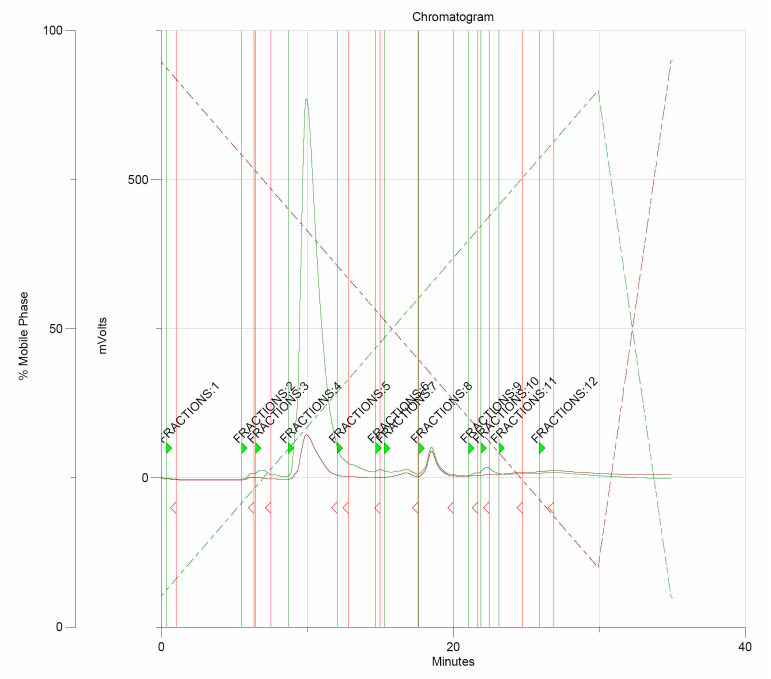

Figure 6.6 - Reverse phase HPLC trace of the lyophilised products from the solid phase synthesis of scrambled $NT_{(8-13)}$. With the absorption at 254 nm as a solid green line and the absorption at 280 nm as a solid red line and the percentages of H_2O and acetonitrile in dashed red and green lines respectively.

The HPLC trace clearly shows a dominant peak occurring 10 minutes into the solvent gradient, picked as fraction 4, which makes up the majority of the cleavage product. This peak was verified as being the desired peptide product using MALDI-TOF, the mass spectrum being shown in Figure 6.7.

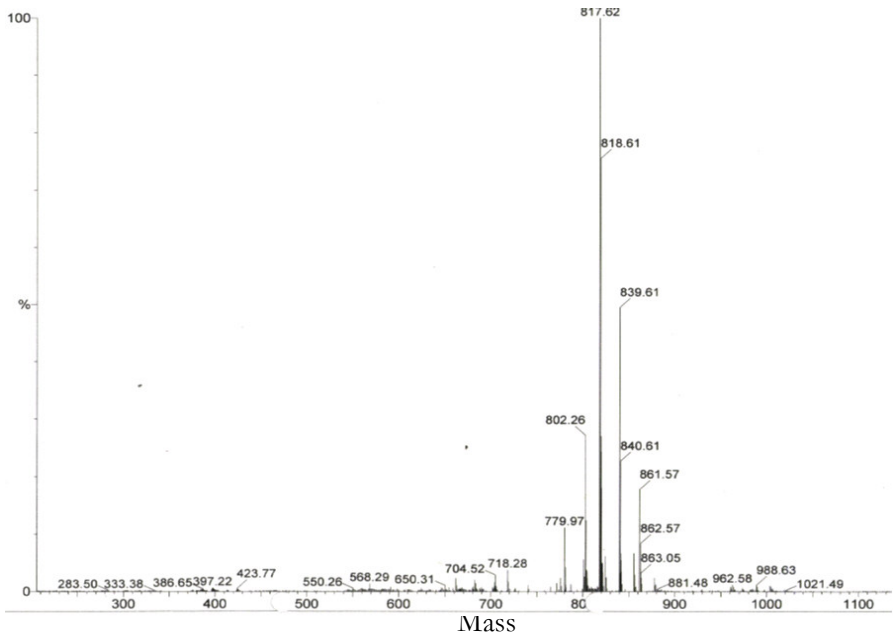

Figure 6.7 – MALDI-TOF mass spectrum of the dominant peak in the HPLC purification of solid phase synthesised $NT_{(8-13)}$.

The mass spectrum (Figure 6.7) shows the correct peptide weight of 817.82 with the ion plus sodium at 839.61 as the dominant feature and component of fraction 4 from the HPLC (Figure 6.6). The yield from one of these syntheses was 0.0686g which is a yield of 81% of the theoretical maximum for this synthesis. This shows that with careful monitoring of the synthesis process the need for excess amino acids can be circumvented, at least in smaller peptides, facilitating more cost effective labelling for NMR purposes.

With the protocol established for the synthesis of $NT_{(8-13)}$ using stoiciometric amounts of amino acids a peptide was synthesized with a labelling scheme designed to investigate the region of the $NT_{(8-13)}$ peptide that has an element of structure in solution. This peptide, dubbed NCCN-$NT_{(8-13)}$ (pArg-Arg-(1, 2, 3, 4, 5 ^{13}C, ^{15}N)Pro-(^{15}N)Tyr-Ile-Leu-OH), was designed to look at the torsion angle around the proline peptide bond as in solution it displays

cis/*trans* isomerisation with the populations roughly 20 %/80 % respectively [43, 102]. The peptide was constructed in the same manner as the $NT_{(8-13)}$, using stoiciometric quantities of amino acids to save on expensive NMR visible labels at a scale of 0.1 mmol with a maximal theoretical yield of 0.082 g. The lyophilised cleavage product from the synthesis resin was purified by HPLC and the trace is shown below in Figure 6.8.

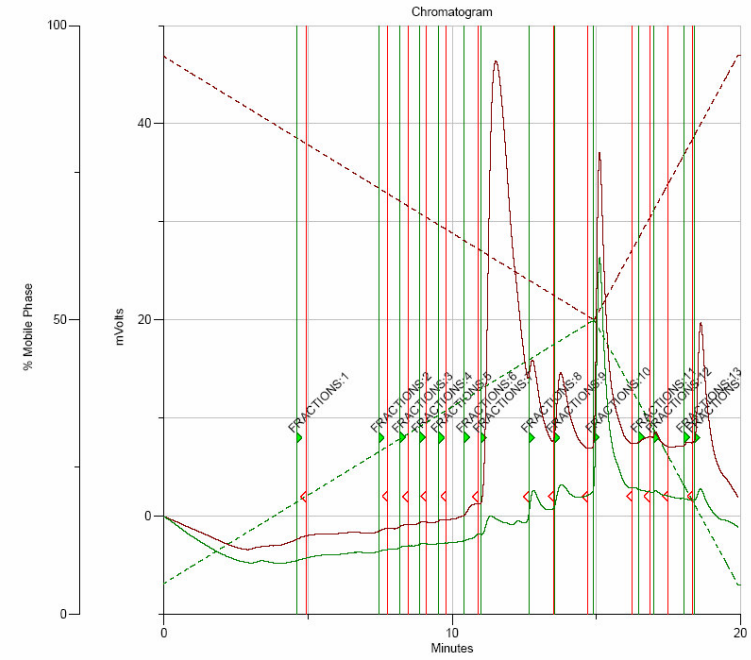

Figure 6.8 – Reverse phase HPLC trace of the lyophilised products from the solid phase synthesis of scrambled NCCN-$NT_{(8-13)}$. With the absorption at 254 nm as a solid green line and the absorption at 280 nm as a solid red line and the percentages of H_2O and acetonitrile in dashed red and green lines respectively.

The HPLC trace shows that the cleavage product was not very pure, though there is one dominant peak around 12 minutes, fraction 7, which was analysed using ESI positive mass spectrometry the results of which are shown below in Figure 6.9.

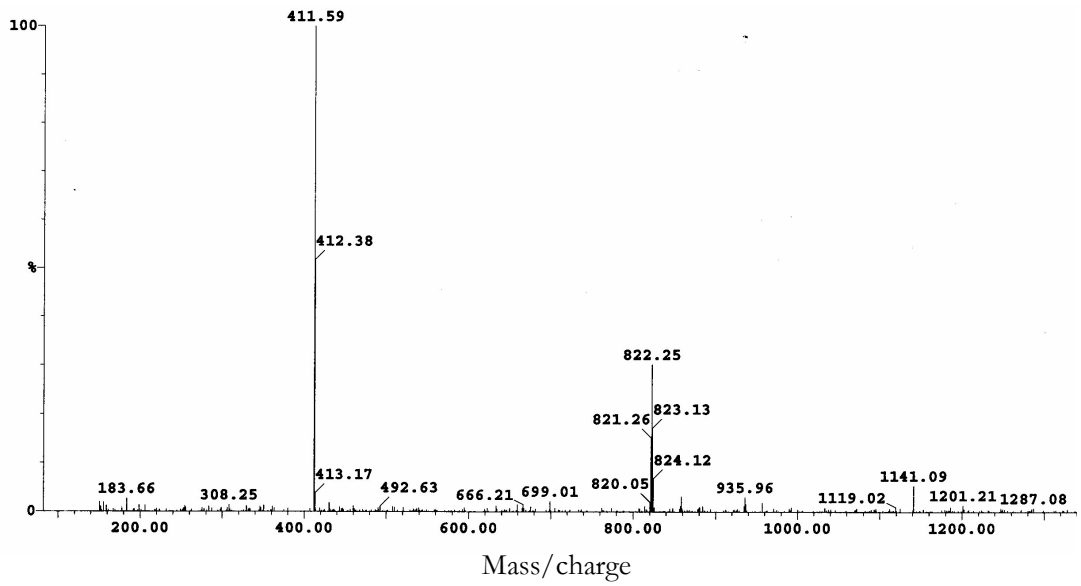

Figure 6.9 – Electrospray ionisation mass spectrum of the dominant peak in the HPLC purification of solid phase synthesised NCCN-$NT_{(8-13)}$.

The mass spectrum clearly show two mass peaks, one at 822.25 which corresponds to the parent ion of NCCN-$NT_{(8-13)}$ and one at 411.59 which is the doubly charge ion of the peptide verifying that the fraction 7 peak is in fact the desired labelled NTS1 agonist peptide.

6.5.2 Solution and solid spectra of the NCCN-$NT_{(8-13)}$ peptide

Figure 6.10 shows one dimensional solid and solution NMR spectra of the NCCN-$NT_{(8-13)}$. The left-hand resonance in the spectrum (Figure 6.10) is from the carbonyl moieties since the de-shielding effect of the oxygen atom gives the characteristically large down field chemical shift.

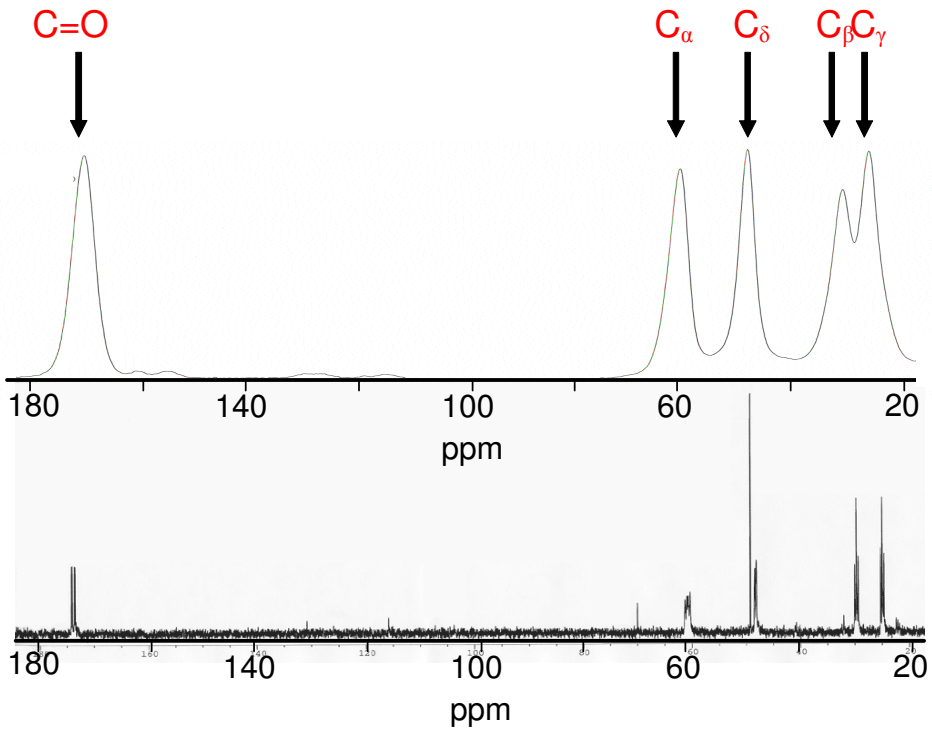

Figure 6.10 - ^{13}C CP-MAS NMR of solid lyophilised (top) and of NCCN-labelled $NT_{(8-13)}$ (10mg) acquired on a 200MHz Varian/Chemagnetics CMX infinity spectrometer with at room temperature proton field strength of 69 kHz for CP a contact time was 1.5 ms; and 63kHz decoupling during acquisition and 12 kHz spinning speed. Also a one pulse with decoupling solution (in water) (bottom) spectrum at 200MHz.

Although there is some overlap between the Cβ & Cγ resonances in the solid state NMR spectrum, each of the labelled carbon atoms in the proline residue is well resolved. The larger than expected line widths seen in this solid sample are due to homogeneous line broadening caused by the nature of the lyophilised powder and the number of conformations and crystallite forms produced in this sample type. The NMR spectra (Figure 6.10), along with the mass spectrometry, verifies that the labelling scheme for the carbon atoms in the NCCN peptide is correct. However, these preliminary assignments need to be confirmed by a two-dimensional experiment.

The $R14^5_4$ spectrum (appendix 2.8.3) obtained from the single quantum-single quantum NMR experiment (Figure 6.11) for the solid can be interpreted in much the same way as a COSY spectrum in solution state NMR.

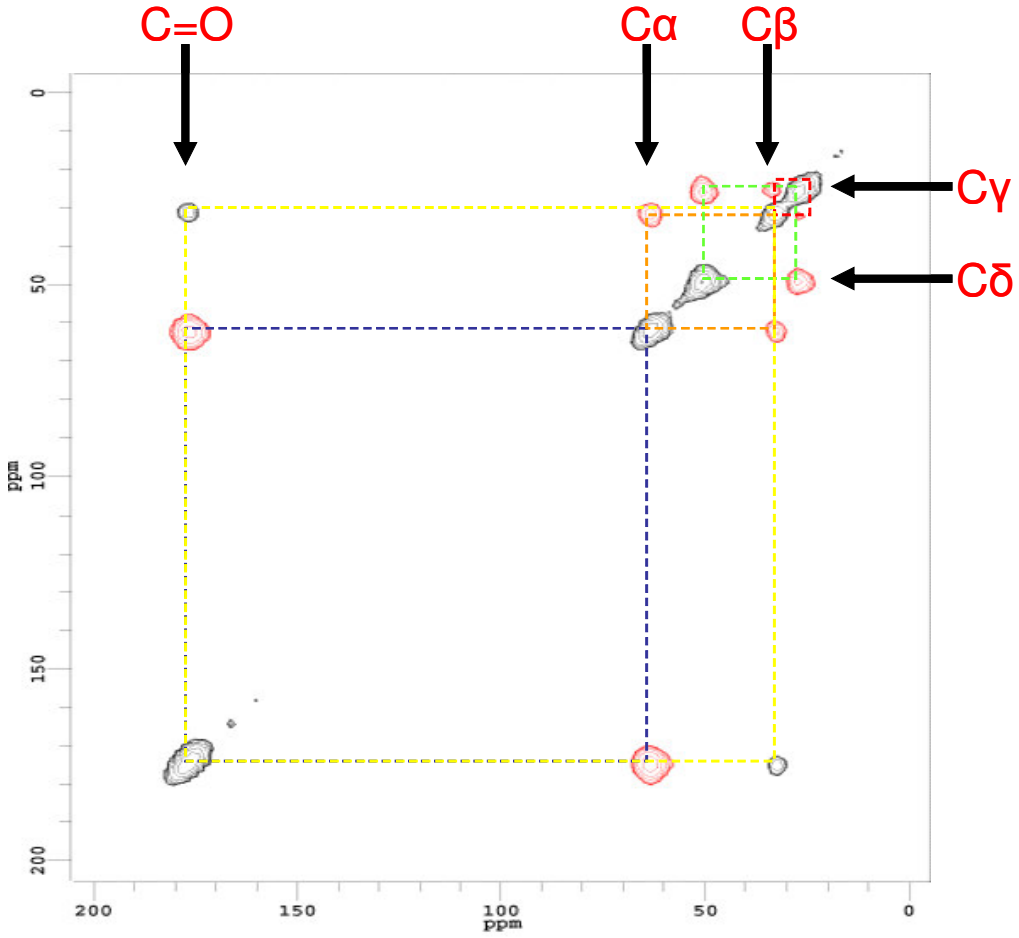

Figure 6.11 - $R14^5_4$ NMR spectrum of NCCN $NT_{(8-13)}$ using the 200 MHz Varian/Chemagnetics CMX infinity spectrometer with a 9 kHz spinning frequency and 64 acquisitions, proton field strength of 71 kHz and a ^{13}C field strength of 73 kHz with a contact time of 1.5 ms; and 70 kHz and 63 kHz decoupling during R sequence and acquisition respectively. Couplings between nearest neighbours include carbonyl-Cα (blue), Cα - Cβ (orange), Cδ - Cγ (green), and Cβ - Cγ (red). A coupling between the carbonyl and Cβ, which are not nearest neighbours, is shown in yellow.

Cross-peaks appear in the spectrum where through-bond interactions occur. The mixing time selected ensured that transfer of magnetisation only occurred between nearest neighbours although, in one case, transfer through two bonds can be seen. Due to the nature of the single

quantum experiment, cross-peaks arising from magnetisation transfer through a single bond have negative intensity (black), while cross peaks arising from transfer through two bonds have positive intensity (red).

The lines along the diagonal of the spectrum correspond well with the 1D ^{13}C spectrum obtained previously (Figure 6.10), allowing preliminary assignment as shown in Figure 6.11. The assignments are confirmed when cross-peaks between neighbouring ^{13}C atoms are analysed using sequential assignment. Assuming the characteristic carbonyl peak at 172.7 ppm to be correct, the dipolar couplings between neighbouring atoms can be sequentially assigned around the labelled proline residue, as shown in Figure 6.11.

Table 6.1 - ^{13}C Assignment of NCCN-labelled $NT_{(8-13)}$ taken from spectrum presented Figure 6.11

Proline Carbon Atoms	Chemical Shift (ppm)
C=O	172.7
C_α	59.8
C_β	28.3
C_γ	23.6
C_δ	47.9

The spectrum obtained from the single quantum-double quantum correlation is shown in

Figure 6.12. All expected correlations have occurred which confirms the labelling scheme and the assignment made previously.

The five peaks in the t2 (single quantum) dimension (x-axis on the spectrum) correspond to the resonances of the five ^{13}C labels, as shown. The four peaks in the t1 (double quantum) (y-axis on the spectrum) dimension correspond to the four 'pairs' of ^{13}C labels formed from direct bonding. Lines are the sum of the frequencies of the two atoms concerned, for example the peaks corresponding to the C=O, Cα pair have a resonance at 232.5 ppm i.e. 172.7 + 59.8 ppm, other connectivities are labelled in red.

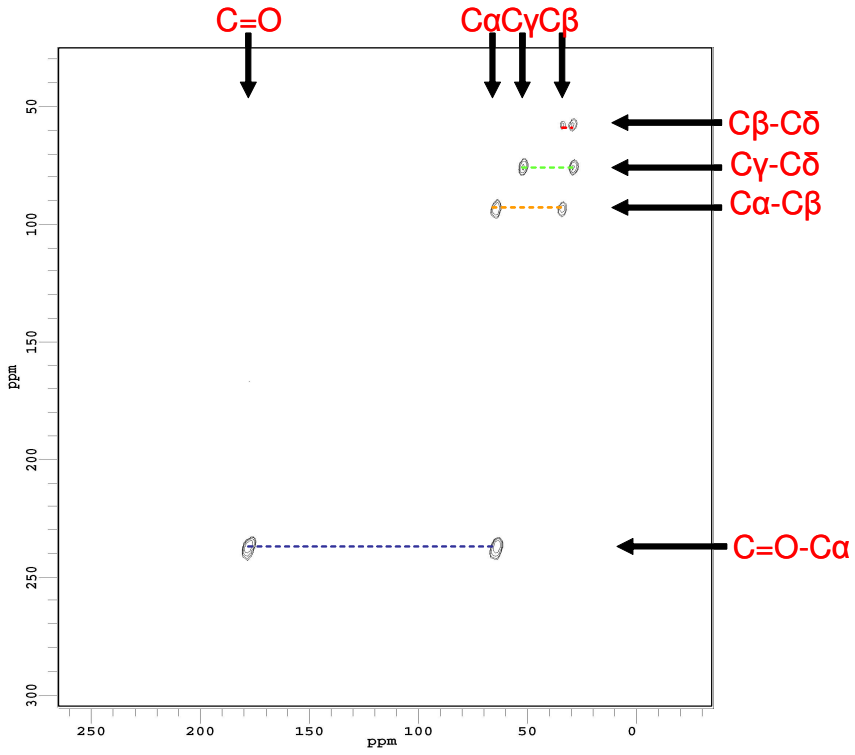

Figure 6.12 - R14[5]$_4$ Single quantum-double quantum ^{13}C correlation spectrum of fully ^{13}C $NT_{(8-13)}$ the spectrum was obtained on a 400 MHz CMX instrument, with a 7 kHz spinning frequency at room temperature, proton field strength of 71 kHz and a ^{13}C field strength of 71 kHz with a contact time of 1.5 ms; and 70 kHz and 63 kHz decoupling during R sequence and acquisition respectively.

Figure 6.13 shows the ^{15}N 1D CP MAS spectrum obtained from the NCCN peptide. The two ^{15}N labels in the sample (Pro^{10} and Tyr^{11}) are defined in two separate peaks, indicating correct labelling of the peptide. Spinning side bands (separated by 5 kHz) can also be seen either side of the central peaks which are inherent at the relatively low spinning of 5 kHz. Although the larger 6 mm rotor could not reach such high spinning frequencies as the smaller 4mm rotor used in the previous experiments, the 11.7 T instrument has the advantage of better resolution afforded by the higher field strength.

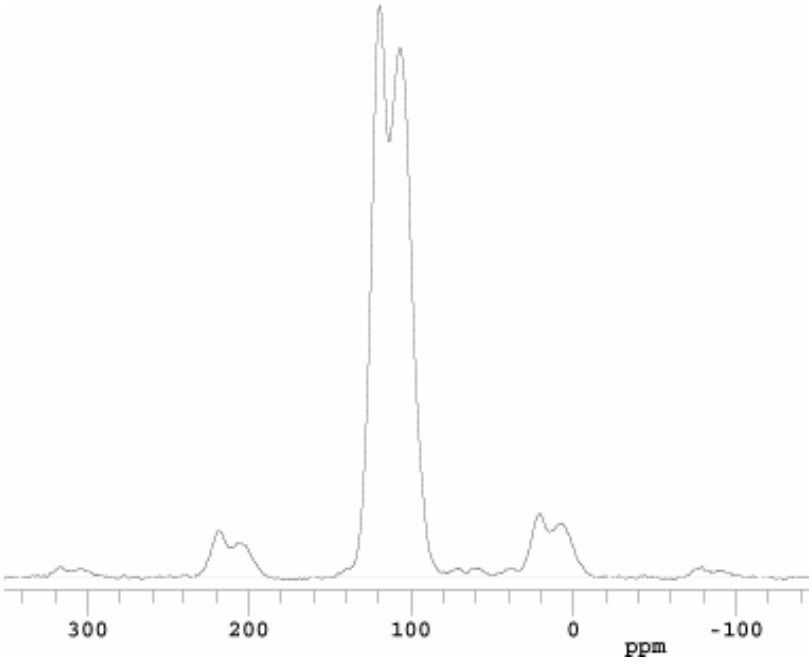

Figure 6.13 - ^{15}N 1D CP MAS spectrum of 20 mg lyophilised NCCN labelled NT_{8-13} obtained using 500 MHz CMX infinity NMR instrument with a proton field strength of 50 kHz during CP, 50kHz decoupling, 5 kHz spinning and 5000 acquisitions.

Figure 6.14 shows a ^{13}C solution spectrum of NCCN-$NT_{(8-13)}$ in the detergent buffer used to purify NTS1-A. Well defined spectral lines were observed with a linewidth on the order of 1-2 ppm. This is to be expected given the averaging of anisotropic interactions in the liquid phase. Precise assignments can therefore be made. All ^{13}C labels in the NCCN peptide can be

accounted for along with two characteristic glycerol peaks, which arise from the relatively large amounts of glycerol in the buffer (30 % w/v). Other small peaks are likely to represent other detergent components of the buffer.

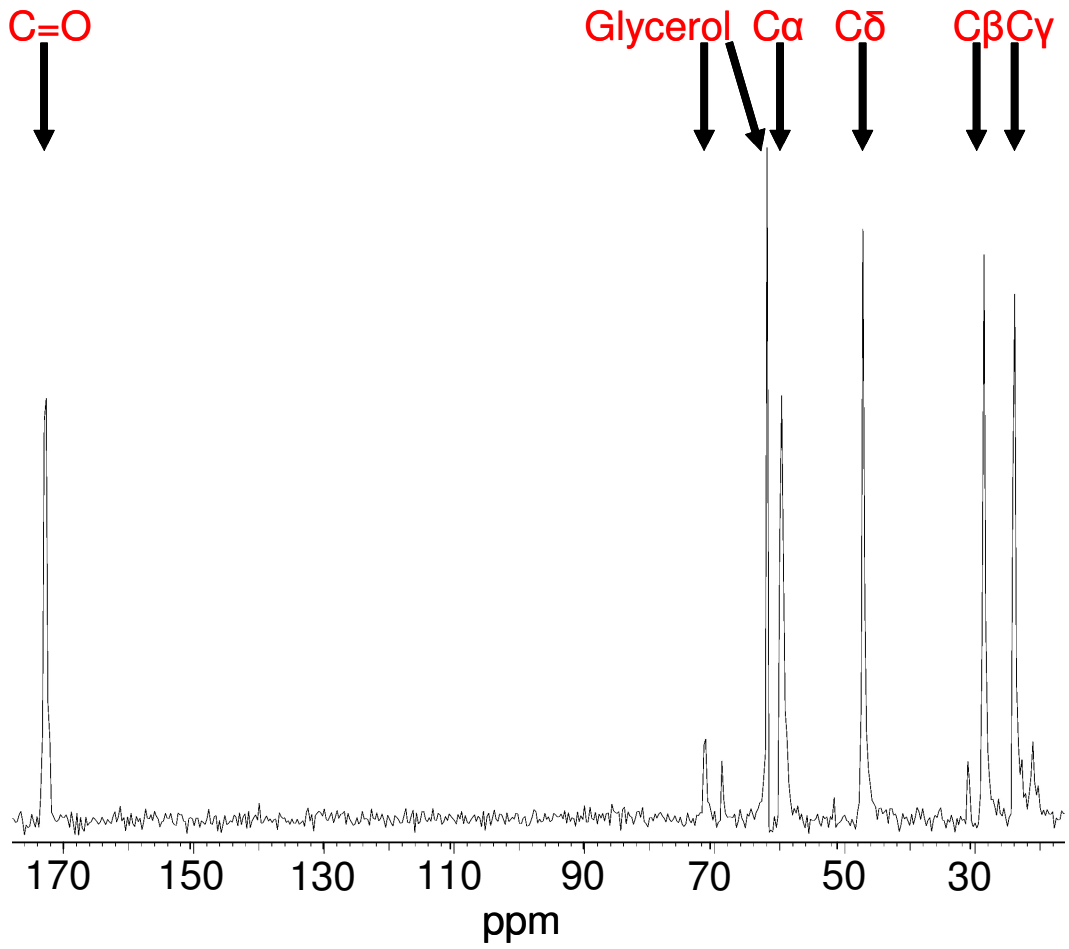

Figure 6.14 - One pulse with decoupling ^{13}C spectrum of 3mg NCCN peptide in 100µl NTR lysis buffer acquired on a 700 MHz Varian / Chemagnetics CMX infinity plus spectrometer with 80 Hz spinning frequency at room temperature.

6.5.3 Peptide synthesis of fully ^{13}C and ^{15}N labeled NT

Fully labeled $NT_{(8-13)}$ was produced by Maureen Pickethly for the purposes of NMR studies bound to NTS1-A, a mass spectrum verifying this synthesis is show in Figure 6.15.

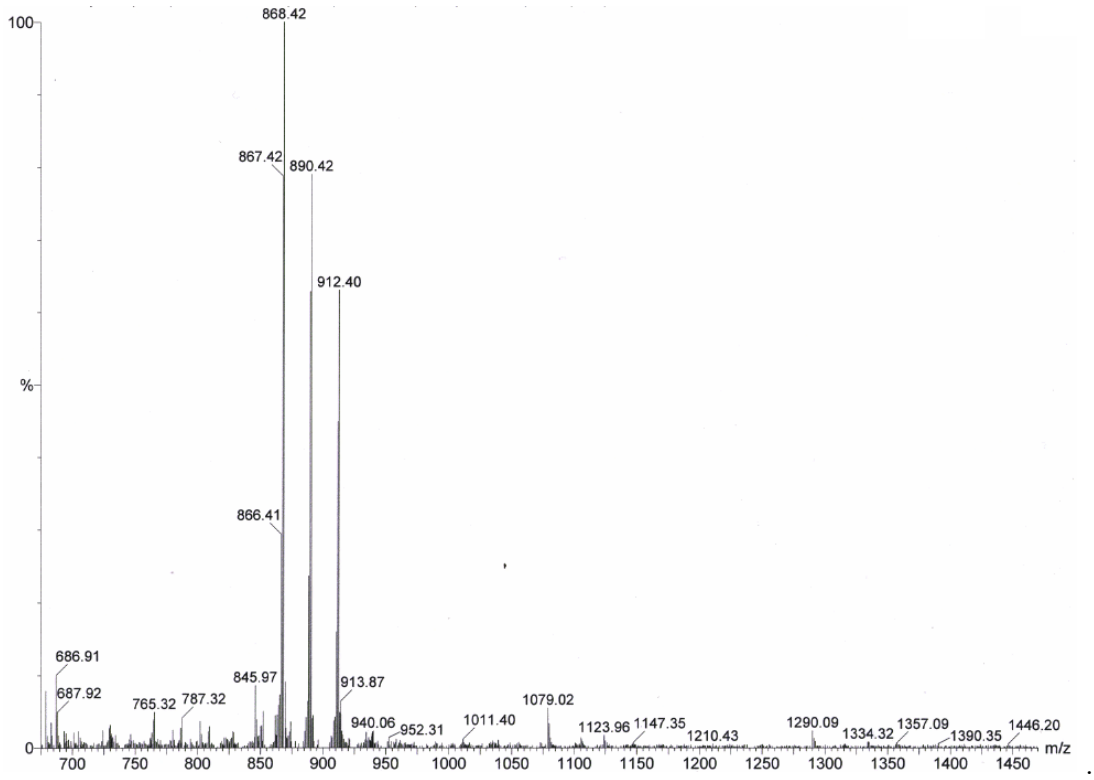

Figure 6.15 – MADLI-TOF ionisation mass spectrum of fully ^{13}C and ^{15}N labelled $NT_{(8-13)}$

The mass spectrum shows the correct peptide weight of 868.42 with the parent ion plus sodium at 890.42 and parent ion plus potassium at 912.40.

6.5.4 Solution Spectra of fully ^{13}C labeled $NT_{(8-13)}$

Assignment of the ^{13}C chemical shifts of $NT_{(8-13)}$ in lysis buffer, the 1D ^{13}C spectrum is shown in Figure 6.16. With the exception of the two resonances arising from the natural abundance of glycerol (62.2 ppm and 71.79 ppm), all the other resonances can be assigned to uniformly ^{13}C labelled $NT_{(8-13)}$ and are in agreement with past assignment [111] and the assignment is given is Table 6.2.

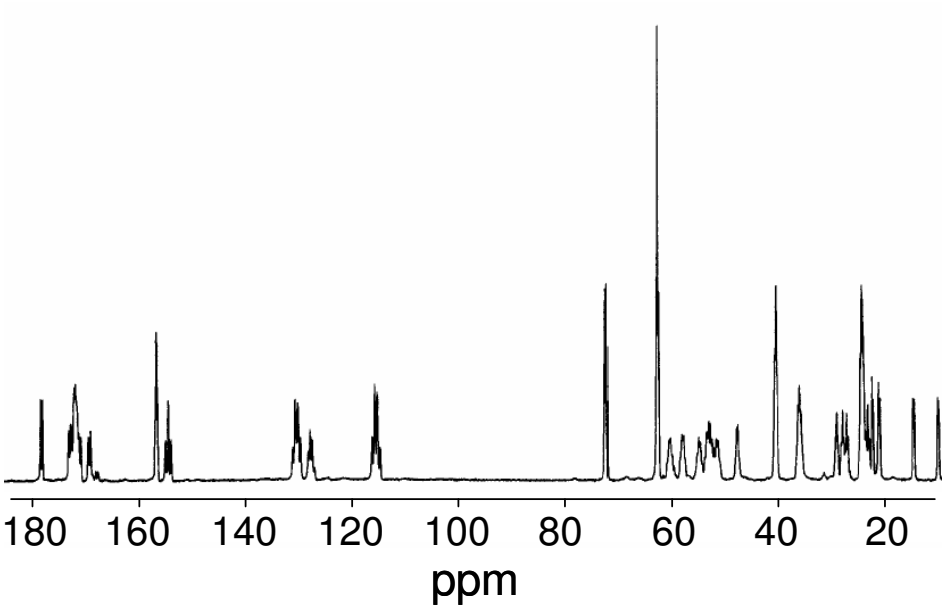

Figure 6.16 – Proton decoupled 13C MAS spectrum of 4mg of uniformly ^{13}C labelled NT(8-13) in lysis buffer. Data were acquired at 5°C and averaged over 1024 acquisitions. The assignment is given in Table 6.2.

Residue	Table 6.2 – Table of the assignment of all the ^{13}C resonances in $NT_{(8-13)}$ ^{13}C chemical shift (ppm)					
	C=O	Cα	Cβ	Cγ	Cδ	other
Arg1	169.4	52.1	28.3	24.2	40.4	156.4(Cε)
Arg2	171.2	50.9	27.5	24.2	40.4	156.4(Cε)
Pro3	172.7	59.8	28.3	23.6	47.9	
Try4	172.0	54.2	35.7			127.3 (C1) 130.4 (C2,6) 115.1 (C3,5) 154.2 (C4)
Ile5	171.8	57.4	35.6	14.3 23.16	9.7	
Leu6	178.1	52.8	40.4	24.2	20.8 22.0	

6.5.5 NMR of Fully ^{13}C labelled $NT_{(8-13)}$ bound to NTS1-A

Figure 6.17 shows a ^{13}C CP-MAS spectrum of purified rNTR-1 receptor in lysis buffer. The glycerol and other buffer peaks dominate the spectrum, but the shoulder on the resonance at 175-180 ppm corresponding to the rNTR-1 carbonyl signal indicates the presence of receptor

protein. Moreover any assignment of the $NT_{(8-13)}$ bound to receptor in 1D is not possible and requires other NMR approaches since the intensity from the natural abundance ^{13}C masks the labelled signal.

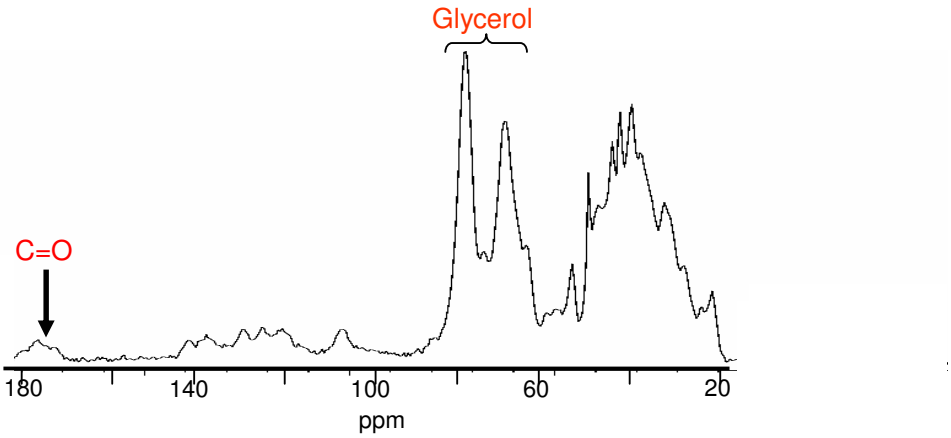

Figure 6.17 - ^{13}C CP-MAS spectrum of purified rNTR-1 receptor in lysis buffer at -130°C. The spectrum was obtained on a 400 MHz CMX spectrometer, with a 5 kHz spinning frequency and accumulated over 48,000 acquisitions, proton field strength of 71 kHz with a contact time of 1 ms; and 63 kHz decoupling during acquisition.

Subtraction of an identical experiment in everything but the presence of labelled ligand in the sample proved difficult as the heights of the glycerol peaks varied over time due to small temperature fluctuations over the course of the long time needed to obtain sufficient signal to noise. To alleviate the problem of the natural abundance background an experimental filter was applied, Figure 6.18 shows a single quantum-single quantum ^{13}C correlation spectrum, the natural abundance resonances are filtered out in the cross peaks. Although further experiments are required for assignment of atoms which give rise to these resonances, it is possible to identify resonances arising from 5 of the carbonyl labels and 4 of the Cαs in the ligand.

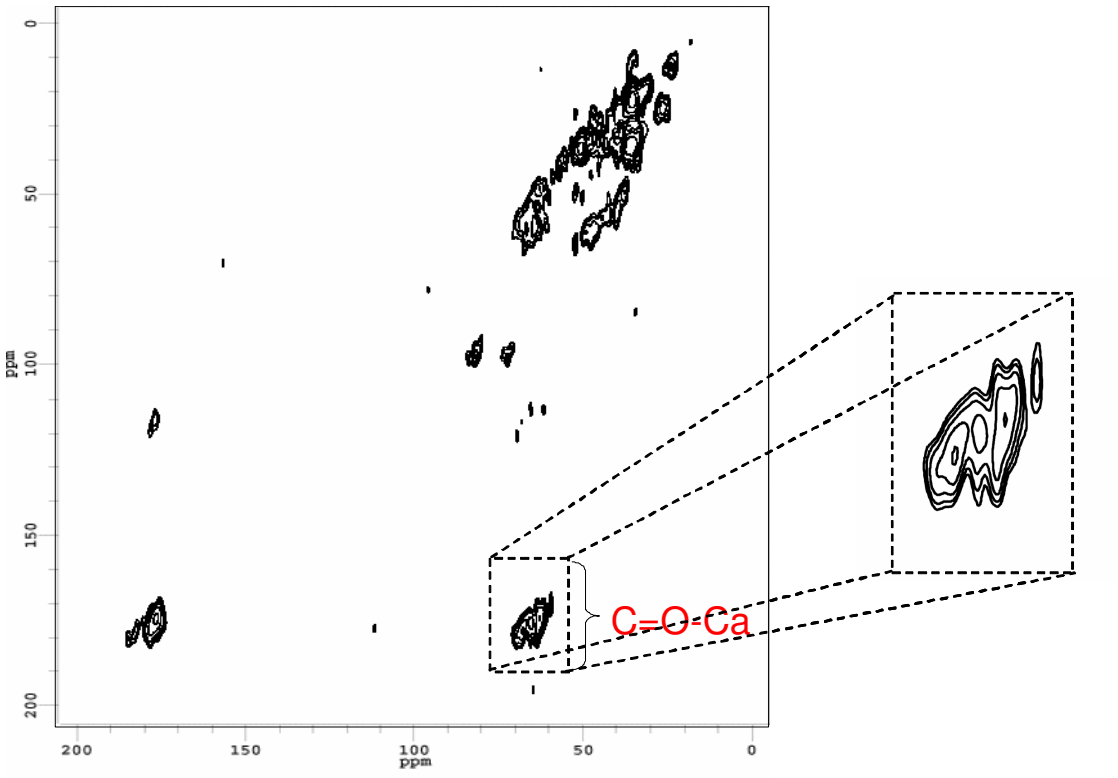

Figure 6.18 – $R14^5_4$ Single quantum-single quantum ^{13}C correlation spectrum of fully ^{13}C $NT_{(8-13)}$ bound to rNTR1 in lysis buffer at -130°C, the spectrum was obtained on a 400 MHz CMX spectrometer, with a 7 kHz spinning frequency, proton field strength of 71 kHz and a ^{13}C field strength of 71 kHz with a contact time of 1.5 ms; and 70 kHz and 63 kHz decoupling during R sequence and acquisition respectively. The rotor contained 21.6 nM of receptor which binds 19µg of labelled $NT_{(8-13)}$.

The $R14^5_4$ 1Q 2Q correlation spectrum in Figure 6.18 clearly has resonances missing; no resonances are visible in the aromatic region (~100-150 ppm); this could be due to rapid motions in these regions of the peptide which would broaden and lower intensities arising from these moieties, reducing them below the noise level in this spectrum. None-the-less the quality of the spectrum considering the amount of label present is very satisfactory.

6.6 Discussion

For the assignment of multiply labelled ligand bound to the receptor it is necessary to filter the natural abundance background generated from the receptor itself and its detergent buffer. Using an $R14^5_4$ experiment it has been possible to do this (Figure 6.18), the choice of the R14 type experiment over a C7 was due entirely to instrumentation, the R14 pulse sequences require less power and present fewer phasing difficulties than the C7 though achieving comparable results. This is the first time that a $R14^5_4$ experiment has been carried out on this type of system, and the preliminary results show it could be an effective method for assignment of multiply labelled ligands bound to membrane receptors in detergent or lipid membranes. Detergent miceller samples are not ideal for these experiments; to improve the signal to noise level reconstitution of the receptor into lipid vesicles would overcome the problems of aggregation when concentrating detergent solubilised receptor, by enabling us to spin down lipid pellets for the NMR. During the course of this work *Luca et al.* published the assignment of the backbone α-carbon residues and the β-carbon of $NT_{(8-13)}$bound to NTS1 using the 2Q filter POST-C7 pulse program [118], modelling of the chemical shifts derived from these assignments indicate that the peptide backbone is in an extended almost β-sheet like conformation though no information was derived about the structure of the side chains of the residues.

Chapter 7 DNA-nanotechnological approaches to membrane protein crystallization and structure determination using NTS1-A as a test case

7.1 Introduction

7.1.1 Nanotechnology and DNA

Nanotechnology is the utilisation of materials, devices and systems through the control of matter scale exploiting the novel properties and phenomena derived from working at the nano scale. DNA, with a diameter of 2 nm and a helical pitch of 3.4 – 3.6 nm which are molecular dimensions suitable for nano-scale constructs and a persistence length (a measure of stiffness) of ~50 nm of the DNA duplex, presents a useful, rigid, structural tool for nanotechnology. Using branched DNA molecules, with the specific bonding and molecular recognition between base pairs driving the formation of self-assembling structures, nonlinear and multidimensional constructs can be formed. DNA, therefore, constitutes a malleable and programmable scaffold that allows precise and specific control over intermolecular interactions, providing a powerful chemically based assembly system [119].

7.1.2 Two-dimensional DNA arrays and crystal structure engineering

An interesting application of this nanotechnology is to use it to produce two dimensional DNA crystals, the basic building block of which is the Holliday junction, an important intermediate in a variety of genetic processes [120]. Periodic arrays are formed by linking multiple copies of this branching DNA structure using complementary "sticky" ends (Figure 7.1).

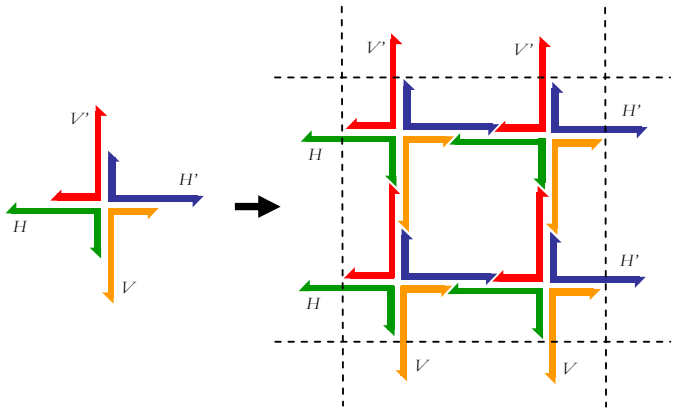

Figure 7.1 – Illustration of how Holliday junctions may be assembled into a 2D array, with the four way junctions being held together by "sticky" end interactions (complementary single-strand regions on different junctions) with the unit cell contained in the dotted lines [121].

By controlling the length and base pair sequence of the constituent oligomers it is possible to tailor the size, periodicity and symmetry of the unit cell to provide a self-assembling repeating 2D array of predetermined proportions.

Arrays are formed through temperature-dependent annealing reactions. Complementary oligonucleotides are heated to a point where there is complete strand separation (typically 75-95 °C). Annealing is then controlled by reducing the temperature over an extended period of time. In this instance, on cooling, individual junctions are thought to form at elevated

temperatures during the cooling process, usually above 40-50 ºC, with the interaction between junctions, which rely on a smaller number of H-bonds, likely to occur at a lower temperature, 30-40 ºC or below.

To date, many such DNA arrays have been generated experimentally and a wide range of potential applications have been put forward for these structures, most involving the use of DNA arrays as scaffold for the assembly of other nano-scale objects. In terms of structural biology, probably the greatest potential application of this technology is in the engineering of crystalline arrays in the form of proteins bound at regular intervals on arrays (Figure 7.2).

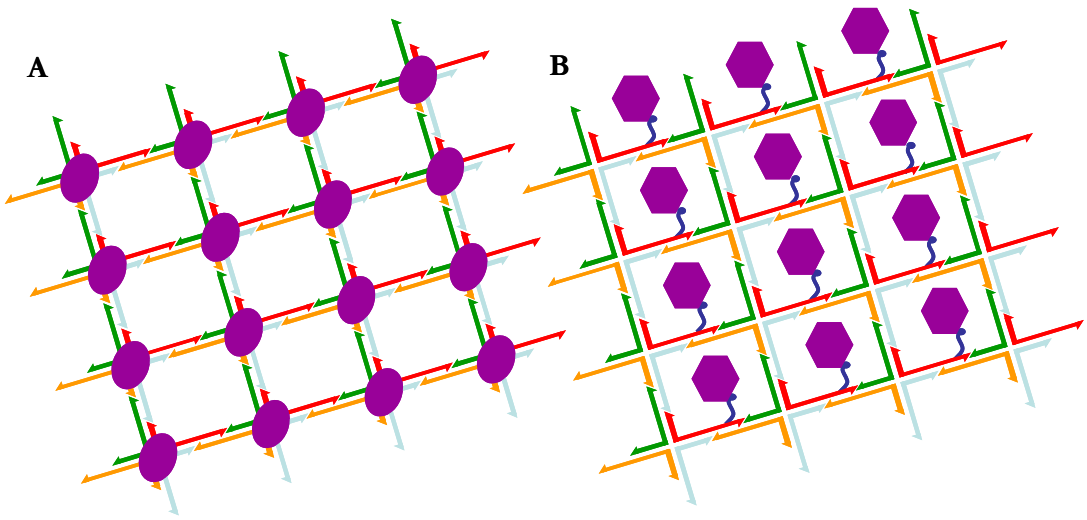

Figure 7.2 – Illustration of the use of DNA arrays to engineer 2D protein crystals with proteins (in purple) binding to the array, either **A** where you have the protein binding to a specific sequence of DNA or **B** the oligonucleotides are derivised with a ligand (in dark blue) which binds the protein to the array in a regularly spaced fashion.

7.1.3 DNA oligonucleotides and the design of DNA arrays

DNA arrays were produced by synthesising oligonucleotides to form Holliday junctions. The sequence details of the oligonucleotides are shown in Figure 7.3. The sequences were designed using secondary structural prediction and energetic predictions made by the *Mfold* program [122], the crystal structure of the DNA Holliday junction [123], and theoretical calculations on the structural properties of DNA [124]. Specific binding of NTS1-A was achieved by a custom synthesis of an oligonucleotide with the 5' guanidine covalently modified with a alkyl chain consisting of six carbons ending in a sulphahydride group attached to the DNA via a SSPY (pyridine-based) linker. This linker was then used to form a disulphide bond with cys-$NT_{(5-13)}$, a truncated from of NT cystinylated to allow the covalent attachment to the oligonucleotide and containing the c-terminal six amino acids of NT vital for receptor binding. Unmodified and thiolated oligonucleotides were obtained from Sigma Geneosys UK, MWG AG Germany, and the $NT_{(5-13)}$ construct was synthesized by Eurogentec Belgium.

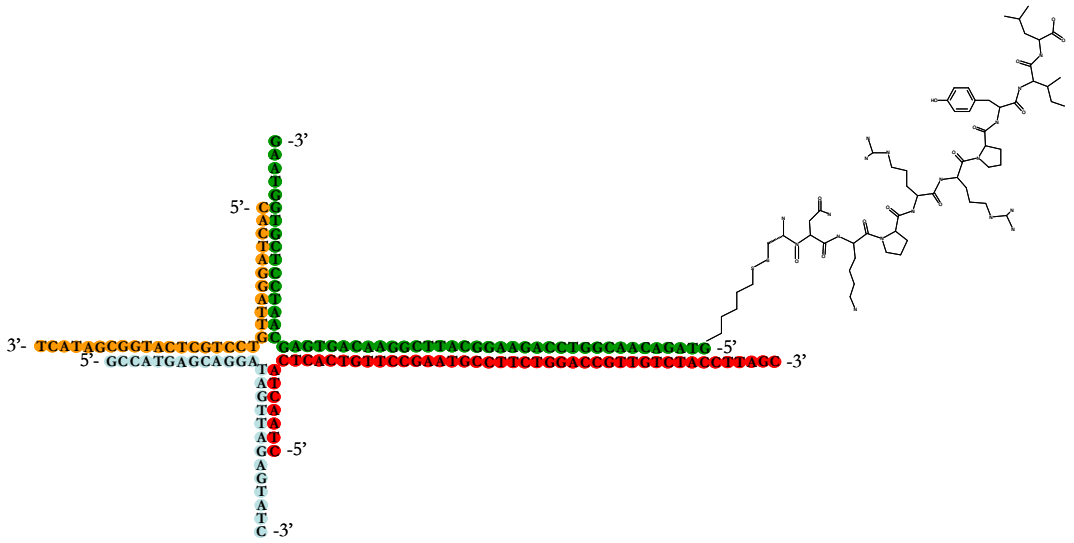

Figure 7.3 – The basic structural unit of the DNA array used, a four-arm Holliday junction [120]. One oligonucleotides (in green) has NT covalently bound to the 5' nucleotide. The different colours denote different strands of DNA, complementary sticky end regions are denoted by contrasting colours (blue to orange and green to red).

The Holliday junction has one long arm (36bp) and three shorter arms (7-13bp), this asymmetry was introduced to position the ligand specifically within the structure of the array. The structure of the assembled array can be seen in Figure 7.4.

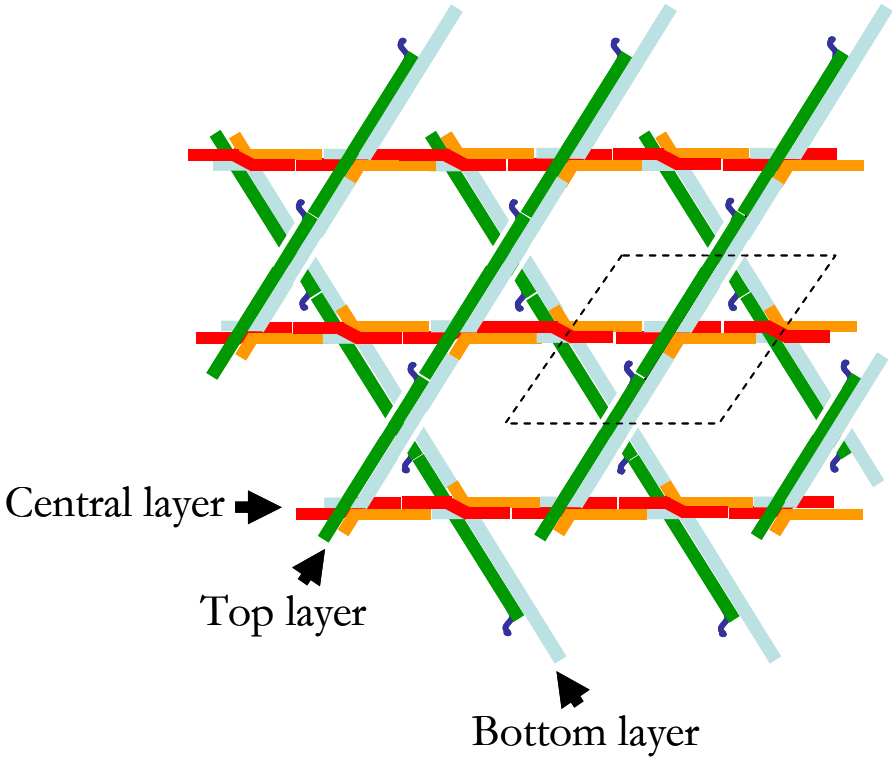

Figure 7.4 – Diagram demonstrating the arrangement of Holliday junctions in the proposed DNA array, with the oligonucleotide colour corresponding to that shown in Figure 7.3, with the NT ligand analogue in dark blue and the unit cell outlined.

The structure of the annealed array forms three parallel interconnected layers of duplex DNA in a honey-style pattern Kagome lattice [125], with the NTS1-A ligand $NT_{(5\text{-}13)}$ pointing down from the upper most layer and up from the bottom most layer into the matrix of the array.

7.1.4 Aims of this study

Historically it has proven notoriously difficult to crystallise membrane proteins with the few successful attempts not appearing to follow any trend or rule. Here DNA nano-technology is used to build a scaffold array of DNA Holliday junctions containing the ligand for NTS1-A in order to generate regular arrays of the GPCR for possible future 2D crystallographic study.

7.2 Methods

Methods are described in 2.9 above.

7.3 Results

7.3.1 Spectrophotometric analysis of array annealing

When single stranded DNA anneals to form a duplex its UV absorbance decreases significantly at most wavelengths [126, 127], providing a means of monitoring the annealing of arrays. This phenomenon, the hyper/hypochromic effect, results from the formation/disruption of the hydrogen bonding between neighbouring bases which alines the pi-electrons in the aromatic rings, so that they are more constrained in sandwich layers overlapping with each other, forming/disrupting pi-pi stacking interactions, and is typically monitored at 260 nm. As the generation of these arrays involves several consecutive annealing steps, oligonucleotides annealing to form individual Holliday junctions, which in turn associate to form ordered crystalline arrays, UV temperature scans provide an attractive means of monitoring the various stages of array formation.

For the formation of a regular DNA array to occur, a large number of Holliday junctions have to anneal together in the correct fashion, and therefore array growth is a highly cooperative process. Conversely, for the melting of an array to occur, several "sticky" end contacts need to

be broken in a concerted fashion with four melting events needed for each separation of a single Holliday junction section from the array which is energetically and kinetically highly unfavourable. As a result, the temperature dependence of the DNA annealing and melting events are distinct, giving rise to hysteresis in the UV temperature scans. The temperature profile of annealing is shown below (Figure 7.5).

The absorbance changes can be broken down into three defined regions of annealing or melting events separated by periods of structural equilibrium. The first of these events, bracket 1 in Figure 7.5, which occurs between 80 °C → 70 °C, is likely to be due to the annealing of the long arm of the Holliday junction units, from calculated annealing temperatures of the base pairing in this region.

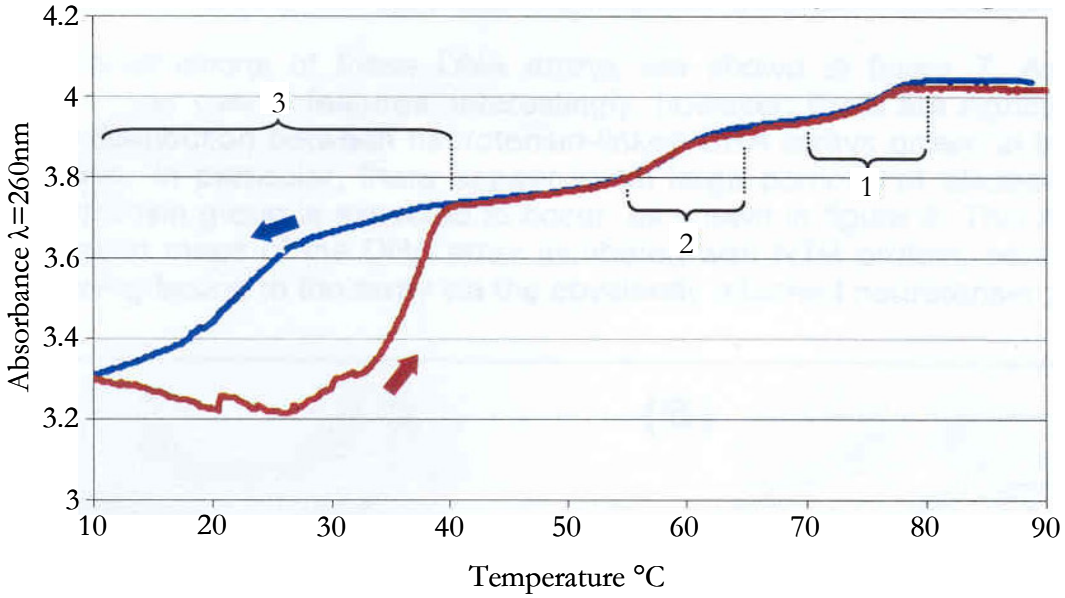

Figure 7.5 – UV temperature scan to monitor the formation of the DNA array, with decreasing temperature shown in blue, increasing temperature in red and notable regions marked with brackets.

The second event, bracket 2 in Figure 7.5, which occurs between 65 °C → 55 °C, from calculated annealing temperatures of the base pairing in this region, is likely to be the formation of the three smaller arms of the Holliday junction completing the annealing on the basic unit of the array. The final event, bracket 3 in Figure 7.5, occurring between 40 °C → 10 °C corresponds to the formation of the "sticky" end interactions, between Holliday junction units, building up the matrix of the array itself. The first two of these events are essentially identical for annealing (decreasing temperature) and melting (increasing temperature), but the third event, the "sticky" end association and dissociation differs markedly, it appears that association occurs from 40 °C → 10 °C but that dissociation, melting, of this interaction occurs between 30 °C → 40 °C with the intervening trace from 10 °C → 30 °C ascribed to abortive melting of "sticky" ends due to lack of energy.

Similar UV annealing profiles have been obtained from previously studied crystalline arrays [128]. The significant annealing occurs between 15 ºC and 30 ºC, which is considerably lower than for earlier arrays studied. This temperature difference in the annealing profile led to the choice of an annealing protocol with a temperature range from 70 ºC to 10 ºC which was a lower range than that used to form arrays in previous studies.

7.3.2 Electron microscopy of protein bound DNA arrays

A number of $NT_{(5\text{-}13)}$ linked DNA arrays were tested, some producing regular micrometer sized arrays in the presence and absence of NTS1-A. These array crystals were visualized using negative-stain electron microscopy; an example micrograph is shown below in Figure 7.6. Electron micrographs were recorded on Kodak SO163 film under low dose conditions using a Philips CM120 electron microscope at 100-kV acceleration. The nominal defocus range was between 400 and 700 nm, the nominal magnification was 45000×. Electron micrographs were

scanned with a UMAX Powerlook 3000 scanner at a sampling raster of 8.33 μm corresponding to a pixel size of 1.9Å.

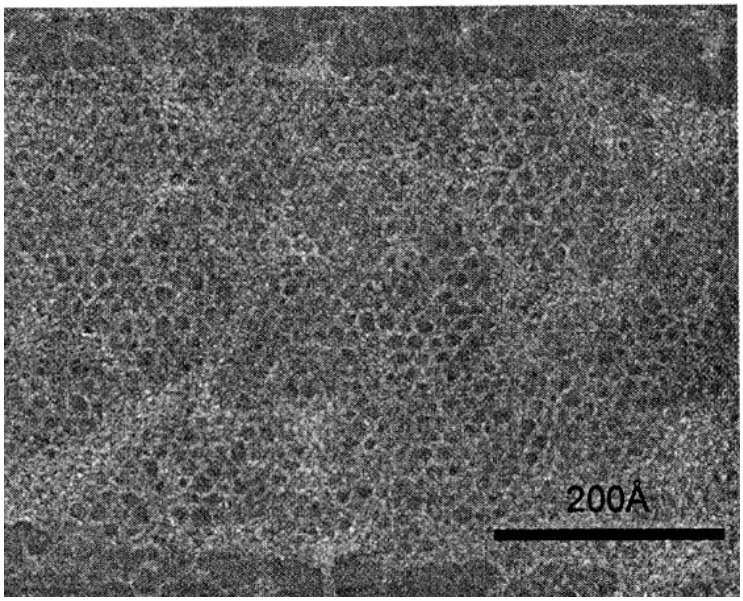

Figure 7.6 - An electron micrograph of a negatively stained with 2 % uranyl acetate DNA array containing $NT_{(5-13)}$The micrograph above appears to show a regular honeycomb-like hexagonal array has been formed though image processing is necessary for confirmation of this.

Image processing was carried out using the MRC program package [66] as well as the CCP4 package [67]. Fourier transformation of this image-processed micrograph shows strong first and second order spots which are indicative of the presence of an ordered structure Figure 7.7.

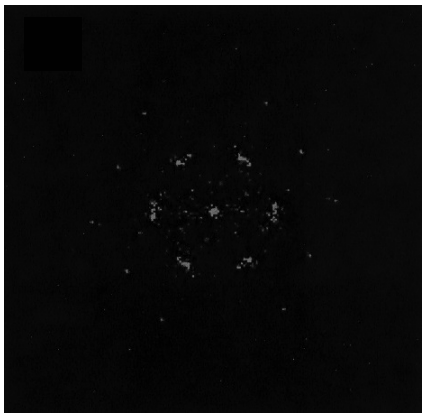

Figure 7.7 – A fourier transform of an image-processed micrograph of the macrograph of negatively stained DNA arrays containing $NT_{(8-13)}$ above (Figure 7.6).

Image reconstructions of these data are shown in Figure 7.8. As expected, the projection maps are superficially similar in their overall features. There are significant differences, however, in electron density around the liganded areas between arrays grown in the presence and absence of NTS1-A.

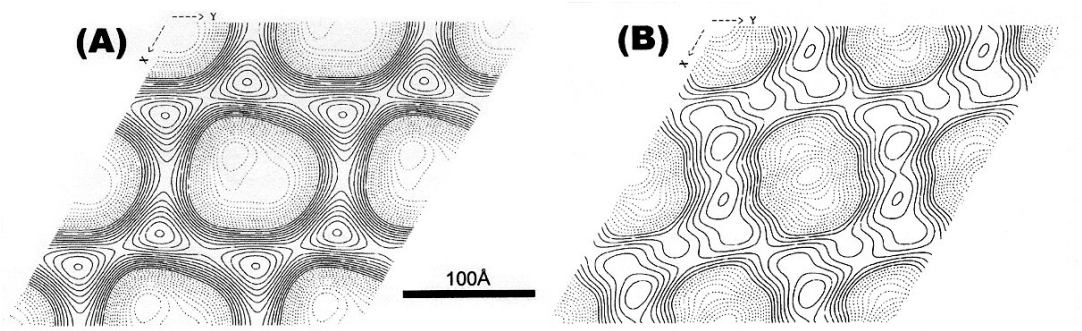

Figure 7.8 – EM image reconstruction of DNA arrays with covalently bound NT(5-13) (A) with no NTS1-A present during the last stages of annealing and (B) NTS1-A added during the final stages of annealing.

The projection map of the neurotensin-linked DNA three-layer honeycomb-type DNA array in the absence of NTS1-A, shown in Figure 7.8 (A), has a P1 spacegroup, the unit cell dimensions of which are: a = b = 132 Å, y = 120.1°. The projection map for honeycomb-type DNA arrays formed in the presence of NTS1-A, shown in Figure 7.8 (B), also has P1 spacegrouping, with an altered unit cell: a = 134 Å, b = 135 Å, y = 119.9°. This density difference could be ascribed to NTS1-A binding to the covalently bound $NT_{(5\text{-}13)}$ on the crystals. In both cases no higher order symmetry was used in the image reconstruction. Although the overall shape of the two projections is similar, the peak density of the maps with and without NTS1-A occurs in different regions, suggesting that there is a structural difference between the two crystals indicative of NTS1-A binding to the arrays. The density unique to

arrays formed in the presence of NTS1-A are highlighted below; the regions approximate to where the ligand is expected to appear in the architecture of the arrays Figure 7.9.

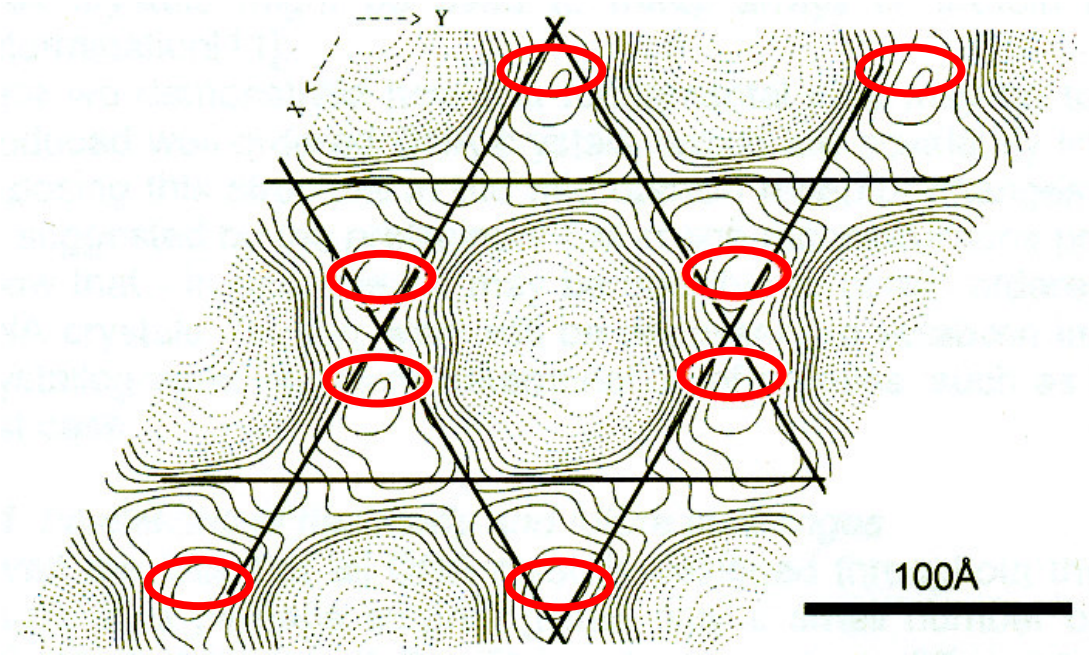

Figure 7.9 – Image reconstruction of DNA arrays formed in the presence of NTS1-A with the locations of the unique density seen in the presence of the receptor highlighted (from Figure 7.8 **(B)**).

Although all of the projection maps of the arrays formed with NTS1-A present show higher density in the region of expected receptor binding, only a small number of images were processed and analyzed. For definitive proof of DNA-NTS1-A forming a regular co-crystalline array more images need to be produced and results should be merged from different preparations to clarify the statistical significance of these results.

The arrays analysed have consistent unit cell dimensions, a≈b≈130-140 Å and y≈120°. The repeating unit for the arrays, some 53 bp, gives an average length of the duplex DNA in the Holliday junctions of ≈2.5 Å per bp. This is similar to the secondary structure of A-type DNA, which has a "rise" (the average length of the DNA per bp) of 2.3 Å, a structure which

tends to be common in dehydrated DNA duplex differing from the more common B-type secondary structure with a "rise" of 3.3 Å and could be an artefact of the staining process, causing a dehydration shrinkage of the DNA when it is mounted onto the glow-discharged, carbon-coated EM grids.

7.4 Discussion

DNA may be regarded as a powerful molecular recognition system, which can be manipulated to form self-assembling nano-structure scaffolds, which in turn can be used to form regular repeating arrays. It has long been thought that such nano-structures could be used to form two-dimensional arrays of protein molecules for the application of crystallographic structural methods [129]. Here this theory has become experimental reality: well-ordered DNA crystals have been produced with a covalently linked truncated ligand analogue, for NTS1-A, $NT_{(5\text{-}13)}$. Similar studies have been carried out using the soluble Holliday junction binding protein RuvA [130], though this is the first instance of using a non DNA binding protein and certainly a membrane proteins to generate and study such arrays. Addition of NST1-A towards the end of the annealing process of the arrays changes final nano-constructs surface properties in the area of the covalently linked receptor ligand, as seen in the preliminary EM image reconstructions presented above. This work demonstrates the principle that it could be possible to produce crystalline 2D DNA arrays as a scaffold for obtaining an ordered arrangement of, notoriously hard to crystallise, membrane proteins that can then be used for the application of crystallographic structural techniques.

The arrays used throughout this investigation were modifications of previous experimentally produced nanostructures and it is curious that only a small number of these array designs could be produced and visualized experimentally in this study. This could be attributed to the high degree of asymmetry in the Holliday junctions from which the array matrix is formed; as

seen in Figure 7.3, one arm of the Holliday junction is considerable longer than the others, which could have a destabilizing effect on the junction itself and it is worth noting that other arrays using junctions with even more pronounced asymmetry failed to produce ordered structures. The presence of $NT_{(5\text{-}13)}$, a relatively bulky derivative, at the 5' end of the long arm of the Holliday junction could add to this instability with steric hindrance causing the destabilization of the "sticky" end preventing or impairing array formation. This possibility is supported by the fact that the $NT_{(5\text{-}13)}$ bound arrays grow in a highly anisotropic manner, given the three-layer architecture of the arrays and the fact that the ligand is on only the outer layers facing into the array (Figure 7.4), its steric hindrance could slow array growth along the axis of the structure. More isotropically designed arrays, where increased "sticky" end length provides compensation for the lost binding due to the presence of the ligand, have so far been unsuccessful.

Subtle factors such as different conformations of constituent Holliday junction and the presence of particular nucleotide sequences which may have an effect on the secondary and tertiary structure of the constituent DNA may also be playing a role in whether a conceptual array is experimentally achievable. Annealing conditions of the $NT_{(5\text{-}13)}$ linked arrays are extremely sensitive to the concentration of magnesium ions and temperature gradients used in the incubations, despite being based on array designs that have previously been seen to be robust in these aspects [128]. The liganded arrays are extremely unstable and it remains to be seen whether it will be possible to stabilise them by extending annealing contacts in the form of "sticky" end linkage between the Holliday junctions. Further experimental difficulties arise from the tendency of the arrays themselves to aggregate. Analysis of EM micrographs suggest that most of the assemblies are either bound to other arrays or folded over on themselves, with only a small fraction of single layer structure present. The largest and often the most well

ordered nanostructures tend to be multilayered and attempts to separate them for EM analysis have met only limited success.

Chapter 8 Conclusions

The work presented in this thesis demonstrates a number of techniques for the study of GPCRs. Its starts with describing a means of obtaining sufficient quantities of pure and active NTS1, in the form of a truncated fusion protein, for biophysical studies, presents the first example in this work of the synthesis of NT and NT like peptides to facilitate the study of this system and the reconstitution of the pure detergent solubilized receptor into a model membrane system (Chapter 3). The receptor samples produced using the methods described in Chapter 3 were then used in a variety of biophysical studies in order to elucidate more information as to its function. Studies of the kinetics of NT binding to NTS1-A were carried out using surface plasmon resonance (SPR) (Chapter 4) and have provided insight into the mechanism of receptor activation. Studies of the dynamics of the putatively non-binding region of NT (amino acids 1-7) investigated using electron spin resonance (Chapter 5) demonstrated a possible role for this region *in vivo*. Solid state NMR was used with ^{13}C and ^{15}N labelled $NT_{(8-13)}$ to investigate means of obtaining assignment of the ligand bound to its receptor (Chapter 6) in the presence of a huge natural abundance signal. Finally, DNA was used as a scaffold, in the form of arrays of Holliday junctions modified to contain an NT agonist analogue covalently bound to one of the oligonucleotides, for generating a regular array

of NTS1-A (Chapter 7) with the view to obtaining 2D-crystalographic data from a notoriously difficult to crystallise membrane proteins.

Expression, Purification and Reconstitution of the G-Protein Coupled Receptor (GPCR) NTS1

It is an attractive option to express proteins in *E. coli* as it constitutes a cost effective easily manipulated host, but problems arise when one wishes to use *E. coli* as a host for the expression of a eukaryotic protein, especially a membrane protein, as it lacks the post-translational mechanisms present in eukaryotes for folding and modification. This chapter described a system in which these difficulties have been overcome using truncation to remove the N-terminal sites of glycosylation from NTS1, fusion proteins to target the N-terminus to the periplasmic space and stabilise both of the termini and an affinity tag to assist in purification. The two step affinity purification process, His_{10} tag and native ligand, facilitates a high level of pure, and initially active, NTS1-A though lability is a problem with detergent soluble receptor needing to be kept at 4 °C during experimentation and – 80 °C for storage. At small scale the expression system is an inefficient way of producing the quantities of receptor needed in this study, though the system was scalable and movement to large volume fermentation enabled the production of large amounts of cell base rapidly. Although the number of active receptors per cell may not be increased, the time taken to produce a sample can be cut drastically by using large scale fermenters which not only allow for much larger volumes to be processed at any one time but also give much more automated control and fine tuning of the growth conditions, for example by controlling the dissolved oxygen content and pH of the media. Radio ligand activity assays show an average yield of 2.7 nmol ± 2.3 nmol active NTS1-A per 20 g of purified cell base which is approximately half of the total protein eluted. Future prospects for this work involve the investigation of new cell lines C 41 and C43 [131], mutated in such a way as to have extensive invaginations in their membrane increasing

the surface area of membrane per cell extensively, in the hope that this increases the area which NTS1 can be correctly folded into. During the course of this write up a new plasmid construct has been made (pNTS1-B) in which we have placed Tev protease sites to remove the fusions from the NTS1 receptor itself and this needs to be investigated in all aspects of the work to see whether the fusions have been generating anomalous results. For the reconstitution protocol it would be nice to examine the samples under EM, this would provide information as to whether we were getting occluded sites in reconstituted samples which seemed to hinder the acquisition of ESR data from protein in this state.

Surface Plasmon Resonance studies of NTS1-A

Surface plasmon resonance (SPR) represents an attractive technique for the direct observation of the binding interactions of biomolecules. The very nature of the interaction of neurotensin receptors with their native ligand lends itself to study with SPR as it is possible to bind the N-terminus of the peptide ligand to large entities and still observe a binding interaction. This study has yielded the first SPR kinetic data for a detergent-solubilised ligand-binding GPCR and also investigates techniques for the direct kinetic study of reconstituted receptor. Using the receptor molecule as the analyte overcomes the problem of the small responses encountered in the reverse orientation, as this orientation of the interaction elicits larger difference in mass concentration at the surface of the chip during a binding event. The data yielded an overall apparent K_D in the nanomolar range of 37.3 ± 11.3 nmol, this value is larger than the K_D of 0.4 ± 0.11 nmol that was obtained for detergent-solubilised NTS-1A from saturation radioligand binding experiments [68] which could be because of the presence of the fusions on NTS1-A or steric hindrance from the surface of the chip itself. This technique will have useful applications to other suitable GPCR systems, where binding can still be observed when the ligand is tethered to the sensor surface, not only providing insights into the kinetics and mechanisms involved in ligand binding, but also in the search for novel ligands and in the

more rigorous optimisation of detergent solubilisation procedures than is currently possible using conventional techniques. The study of possible conformational changes which occur upon ligand binding to NT receptors and other GPCRs will be crucial to gaining an understanding of how ligand binding at the cell surface is coupled to downstream signalling events. Future work here would involve repeating the detergent studies using another sensor surface (e.g. the planar CM1 chips), attempting measurements in the reverse orientation (with the NT as the analyte and the NTS1-A as the ligand), and also once the protocol has been established for the production of NTS1-B and NTS1 without its fusions in detergent these experiments could be repeated to determine the effect if any of the fusions in the experiments here.

Electron Spin Resonance studies to investigate the mobility of NT at its binding site on NTS1-A

The main focus of studies on NTSs and their interaction with NT have focused on $NT_{(8-13)}$ in the main due to the fact that it is all that is required for receptor activation. It has become so engrained in the field that statement likes "$NT_{(8-13)}$ is a peptide fragment of neurotensin (NT) and is more biologically relevant than the parent peptide" [50] start to arise in the literature, but this is misguided as this truncated analogue of NT never occurs *in vivo* even as a degradation product of NT. This chapter demonstrated that there is an induced restriction of motion in the N-terminus of NT upon binding to NTS1-A, with the correlation time increasing approximately by an order of magnitude at least (1.9 ns to 11.4 ns) in the presences of excess receptor binding sites. These results indicate that the 1-7 region of NT is associating with the receptor on binding and although it is not responsible for inducing communication through the NTS1 to G-proteins, as the 8-13 region alone can accomplish this, it could have a role other than inducing the conformational change which communicates the signal into the cell. Since $NT_{(8-13)}$ does not occur *in vivo* and given the observations in this chapter, it is biologically

relevant to study the native ligand NT. Clearly this initial study now opens up the way for more similar studies to elucidate these possibilities. Prospects for this work involve a more in depth study of the systems already used addressing the possible issues of their being a number of species present in the experiments in the presence of receptor. Also plans are underway for the labelling of the receptor itself to examine the motions of exposed cysteine residues and possibly obtain a Stokes radius measurement, again examination of NTS1-B would be interesting in this case.

Nuclear magnetic resonance (NMR) studies of the NT agonist analogue $NT_{(8-13)}$

The natural abundance background arising from detergent/lipids and indeed the protein itself mask the signal arising from labelled ligand bound to receptor. For detergent samples subtractions of the background were made difficult because of the quantity of glycerol in the buffer making it difficult to freeze out the motions of the resonance arising from this cryo-protectant. Using an $R14^5_4$ experiment it has been possible to filter resonances arising from labelled ligand from the natural abundance background. This is the first time that a $R14^5_4$ 1Q-2Q correlation experiment has been used to study a ligand bound to a membrane protein, and the preliminary results show it could be an effective tool for assignment of multiply labelled ligands bound to membrane receptors in detergent or lipid membranes. Detergent miceller samples are not ideal for this these experiments; to improve the signal to noise level reconstituted receptor would over come the problems of aggregation when concentrating detergent solubilised receptor, by enabling us to spin down lipid pellets for the NMR. Further work here would focus on assignments of the residues arising from the side chains of $NT_{(8-13)}$ as so far only backbone α-carbon resonances and the β-carbon resonances have been assigned. Distance measurements in the form of rotational resonance and REDOR experiments would

also be needed using new labelling schemes to achieve accurate single distance measurements, an area in which solid state NMR excels.

DNA-nanotechnological approaches to membrane protein crystallization and structure determination using NTS1-A as a test case

The use of three-dimensional scaffolds of DNA to generate a repeating crystalline array of proteins for X-ray crystallography, where the structural order is generated by the regular array of Holliday junctions rather than protein to protein contacts, has been demonstrated. Well-ordered DNA crystals have been produced with a covalently linked truncated ligand analogue, for NTS1-A, $NT_{(5-13)}$, similar studies have been carried out using the soluble Holliday junction binding protein RuvA [130], though this is the first instance of using a non DNA binding protein and certainly a membrane proteins to generate and study such arrays. The addition of NTS1-A towards the end of the annealing process, of the DNA scaffold, produced an increased electron density, around the area of the arrays where the receptors ligand is covalently bound to the DNA, from arrays formed in the absence of NTS1-A. The arrays analysed have consistent unit cell dimensions, a≈b≈130-140 Å and y≈120°. The repeating unit for the arrays, some 53 bp, gives an average length of the duplex DNA in the Holliday junctions of ≈2.5 Å per bp. Electron microscopy of 2D crystals has achieved resolutions of up to 3.5 Å [132] and has the advantage of requiring very small amounts of protein (approximately 1 μg per grid). The work carried out here has demonstrated a principle by which membrane proteins, notoriously hard to crystallise by conventional means, can be induced to form regular arrays for the application of crystallographic techniques. The further prospects of this work involves investigation of more stable arrays, in order to combat the problems faced with the aggregation of arrays in the presence of NTS1-A. This achieved, more EM studies would be carried out in the hope of achieving much higher resolutions and

obtaining structural information about the receptor. Again here application of the techniques used here on NTS1-B could also prove very insightful.

Bibliography

1. Van-Holde, K.E. and C.K. Mathews, *Biochemistry*. 1990: The Benjamin/Cummings Publishing Comoany.

2. Liang, F., et al., *Gene Index analysis of the human genome estimates approximately 120,000 genes.* Nature Genetics, 2000. **25**(2): p. 239-240.

3. Liang, F., *Gene Index analysis estimates the human genome contains 120,000 genes (vol 25, pg 239, 2000).* Nature Genetics, 2000. **26**(4): p. 501.

4. Garavito, R.M., D. Picot, and P.J. Loll, *Strategies for crystallizing membrane proteins.* Journal of Bioenergetics and Biomembranes, 1996. **28**(1): p. 13-27.

5. Consortium, I.H.G.S., *Initial sequencing and analysis of the human genome.* Nature, 2001. **409**: p. 860-921.

6. Bargmann, C.I., *Neurobiology of the Caenorhabditis elegans genome.* Science, 1998. **282**(5396): p. 2028-2033.

7. Plakidou-Dymock, S., D. Dymock, and R. Hooley, *A higher plant seven-transmembrane receptor that influences sensitivity to cytokinins.* Current Biology, 1998. **8**(6): p. 315-324.

8. Dohlman, H.G., et al., *Model systems for the study of 7-transmembrane segment receptors.* Annual review of biochemistry, 1991. **60**: p. 653-688.

9. Devreotes, P.N., *G-protein-linked signaling pathways control the developmental program of Dictyostelium.* Neuron, 1994. **12**(2): p. 235-241.

10. Vernier, P., et al., *An evolutionary view of drug-receptor interaction - The bioamine receptor family.* Trends in Pharmacological science, 1995. **16**(11): p. 375-381.

11. New, D.C. and J.T.Y. Wong, *The evidence for G-protein-coupled receptors and heterotrimeric G proteins in protozoa and ancestral metazoa.* Biological signals and receptors, 1998. **7**(2): p. 98-108.

12. Baldwin, J.M., *The probable arrangement of the helices in G-protein coupled receptors.* EMBO, 1993. **12**(4): p. 1693-1703.

13. Krasnoperov, V.G., et al., *Alpha-latrotoxin stimulates exocytosis by the interaction with a neuronal G-protein-coupled receptor.* Neuron, 1997. **18**(6): p. 925-937.

14. Davletov, B.A., et al., *Alpha-Latrotoxin stimulates vesicle exocytosis via latrophilin- and PLC-mediated coupling of external and stored Ca^{-2} and induces Ca^{2+}-independent membrane pores.* European Journal of Neuroscience, 1998. **10**: p. 217-217.

15. Pin, J.P. and J. Bockaert, *Get receptive to metabotropic glutamate receptors.* Current opinion in neurobiology, 1995. **5**(3): p. 342-349.

16. Kaupmann, K., et al., *Expression cloning of GABA(B) receptors uncovers similarity to metabotropic glutamate receptors.* Nature, 1997. **386**(6622): p. 239-246.

17. Bargmann, C.I., *Olfactory receptors, vomeronasal receptors, and the organization of olfactory information.* Cell, 1997. **90**(4): p. 585-587.

18. Dulac, C. and R. Axel, *A novel family of genes encoding putative pheromonereceptors in mammals.* Cell, 1995. **83**(2): p. 195-206.

19. Uhl, G., E. Bennet, and C. Nemeroff, *Neurotensin, a central nervous system peptide: apparent receptor binding in brain membranes.* Brain Research, 1977. **130**: p. 299.

20. Tanaka, K., M. Masu, and S. Nakanishi, *Structure and Functional Expression of the Cloned Rat Neurotensin Receptor*. Neuron, 1990. **4**(6): p. 847-854.

21. Chalon, P., et al., *Molecular cloning of a levocabastine-sensitive neurotensin binding site*. FEBS Letters, 1996. **386**(2-3): p. 91-94.

22. Mazella, J., et al., *Structure, Functional Expression, and Cerebral Localization of the Levocabastine-Sensitive Neurotensin/Neuromedin N Receptor from Mouse Brain*. The Journal of Neuroscience, 1996. **16**(18): p. 5613-5620.

23. Mazella, J., et al., *The 100-kDa Neurotensin Receptor Is gp95/Sortilin, A Non-G-Protein-coupled Receptor*. Journal of Biological Chemistry, 1998. **273**(41): p. 26273-26276.

24. Vita, N., et al., *Cloning a and Expression of a Complementray-DNA Encoding a High-Affinity Human Neurotensin Receptor*. FEBS Letters, 1993. **317**(1-2): p. 139-142.

25. Dubuc, I., et al., *The Nonpeptide Neurotensin Antagonist, SR 48692, Used as a Tool to Reveal Putative Neurotensin Receptor Subtypes*. British Journal of Pharmacology, 1994. **112**(2): p. 352-354.

26. Gully, D., et al., *Biochemical and Pharmacological Activities of SR 142948A, a New Potent Neurotensin Receptor Antagonist*. Journal of Pharmacology and experimental Therapeutics, 1997. **280**(2): p. 802-812.

27. Botto, J.M., et al., *Effects of SR 48692 on neurotensin-induced calcium-activated chloride currents in the Xenopus oocyte expression system: Agonist-like activity on the levocabastine-sensitive neurotensin receptor and absence of antagonist effect on the levocabastine insensitive neurotensin receptor*. Neuroscience Letters, 1997. **223**(3): p. 193-196.

28. Vita, N., et al., *Neurotensin is an antagonist of the human neurotensin NT2 receptor expressed in Chinese hamster ovary cells*. European Journal of Pharmacology, 1998. **360**(2-3): p. 265-272.

29. Petersen, C.M., et al., *Molecular Identification of a Novel Candidate Sorting Receptor Purified from Human Brain by Receptor-associated Protein Affinity Chromatography*. Journal Of Biological Chemistry, 1997. **272**(6): p. 3599-3605.

30. Carraway, R. and S.E. Leeman, *Discovery of neurotensin*. Journal of biological Chemistry, 1973. **248**: p. 6854-6861.

31. Kitabgi, P., R.E. Carraway, and S.E. Leeman, *Isolation of a tridecapeptide from bovine intestinal tissue and its partial characterisation as neurotensin*. Journal of Biological Chemistry, 1976. **251**: p. 7053-7058.

32. Kasckow, J. and C.B. Nemeroff, *The Neurobiology of neurotensin: focus on neurotensin-dopamine interactions*. Regulatory Peptides, 1991. **36**(2): p. 153-164.

33. Elliott, P.J. and C.B. Nemeroff, *Repeated neurotensin administration in the ventral tegmental area: effect on baseline and D-ampetamine-induced locomotor activity*. Neuroscience Letters, 1986. **68**(2): p. 239-244.

34. Clineschmidt, B.V., J.C. mcGuffin, and P.B. Bunting, *Neurotensin:antinocisponsive action in rodents*. European Journal of Pharmacology, 1979. **52**(1-2): p. 129-139.

35. Bissette, G., et al., *Hypothermia and intolerance to cold induced by intracisternal administration of the hypothalamic peptide neurotensin,*. Nature, 1976. **262**: p. 607-609.

36. Bissette, G., et al., *Modification of pentobarbital-induced sedation by natural and synthetic peptides*. Neuropharmacology, 1978. **17**: p. 229-237.

37. Kinkead, B., E.B. Binder, and C.B. Nemeroff, *Does neurotensin mediate the effects of antipsychotic drugs*. Society of biological Psychiatry, 1999. **46**: p. 340-351.

38. Schimpffa, R.M., et al., *Increased plasma neurotensin concentrations in patients with Parkinson's disease.* Journal of Neurosurgery Psychiatry, 2001. **70**: p. 784-786.

39. Kitabgi, P., *Effects of neurotensin on intestine smooth muscle: application to study structure activity relationships.* Annual New York academy of science, 1982. **400**: p. 37-55.

40. Kachur, J.F., et al., *Neurohormal control of ileal electrolyte transport.* Journal of Pharmacology and experimental therapeutics, 1982. **220**: p. 456-483.

41. Evers, B.M., et al., *Neurotensin Expression and Release in Human Colon Cancers.* Annals of Surgery, 1992. **216**(4): p. 423-431.

42. Moody, T.W., et al., *SR48692 is a neurotensin receptor antagonist which inhibits the growth of small cell lung cancer cells.* Peptides, 2001. **22**(1): p. 109-115.

43. Xu, G.Y. and C.M. Deber, *Conformations of Neurotensin in Solution and in Membrane Enviroments Studied by 2-D NMR-Spectroscopy.* International Journal of Peptide and Protein Research, 1991. **37**(6): p. 528-535.

44. Gully, D., et al., *Biochemical and Pharmacological Profile of a Potent and Selective Nonpeptide Antagonist of the Neurotensin Receptor.* Proceedings of the national academy of Science, 1993. **90**: p. 65-69.

45. Steinburg, R., et al., *SR-48692, A Nonpeptide Neorotensin Receptor Antagonist Differentially Affects Neurotensin-Induced Behaviour and Changes in Dopaminergic Transmission.* Neuroscience, 1994. **59**(4): p. 921-929.

46. Pugsley, T.A., et al., *Differential Effects of the Nonpeptide Neurotensin Antagonist, SR 48692, on the Pharmacological Effects of Neurotensin Agonists.* Peptides, 1994. **16**(1): p. 37-44.

47. Le, F., B. Cusack, and E. Richelson, *The neurotensin receptor: is there more than one subtype?* Trends in Pharmacological Science, 1996. **17**(1): p. 1-3.

48. Cusack, B., et al., *Pharmatological and Biochemical Profiles of Unique Neurotensin-8-13 Analogs Exhibiting Species Selectivity, Sterioselectivety, and Superagonism.* Journal of Biological Chemistry, 1995. **270**(31): p. 18395-18366.

49. Gilbert, J.A., et al., *Neurotensin(8-13) - Comparison of Novel Analogs for Stimulation of Cyclic-GMP Formation in Neuro-Blastoma Clone N1E-115 and Receptor-Binding to Human-Brain and Intact N1E-115 Cells.* Biochemical Pharmacology, 1989. **38**(19): p. 3377-3382.

50. Pang, Y., et al., *Proposed Ligand Binding Site of the Transmembrane Receptor for Neurotensin(8-13).* Journal of Biological Chemistry, 1996. **271**(25): p. 15060-15068.

51. Tyler-McMahon, B.M., et al., *In vitro binding and CNS effects of novel neurotensin agonists that cross the blood brain barrier.* Neuropharmacology, 1999. **38**: p. 1027-1034.

52. Botto, J., et al., *Identification in the rat neurotensin receptor of amino-acid residues critical for the binding of neurotensin.* Molecular Brain Research, 1997. **46**(1-2): p. 311-317.

53. Labbé-Jullié, C., et al., *Mutagenesis and Modeling of the Neurotensin Receptor NTR1 Identification of Residues that are Critical for Binding SR 48692, a Nonpeptide Neurotensin Antagonist.* Journal of biological Chemistry, 1998. **273**(26): p. 16351-16357.

54. Barroso, S., et al., *Identification of Residues Involved in Neurotensin Binding and Modeling of the Agonist Binding Site in Neurotensin Receptor 1.* Journal Of Biological Chemistry, 2000. **275**(1): p. 328-336.

55. Probst, W.C., et al., *Sequence alignment of the G-protein coupled receptor superfamily.* DNA cell Biology, 1992. **11**: p. 1-20.

56. Cohen, S.N., et al., *Construction of biologically functional bacterial plasmid in vitro.* National Academy of Sciences of the Unites States of America, 1973. **70**(11): p. 3240-3244.

57. Witholt, B., et al., *Efficient and reproducible procedure for formation of sphereoplasts from variously grown Escherichia-coli.* Analytical Biochemistry, 1976. **74**(1): p. 160-170.

58. Hartmann, S.R. and E.L. Hahn, *Nuclear double resonance in the rotating frame.* Physics Review, 1962. **128**: p. 2024-2053.

59. Hediger, S., B.H. Meier, and R.R. Ernst, *Adiabatic Passage Hartmann-Hahn Cross-Polarisation in NMR Uunder Magic-Angle Sample-Spinning.* Chemical Physics Letters, 1995. **240**(5-6): p. 449-456.

60. Bennett, A.E., et al., *Heteronuclear decoupling in rotating solids.* Journal of Chemical Physics, 1995. **103**(16): p. 6951-6958.

61. Carravetta, M., *Estinmation of carbon-carbon bond lengths and medium-range internuclear distances by solid-state NMR.* J. Am. Chem. Soc., 2001. **123**: p. 10628.

62. Levitt, M.H., *Symmetry-Based Pulse Sequences in Magic-angle Spinning Solid-state NMR.* Ency, Nuc. Mag. Res., 2002. **9**.

63. Andrew, E.R. and e. al., *The narrowing of NMR spectra of solids by high-speed specimen rotation and the resolution of chemical shift and spin multiplet structures for solids.* Prog. NMR Spectr., 1971. **8**: p. 1.

64. Davis, J.H. and M. Auger, *static and magic angle spinning NMR of membrane peptides and proteins.* Prog. Nuc. Mag. Res. Spec., 1998. **35**: p. 1.

65. Harris, J.R. and R.W. Horne, *Electron Microscopy in Biology: a practical approach*, ed. J. Harris. 1991. 203-228.

66. Crowther, R.A., R. Henderson, and J.M. Smith, *MRC image processing programs.* Journal of Structural Biology, 1996. **116**(1): p. 9-16.

67. Bailey, S., *The CCP4 Suite: Programs for protein crystallography.* Acta Crystallographica section D-biological crystallography, 1994. **50**: p. 760-763.

68. Tucker, J. and R. Grisshammer, *Purification of a rat neurotensin receptor expressed in Escherichia coli.* Biochemical Journal, 1996. **317**: p. 891-899.

69. Decaluwe, G.L.J., et al., *Effect of carboxyl mutations on functional-properties of bovine rhodopsin.* Biophysical Chemistry, 1995. **56**(1-2): p. 79-87.

70. Smith, S.O., *Nuclear-magnetic-resonance studies on the structure and function of rhodopsin.* Behavioral and brain science, 1995. **18**(3): p. 488-489.

71. Langen, R., et al., *Structural Features of the C-Terminal Domain of Bovine Rhodopsin: A Site-Directed Spin-Labeling Study.* Biochemistry, 1999. **38**(25): p. 7918-7924.

72. Kane, J.F., *Effects of rare codon clusters on high-level expression of heterologous proteins in Esherichia coli.* Current Opinion in Biotechnology, 1995. **6**: p. 494-500.

73. Pedersen-Lane, J., et al., *High-Level Expression of Human Thymidylate Synthase.* Protein Expression and Purification, 1997. **10**(2): p. 1997.

74. Stanasila, L., et al., *Coupling Efficacy and Selectivity of the Human mu-Opioid Receptor Expressed as Receptor-Galpha Fusion Proteins in Escherichia coli.* Journal of Neurochemistry, 2000. **75**: p. 1190-1199.

75. Hulme, E.C. and C.A.M. Curtis. in *Biochemical Society Transcripts*. 1998.

76. Sambrook, J., E.F. Fritsh, and T. Maniatis, *Molecular Cloning*. 2nd ed. 1992: Cold Spring Harbour Laboratory Press.

77. Grisshammer, R. and C.G. Tate, *Overexpression of integral membrane proteins for structural studies*. Quarterly review of biophysics, 1995. **28**: p. 315-422.

78. Grisshammer, R., R. Duckworth, and H. Henderson, *Expression of a rat neurotensin receptor in E. coli*. Biochemical Journal, 1993. **317**: p. 891-899.

79. Knol, J., K. Sjollema, and B. Poolman, *Detergent-mediated reconstitution of membrane proteins*. Biochemistry, 1998. **37**: p. 16410-16415.

80. Rigaud, J., B. Pitard, and D. Levy, *Reconstitution of membrane proteins into liposomes: application to energy-transducing membrane proteins*. Biochimica et Biophysica Acta, 1995. **1231**: p. 223-246.

81. Jackson, M.L., et al., *Solubilization of phosphatidylcholine bilayers by octyl glucoside*. Biochemistry, 1982. **21**: p. 4576-4582.

82. Rigaud, J., M. Paternostre, and A. Bluzat, *Mechanisms of Membrane Protein Insertion into Liposomes during Reconstitution Procedures Involving the Use of Detergents. 2. Incorporation of the Light-Driven Proton Pump Bacteriorhodopsin*. Biochemistry, 1987. **27**: p. 2677-2688.

83. Levy, D., et al., *Phospholipid Vesicle Solubilization and Reconstitution by Detergents. Symmetrical Analysis of the Two Processes Using Octaethylene Glycol*

Mono-n-dodecyl Ether. Biochemistry, 1990. **29**: p. 9480-9488.

84. McDonnell, J.M., *Surface plasmon resonance: towards an understanding of the mechanisms of biological molecular recognition.* Current Opinions in Chemical Biology, 2001. **5**(5): p. 572-577.

85. Kroger, D., F. Hucho, and H. Vogel, *Ligand binding to Nicotinic Acetylcholine Receptor Investigated by Surface Plasmon Resonance.* Analytical Chemistry, 1999. **71**: p. 3157.

86. De Crescenzo, G., et al., *Real-Time Kinetic Studies on the Interaction of Transforming Growth Factor R with the Epidermal Growth Factor Receptor Extracellular Domain Reveal a Conformational Change Model.* Biochemistry, 2000. **39**: p. 9466-9476.

87. Rich, R.L., et al., *Kinetic analysis of estrogen receptor/ligand interactions.* Proceedings of the National Academy of Sciences of the United States of America, 2002. **99**(13): p. 8562-8567.

88. Heyse, S., et al., *Incorporation of Rhodopsin in Laterally Structured Supported Membranes: Observation of Transducin Activation with Spatially and Time-Resolved Surface Plasmon Resonance.* Biochemistry, 1998. **37**: p. 507-522.

89. Karlsson, O.P. and S. Lofas, *Flow-mediated on-surface reconstitution of G-protein coupled receptors for applications in surface plasmon resonance biosensors.* Analytical Biochemistry, 2002. **300**(2): p. 132-138.

90. Stenlund, P., et al., *Capture and reconstitution of G protein-coupled receptors on a biosensor surface.* Analytical Biochemistry, 2004. **316**: p. 243-250.

91. O'Shannessy, D.J. and D.J. Winzor, *Interpretation of Deviations from Pseudo-First-Order Kinetic Behaviour in the Characterisation of Ligand Binding by Biosensor Technology.* Analytical Biochemistry, 1996. **236**: p. 275-283.

92. Van der Merwe, P.A., *Surface Plasmon Resonance in Protein-Ligand Interactions: A Practical Approach.*, ed. S. Harding and P.Z. Chowdry. 2000: Oxford University Press.

93. Weiss, J.M., et al., *The cubic ternary complex receptor-occupancy model .1. Model description.* Journal of Theoretical Biology, 1996. **178**(2): p. 151-167.

94. Weiss, J.M., et al., *The cubic ternary complex receptor-occupancy model .2. Understanding apparent affinity.* Journal of Theoretical Biology, 1996. **178**(2): p. 169-182.

95. Vincent, J.P., J. Mazella, and P. Kitabgi, *Neurotensin and neurotensin receptors.* Trend in Pharmacological Sciences, 1999. **20**(7): p. 302-309.

96. Lipschultz, C.A., *Experimentl Design for Analysis of Complex Kinetics Using Surface Plasmon Resonance.* Methods, 2000. **20**: p. 310-318.

97. McConnell, H.M., *Effect of anisotropic hyperfine interactions on paramagnetic relaxation in liquids.* Journal of Chemical Physics, 1956. **25**: p. 709-.

98. Griffith, O.H., D.W. Cornell, and H.M. McConnell, *Nitrogen Hyperfine Tensor and g Tensor of Nitroxide Radicals.* Journal of Chemical Physics, 1965. **43**: p. 2909-2910.

99. Watts, A., I.D. Volotovski, and D. Marsh, *Rhodopsin-Lipid associations on Bovine rod outer segement membranes - Identification of Immobilized Lipid by spin-labels.* Biochemistry, 1979. **18**(22): p. 5006-5013.

100. Willan, K.J., et al., *Specific spin labelling of fc region of immunoglobulins.* FEBS letters, 1977. **80**(1): p. 133-136.

101. Spooner, P.J.R., et al., *Structural Information on a membrane transport protein from nuclear magnetic resonance spectroscopy using sequence-selective nitroxide labeling.* Biochemistry, 1999. **38**: p. 9634-9639.

102. Hadingham, T., *Structural studies of the peptide neurotransmitter neurotensin*. 2002, Oxford University.

103. Jost, P., et al., *Lipid spin labels in lectin multilayers - Study of motion along fatty acid chains.* Journal of Molecular Biology, 1971. **59**(1): p. 77-.

104. Kitabgi, P., et al., *Biosynthesis, Maturation, Release, and Degradation of Neurotensin and Neuromedin-N.* Annuals of the New York Academy of science, 1992. **668**: p. 30-42.

105. Carraway, R.E., S.P. Mitra, and G. Spaulding, *Posttranslational processing of the Neurotensin Nerromedin-N Precursor.* Annuals of the New York academy of Science, 1992. **668**: p. 1-16.

106. Demura, M., et al., *Structure of Bombyx mori silk fibroin based on solid-state NMR orientational constraints and fiber diffraction unit cell parameters.* Journal of the American Chemical Society, 1998. **120**(6): p. 1300-1308.

107. SHON, K.J., et al., *NMR-studies of the structure and dynamics of membrane-bound bacteriophage-PFL-coat protein.* Science, 1991. **252**(5010): p. 1303-1304.

108. Kim, Y., et al., *Solid-state NMR studies of the membrane-bound closed state of the colicin E1 channel domain in lipid bilayers.* Protein Science, 1998. **7**(2): p. 342-348.

109. Williamson, P.T.F., et al., *Probing the agonist binding pocket in the nicotinic acetylcholine receptor: A high-resolution solid-state NMR approach.* Biochemistry, 1998. **37**(30): p. 10854-10859.

110. Williamson, P.T.F., et al., *Dynamics and orientation of N+(CD3)(3)-bromoacetylcholine bound to its binding site on the nicotinic acetylcholine receptor.* Proceedings of the national academy of sciences of the United States of America, 2001. **98**(5): p. 2346-2351.

111. Williamson, P.T.F., et al., *Probing the enviroment of neurotensin whilst bound to the neurotensin receptor by solid state NMR*. FEBS Letters, 2002. **518**: p. 111-115.

112. Spooner, P.J.R., et al., *Structural information on a membrane transport protein from nuclear magnetic resonance spectroscopy using sequence-selective nitroxide labeling*. Biochemistry, 1999. **38**(30): p. 9634-9639.

113. Middleton, D.A., et al., *The conformation of an inhibitor bound to the gastric proton pump*. FEBS Letters, 1997. **410**(2-3): p. 269-274.

114. Kim, C.G., J.A. Watts, and A. Watts, *Ligand docking in the gastric H+/K+-ATPase: Homology modeling of a reversible inhibitor binding sites*. Journal of Medical Chemistry, 2005. **48**(23): p. 7145-7152.

115. Prosser, R.S., et al., *Magnetically Aligned Membrane Model Systems with Positive Order Parameter: Switching the Sign of S_{zz} with Paramagnetic Ions*. Journal of the American Chemical Society, 1996. **118**(1): p. 269-270.

116. Andrew, E.R., A. Bradbury, and R.G. Eades, *NMR spectra from crystals rotated at high speed*. Nature, 1958. **182**: p. 1659-.

117. Lowe, I.J., *Free induction decays in rotating solids*. Phys. Rev. Lett., 1959. **2**: p. 285-.

118. Luca, S., et al., *The conformation of neurotensin bound to its G protein-coupled receptor*. PNAS, 2003. **100**(19): p. 10706-10711.

119. Seeman, N.C., *Structural DNA nanotechnology*. Abstracts of papers of the American chemical society, 2003. **225**(1): p. 215.

120. Holliday, R., *A mechanism for gene conversion in fungi*. Genetics Research, 1964. **5**: p. 282-304.

121. Seeman, N.C., *Structural DNA nanotechnology*. Abstracts of papers of the American chemical society, 2003. **226**(2): p. 82-.

122. SantaLucia, J., *A unified view of polymer, dumbbell, and oligonucleotide DNA nearest-neighbor thermodynamics*. Proceedings of the national academy of sciences of the United States of America, 1998. **95**(4): p. 1460-1465.

123. Ortiz-Lombardia, M., et al., *Crystal structure of a DNA Holliday junction*. Nature Structural Biology, 1999. **6**(10): p. 913-917.

124. Zuker, M., *Mfold Webserver:* http://www.bioinfo.rpi.edu/applications/mfold.

125. Syozi, I., Progress in Theoretical Physics, 1951. **6**: p. 306.

126. Thomas, R., *Recherches sur la denaturation des acides desoxyribonucleiques*. Biochinica et Biophysica Acta, 1954. **14**(2): p. 231-240.

127. Voet, D. and J.G. Voet, *"Forces stabilizing nucleic acid structures - denaturation and renaturation" in Biochemitery*. 2 ed. 1995, New York: Wiley.

128. Mitchell, J.C. 2003, Oxford University: Oxford.

129. Seeman, N.C., *DNA engineering and its application to nanotechnology*. Trends in Biotechnology, 1999. **17**(11): p. 437-443.

130. Malo, J., et al., *Engineering a 2D Protein-DNA Crystal*. Angewandte Chemie, 2005. **117**: p. 3117-3121.

131. Miroux, B. and J.E. Walker, *Over-production of proteins in Escherichia coli: mutant hosts that allow synthesis of some membrane proteins and globular proteins at high levels.* Journal of Molecular Biology, 1996. **260**: p. 289-298.

132. Henderson, R., et al., *Model for the strucutre of bacteriorhodopsin based on high-resolution electron cryo-microscopy.* Journal of Molecular Biology, 1990. **213**: p. 899-929.